



THESIS APPROVAL

GRADUATE SCHOOL, KASETSART UNIVERSITY

Master of Science (Chemistry)

DEGREE

Chemistry

Chemistry

FIELD

DEPARTMENT

TITLE: The Use of 5,10,15,20-Tetra(p-bromophenyl)Porphyrin and
5,10,15,20-Tetra(p-nitrophenyl)Porphyrin as Chemosensor for Hg²⁺

NAME: Miss Suwaluck Chaitong

THIS THESIS HAS BEEN ACCEPTED BY

THESIS ADVISOR

(Associate Professor Apisit Songsasen, Ph.D.)

THESIS CO-ADVISOR

(Associate Professor Waraporn Parasuk, Dr.rer.nat.)

THESIS CO-ADVISOR

(Mr. Wanchai Pluempanupat, Ph.D.)

DEPARTMENT HEAD

(Associate Professor Supa Hannongbua, Dr.rer.nat.)

APPROVED BY THE GRADUATE SCHOOL ON _____

DEAN

(Associate Professor Gunjana Theeragool, D.Agr.)

THESIS

THE USE OF 5,10,15,20-TETRA(P-BROMOPHENYL)
PORPHYRIN AND 5,10,15,20-TETRA(P-NITROPHENYL)
PORPHYRIN AS CHEMOSENSOR FOR Hg²⁺



SUWALUCK CHAITONG

A Thesis Submitted in Partial Fulfillment of
the Requirements for the Degree of
Master of Science (Chemistry)
Graduate School, Kasetsart University

2012

Suwaluck Chaitong 2012: The Use of 5,10,15,20-Tetra(*p*-bromophenyl)Porphyrin and 5,10,15,20-Tetra(*p*-nitrophenyl)Porphyrin as Chemosensor for Hg²⁺. Master of Science (Chemistry), Major Field: Chemistry, Department of Chemistry. Thesis Advisor: Associate Professor Apisit Songsasen, Ph.D. 143 pages.

5,10,15,20-Tetra(*p*-bromophenyl)Porphyrin (TBTPP) and 5,10,15,20-Tetra(*p*-nitrophenyl)Porphyrin (TNPP) were synthesized the reaction of pyrrole with *p*-bromobenzaldehyde and *p*-nitrobenzaldehyde repectively, in the presence of acid catalyst. FT-IR and ¹H NMR were used to identify the structure of synthesized compounds.

TBTPP and TNPP were used as ratiometric fluorescent chemosensor for determining Hg²⁺ attributed to the metalloporphyrin formation of Hg-TBTPP and Hg-TNPP complexes. There were evidences from the experiments such as spectrofluorometry, which showed the occurrence of Hg-TBTPP and Hg-TNPP complexes. The structures of porphyrin ligand and porphyrin complexes were also investigated by using quantum chemical calculation. The results showed that synthesized TBTPP could coordinate with Hg²⁺ as similar as TNPP. However, TBTPP could coordinate with Hg²⁺ better than TNPP, these results were confirmed by the stablily constants and stabilization energy of complexes. The linear range of detections of Hg²⁺ by TBTPP and TNPP were found to be 8-24 μM and 12-27 μM, respectively.

Student's signature

Thesis Advisor's signature

ACKNOWLEDGEMENTS

I wish to express my sincere gratitude to my supervisor, Associate Professor Dr. Apisit Songsasen for his unwavering support and continuously valuable guidance throughout the duration of my graduate study and research. I also wish to express my appreciation of my advisory committee Assistant Professor Waraporn Parasuk Dr. and Dr. Wanchai Pluempanupat for worthy suggestions. Additionally, I am also appreciated to Mr. Akachai Punyatharakorn, a graduate student in Physical chemistry field, for the advantageous suggestion on the quantum chemical calculation part.

I would also like to thank all of staffs at Department of Chemistry, Faculty of Science, Kasetsart University for their kind helps in everything that they can.

Besides, I myself would like to thank the Center of Excellence for Innovation in Chemistry (PERCH-CIC) for financial support and the Department of Chemistry, Faculty of Science, Kasetsart University for all research facilities.

Last but not least, I wish to express my great appreciation and my gratitude to my family for their hard work, advice, encouragement, understanding and the financial assistance, which made my graduate study possible and I would like to thank all of my friends for their support and unconditional friendship.

Suwaluck Chaitong

May, 2012

TABLE OF CONTENTS

	Page
TABLE OF CONTENTS	i
LIST OF TABLES	iii
LIST OF FIGURES	v
LIST OF ABBREVIATIONS	x
INTRODUCTION	1
OBJECTIVES	30
LITERATURE REVIEW	31
MATERIALS AND METHODS	52
Materials	52
Methods	54
RESULTS AND DISCUSSIONS	63
CONCLUSION AND RECOMMENDATIONS	98
Conclusion	98
Recommendations	100
LITERATURE CITED	101
APPENDICES	106
Appendix A	107
The reaction mechanisms of TBTPP and TNPP synthesis, where R = Br, NO ₂	
Appendix B	113
Calculation of stability constant of TBTPP and Hg ²⁺ by continuous variation method	
Appendix C	117
Calculation of stability constant of TBTPP and Hg ²⁺ by Benesi-Hildebrand's equation	
Appendix D	122
Calculation of limit of detection of the analysis of Hg ²⁺ by TBTPP and TNPP	
Appendix E	127
Determination of linear range of Hg ²⁺ analysis by using TNPP in methanol	

TABLE OF CONTENTS (Continued)

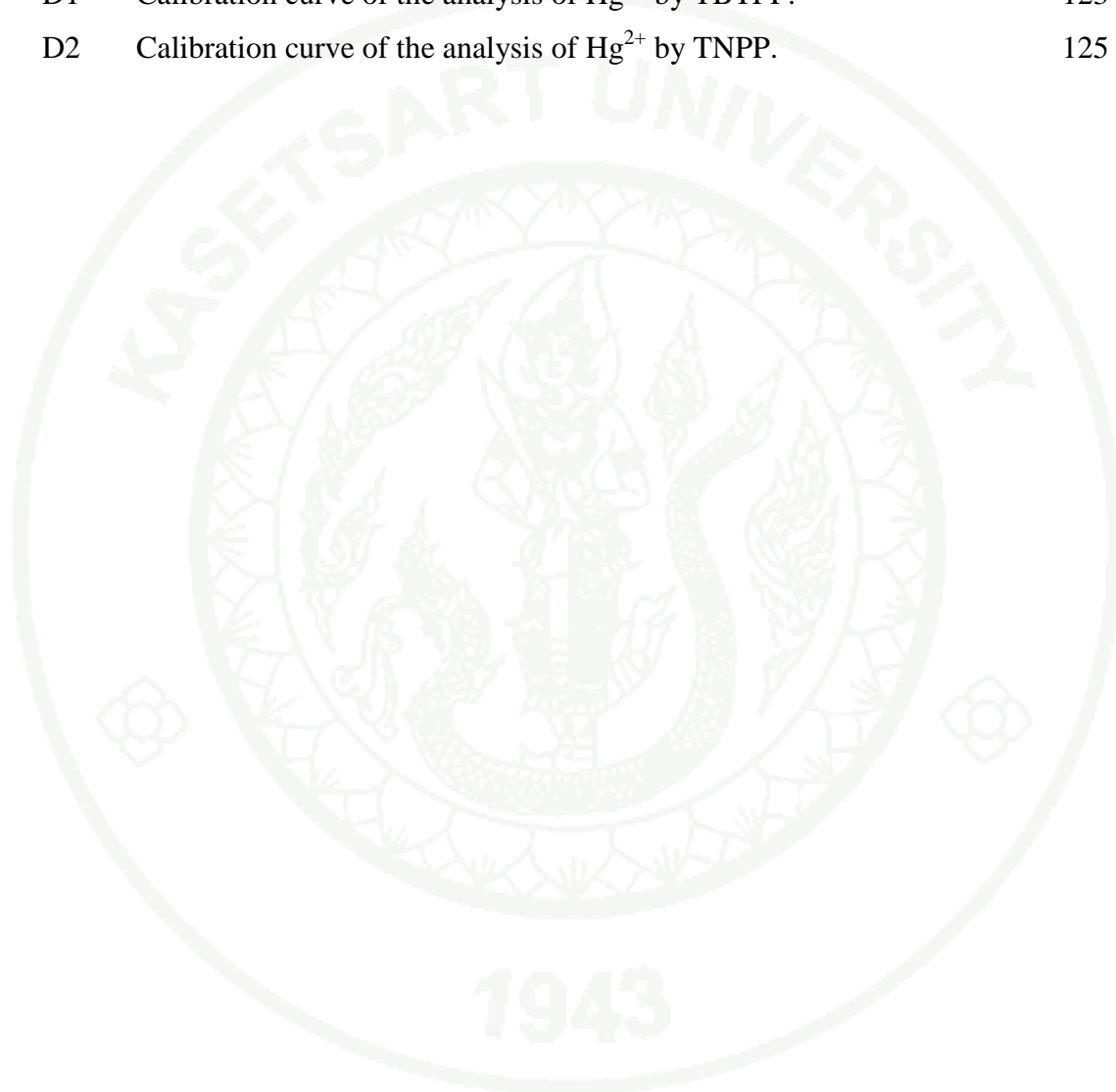
	Page
Appendix F Determination of stabilization energies by quantum chemical calculation and the output data of complexes optimized by Gaussian 03	129
CURRICULUM VITAE	143

LIST OF TABLES

Table		Page
1	Some properties of elemental mercury.	2
2	The amount of metal ion solutions and metal ion salts for the preparation of 1 mM standard metal cation in ethanol.	57
3	The amount of anion salts for the preparation of 1 M standard anion in distilled water.	58
4	Data from the FT-IR spectra of TBTPP.	68
5	Chemical shifts from ^1H NMR spectra of TBTPP.	68
6	Data from the FT-IR spectrum of TNPP.	70
7	Chemical shifts from ^1H NMR spectra of TNPP.	73
8	Fluorescent sensing of Hg^{2+} by using of TBTPP in the presence of interfering cation and anion.	85
9	Fluorescent sensing of Hg^{2+} by using of TNPP in the presence of interfering cation and anion.	86
10	The classification of Lewis acids and bases.	87
11	Ionic radii of some metal cations at coordination number of 6.	92
12	Energetic data of isolated atoms, molecules and possible structure of TBTPP and TNPP complexes calculated at B3LYP level of theory using 6-31G* and LandL2DZ basis set in route (a, c).	96
13	Energetic data of isolated atoms, molecules and possible structure of TBTPP complexes calculated at B3LYP level of theory using 6-31G* and LandL2DZ basis set in route (b).	97

LIST OF TABLES (Continued)

Appendix Table		Page
D1	Calibration curve of the analysis of Hg^{2+} by TBTPP.	123
D2	Calibration curve of the analysis of Hg^{2+} by TNPP.	125



LIST OF FIGURES

Figure		Page
1	A simplified Jablonski diagram with absorbance, internal conversion, fluorescence, vibrational relaxation, intersystem crossing and phosphorescence.	5
2	Electron spins in singlet and triplet excited states.	6
3	Mirror-image rule and Franck-Condon factors, the absorption and emission spectra are for anthracene. The numbers 0, 1 and 2 refer to vibrational energy levels.	10
4	Stokes shift between λ_{\max} of absorption and emission spectra.	11
5	Structures of some typical fluorescent substance.	12
6	Main compositions of fluorescent melocular sensor for cation recognition.	14
7	The general view of the principle of PET fluorescence molecular sensor.	16
8	Interaction of a bound cation with an electron-donating or electron withdrawing group.	17
9	A schematic fluorescence resonance energy transfer system.	19
10	Diagram showing the spectral overlap for fluorescence resonance energy transfer system.	19
11	Molecular structure of porphin which showed a position of each atom and hydrogen bonding.	20
12	Structure of heme b, chlorophyll and vitamin B ₁₂ .	22
13	Typical UV-VIS absorption spectrum of porphyrins.	25
14	Reaction scheme of meso-tetraphenylporphyrin synthesis by Lindsey <i>et al.</i> , (1987).	33
15	Mono(nitrophenyl)triphenyl porphyrin.	34

LIST OF FIGURES (Continued)

Figure		Page
16	The structure of <i>meso</i> -Tetrakis[4-(carboxy-phenyl)porphyrin (H ₂ CPP) and <i>meso</i> -Tetrakis[4-(carboxymethyleneoxy)phenyl]porphyrin (H ₂ T4CPP).	35
17	Synthetic scheme of Shi D. F. developed method.	36
18	The structures of 5-(4-nitroaryl)-10,15,20-triarylporphyrin (a), 5,10-bis(4 nitroaryl)-15,20-diarylporphyrin (b), 5,10,15-tris(4-nitroaryl)-20-arylporphyrin (c) and tri-carboranylporphyrin (d).	37
19	The structures of 5-(4-nitroaryl)-10,15,20-triarylporphyrin, 5,10-bis(4-nitroaryl)-15,20-diarylporphyrin, and 5,10,15-tris(4-nitroaryl)-20-arylporphyrin.	38
20	The synthesis of 5,10,15,20-Tetra[5-{2-(4-alkoxyphenyl)-ethenyl}-6-{2-phenyl-ethenyl}-2,3-dicyano-porphyrin.	39
21	The synthesis of 5,10,15,20-tetraphenylporphyrin in two-step process.	40
22	The synthesis of trans-A ₂ B ₂ -tetraarylporphyrins.	40
23	The structure of compound 5,10,15,20-tetra(<i>p</i> -sulfonatophenyl)porphyrin (TPPS).	41
24	The structure of the porphyrin derivatives (24a-24d).	42
25	A disulfonamide appended porphyrin receptor (25a) and its anion complex (25b).	43
26	The structure of 5-(4-([2, 2':6', 2'']-terpyridin-4-ylcarboxamidyl)phenyl)-10,15,20-triphenylporphyrin (H ₂ TPPTPy).	45
27	The structure of 5-(<i>p</i> -N,N'-bis(2-pyridyl)amino)phenyl-10,15,20-tris(<i>p</i> -methoxyphenyl)porphyrin Zinc.	46

LIST OF FIGURES (Continued)

Figure		Page
28	The structure of compound 5,10,15,20-tetra(<i>p</i> -bromophenyl)porphyrin and 5,10,15,20-tetra(<i>p</i> - <i>N,N</i> -bis(2-pyridyl)amino)phenyl porphyrin zinc.	47
29	The structure of compound of meso-tetraphenylporphyrin derivative, containing two 2-(oxymethyl) pyridine units.	47
30	Preparation of 5,10,15,20-tetra-(3-bromo-4-hydroxyphenyl) porphyrin (TBHPP).	48
31	The structure of compounds tetra(<i>p</i> -dimethylaminophenyl) porphyrin (TDMAPP) and tetra(<i>n</i> -phenylpyrazole)porphyrin (TPPP).	49
32	The structure of compound meso-tetra(<i>p</i> -methoxylphenyl)porphyrin T(<i>p</i> -OCH ₃)PPH ₂ and meso-tetra(<i>p</i> -methoxylphenyl)porphyrin T(<i>p</i> -OCH ₃)PPH ₂ - Ag(I) complex.	50
33	Mechanism of fluorescence enhancement of [Co(TPP)(Ds-pip)] complex upon the addition of ammonia.	51
34	The synthesis pathways of TBTPP and TNPP.	64
35	The components of synthesized TBTPP and TNPP with the best condition on thin layer chromatography (TLC).	65
36	The FT-IR spectrum of TBTPP.	67
37	The ¹ H NMR spectrum of TBTPP in chloroform- <i>d</i> (CDCl ₃).	69
38	The FT-IR spectrum of TNPP.	71
39	The ¹ H NMR spectrum of TNPP in chloroform- <i>d</i> (CDCl ₃).	72
40	The fluorescence spectra of TBTPP in the presence of Hg ²⁺ in methanol, ethanol and propanol.	76

LIST OF FIGURES (Continued)

Figure	Page
41	Continuous variation plot of complex between TBTPP and Hg^{2+} in ethanol. 77
42	The mole ratio plot of complex between TBTPP and Hg^{2+} in ethanol. 78
43	The fluorescence spectra of TNPP in the presence of Hg^{2+} in methanol, ethanol and propanol. 79
44	The mole ratio plot of complex between TNPP and Hg^{2+} in ethanol. 80
45	Fluorescent titration emission spectra of TBTPP (25 μM) upon the addition of different concentration of Hg^{2+} (0-30 μM) in ethanol solution. 81
46	The plot of relative fluorescence intensity (I_0/I) as a function of Hg^{2+} concentration. 81
47	Fluorescent titration emission spectra of TNPP (25 μM) upon the addition of different concentration of Hg^{2+} (0-30 μM) in ethanol solution. 82
48	The plot of relative fluorescence intensity (I_0/I) as a function of Hg^{2+} concentration. 82
49	Postulated structure of M-TBTPP complex, where M = Hg, Pb, Cd. 88
50	Postulated structure of M-TBTPP complex, where M = Hg, Pb. 89
51	The optimized structure of ligand H_2TBTPP . 90
52	The optimized structure of ligand TBTPP^{2-} . 90
53	The optimized structure of ligand H_2TNPP . 91
54	The optimized structure of Hg-TBTPP . 93

LIST OF FIGURES (Continued)

Figure		Page
55	The optimized structure of Pb-TBTPP.	93
56	The optimized structure of Cd-TBTPP.	94
57	The optimized structure of Hg-TNPP.	94
58	The optimized structure of Pb-TNPP.	95
Appendix Figure		
A1	The SN ₁ reaction mechanism of TBTPP and TNPP synthesis, R = Br, NO ₂ .	108
A2	The SN ₂ reaction mechanism of TBTPP and TNPP synthesis, R = Br, NO ₂ .	111
C1	The relationship between [Hg ²⁺]/A and 1/[TBTPP].	120
C2	The relationship between [Hg ²⁺]/A and 1/[TNPP].	121
E1	The plot of relative fluorescence intensity (I ₀ /I) as a function of Hg ²⁺ concentration in methanol.	128

LIST OF ABBREVIATIONS

TPP	=	<i>Meso</i> -tetraphenylporphyrin
TBTPP	=	5,10,15,20-Tetra(<i>p</i> -bromophenyl)porphyrin
TNPP	=	5,10,15,20-Tetra(<i>p</i> -nitrophenyl)porphyrin
Hg-TBTPP	=	5,10,15,20-Tetra(<i>p</i> -bromophenyl)porphyrin mercury(II)
Pb-TBTPP	=	5,10,15,20-Tetra(<i>p</i> -bromophenyl)porphyrin lead(II)
Cd- TBTPP	=	5,10,15,20-Tetra(<i>p</i> -bromophenyl)porphyrin cadmium(II)
Hg-TNPP	=	5,10,15,20-Tetra(<i>p</i> -bromophenyl)porphyrin mercury(II)
Pb-TNPP	=	5,10,15,20-Tetra(<i>p</i> -nitrophenyl)porphyrin lead(II)
H ₂ TBTPP	=	5,10,15,20-Tetra(<i>p</i> -bromophenyl)porphyrin(0)
TBTPP ²⁻	=	5,10,15,20-Tetra(<i>p</i> -bromophenyl)porphyrin(-II)
H ₂ TNPP	=	5,10,15,20-Tetra(<i>p</i> -nitrophenyl)porphyrin
H ₂ T4CPP	=	<i>Meso</i> -Tetrakis[4- (carboxymethyleneoxy)phenyl]porphyrin
H ₂ CPP	=	<i>Meso</i> -Tetrakis[4-(carboxy-phenyl)porphyrin
TPPS	=	5,10,15,20-tetra(<i>p</i> -sulfonatophenyl)porphyrin
H ₂ TPPTPy	=	5-(4-([2,2':6',2'']-terpyridin-4-yl- carboxyamidyl)phenyl)-10,15,20- triphenylporphyrin
TBHPP	=	5,10,15,20-tetra-(3-bromo-4- hydroxyphenyl)porphyrin
TDMAPP	=	Tetra(<i>p</i> -dimethylaminophenyl) porphyrin
TPPP	=	Tetra(<i>n</i> -phenylpyrazole) porphyrin

LIST OF ABBREVIATIONS (Continued)

Pd-TAPP	=	<i>Meso</i> -tetra(4- <i>N,N,N</i> -trimethylanilinium)porphyrin-Palladium
T(<i>p</i> -OCH ₃)PPH ₂	=	<i>Meso</i> -tetra(<i>p</i> -methoxyphenyl)porphyrin
Co(TPP)(Ds-pip)	=	Porphyrin cobalt(II)-dansyl complex
DDQ	=	2,3-dichloro-5,6-dicyano-1,4-benzoquinone
DMAP	=	<i>N,N'</i> -dimethyl-4-aminopyridine
DMF	=	<i>N,N'</i> -dimethylformamide
DPA	=	2,2'-dipyridylamine
EDC	=	1-(3-dimethylaminopropyl)-3-ethylcarbodiimide
EDTA	=	Ethylenediaminetetraacetic acid
THF	=	Tetrahydrofuran
PVC	=	Poly(vinylchloride)
TBAP	=	Tetrabutylammonium perchlorate
DMSO-d ₆	=	Dimethylsulfoxide, D-6
UV-Vis	=	Ultraviolet-visible spectroscopy
FT-IR	=	Fourier Transform Infrared Spectrophotometry
¹ H NMR	=	Proton Nuclear Magnetic Resonance Spectroscopy
TLC	=	Thin Layer Chromatography
PET	=	Photoinduced Electron Transfer
ICT	=	Internal Charge Transfer
HOMO	=	Highest Occupied Molecular Orbital
LUMO	=	Lowest Unoccupied Molecular Orbital
L.O.D	=	Limit of Detection
DFT	=	Density Functional Theory
a.u.	=	Atomic unit

**THE USE OF 5,10,15,20-TETRA(P-BROMOPHENYL)
PORPHYRIN AND 5,10,15,20-TETRA(P-NITROPHENYL)
PORPHYRIN AS CHEMOSENSOR FOR Hg²⁺**

INTRODUCTION

1. Mercury in the environment

Mercury is known to early humans before other metals because it could be found in a free state in nature. Moreover, mercury pollution has become a global problem and seriously endangers human health. Inorganic mercury can be easily released into the environment through a variety of anthropogenic sources, such as the coal mining, solid waste incineration, fossil fuel combustion, and chemical manufacturing. It can also be released through the nonanthropogenic sources in the form of forest fires, volcanic emissions, and oceanic emission. Mercury can be easily transported into the atmosphere as the form of the mercury vapor. The atmospheric deposition of mercury ions leads to the accumulation on plants, in topsoil, in water and in underwater sediments.

1.1 The properties of mercury

Mercury is a heavy, silvery-white metal. As compared to other metals, it is a poor conductor of heat, but a fair conductor of electricity. Mercury has an exceptionally low melting temperature for a d-block metal. A complete explanation of this fact requires a deep excursion into quantum physics. Mercury has a unique electronic configuration where electrons fill all the available 1s, 2s, 2p, 3s, 3p, 3d, 4s, 4p, 4d, 4f, 5s, 5p, 5d and 6s subshells. As such configuration strongly resists removal of an electron, mercury behaves similarly to noble gas elements. Moreover, there are seven stable isotopes of mercury with ²⁰²Hg being the most abundant (29.86%). The

longest-lived radioisotopes are ^{194}Hg with a half-life of 444 years, and ^{203}Hg with a half-life of 46.612 days. Most of the remaining radioisotopes have half-lives that are less than a day. ^{199}Hg and ^{201}Hg are the most often studied NMR-active nuclei, having spins of $\frac{1}{2}$ and $\frac{3}{2}$ respectively.

Table 1 Some properties of elemental mercury.

Properties	Value
Atomic symbol	Hg
Atomic number	80
Atomic weight/g mol ⁻¹	200.59
Electronic configuration	[Xe] 4f ¹⁴ 5d ¹⁰ 6s ²
Density(20°C)/g cm ⁻³	15.534
Melting point/°C	-38.9
Boiling point/°C	357
ΔH_{fus} / kJ mol ⁻¹	2.30
ΔH_{vap} / kJ mol ⁻¹	59.1
ΔH_f (monoatomic gas)/ kJ mol ⁻¹	61.3
Electronegativity (Pauling Scale)	1.9
Electrical resistivity (20°C)/μΩ cm	95.8
Metal radius (12-coordinate)/pm	151
Effective ionic radius (6-coordinate)/pm	
III	102
II	119

Source: Greenwood (1997)

1.2 Application of mercury

Mercury has many benefits, it is used for the manufacture of industrial chemicals, for electrical and electronic, in medicine or using in laboratory.

The alchemist used mercury to make elixirs in order to try to cure all illnesses. Mercury is commonly used for making amalgams, which are solutions of various metals. Another common, liquid mercury is used in mirror telescopes so the mirror is formed by rotating liquid mercury on a disk, the parabolic form of the liquid thus formed reflecting and focusing incident light. In addition, liquid mercury is used in mercury battery as a non-rechargeable electrochemical battery and it can be used as a part of secondary reference electrode in electrochemistry. For Gaseous mercury, it is used in mercury-vapor lamps, fluorescent lamps and cold cathode argon-filled lamps to increase the ionization and electrical conductivity.

1.3 The toxicity of mercury

The use of mercury is becoming more restrictive because of its toxicity. Inorganic mercury, Hg^0 and Hg^{2+} , is released into an environment through a variety of anthropogenic and natural sources. Emitted elementary mercury vapors are easily transported into the atmosphere and are oxidized to Hg^{2+} . Then Hg^{2+} can accumulate on plants, in topsoil and in water. Moreover, a fraction of Hg^{2+} accumulated in environment can be reduced to Hg^0 by microorganisms including algae and cyanobacteria, and can be released back to the atmosphere again. This accumulated mercury reduces photosynthesis and transpiration in plants which may impact the global carbon cycle. Furthermore, the accumulated mercury will enter into a food chain, if animals eat plants or drink water in which mercury accumulates.

Another portion accumulated Hg^{2+} in an environment can be converted from inorganic mercury to methylmercury which is defined as any CH_3HgX species (X = halogen) by some prokaryotes. In particular, methylmercury is the most toxic form of mercury because it can cause severe neurological damages and wild lifes.

Moreover, it is readily absorbed by gastrointestinal (GI) tract and targets the central nervous system. The most dramatic case of severe methylmercury poisoning, which is through seafood consumption, was the Minamata Bay, Japan incident of the 1950s (Diez, 2008). After consumption, methylmercury is accumulated in the liver and kidney, and is dispersed throughout the body by blood flow.

As mentioned before, the critical target for methylmercury toxicity is the central nervous system. Physical lesions may be manifested as tingling and numbness in fingers and toes, loss of coordination, difficulty in walking, generalized weakness, impairment of hearing and vision, tremors and finally loss of consciousness leading to death.

2. Luminescence

Luminescence is an emission of light from any substance and occurs from electronically excited states. Luminescence is divided into two categories (fluorescence and phosphorescence) depending on the nature of the excited state.

2.1 Fluorescence is light emission caused by radiation with light (normally visible or ultraviolet light) and occurring within 10^{-10} to 10^{-8} s after irradiation.

2.2 Phosphorescence is a light emission which occur over much longer times after irradiation (10^{-3} to 10^2 s). It involves storage of energy in metastable states and its release through relatively slow processes. The phenomenon was discovered early on for phosphorus (Valeur *et al.*, 2002).

3. Jablonski diagram and electronic transition

The processes which occur between the absorption and emission of light are usually illustrated by the Jablonski diagram (Valeur *et al.*, 2002). The Jablonski diagram is a summary of the radiative and non-radiative transitions occurring between electronic states in a molecule. The figure below shows the transitions that

are common to all systems. The thick, dark lines labeled S_0 , S_1 and S_2 correspond to singlet electronic states and those labeled T_1 and T_2 represent triplet electronic states. Vibrational levels are shown with thin lines for each state. The vertical arrows with straight lines represent radiative transitions, while the arrows with wavy lines represent non-radiative transitions.

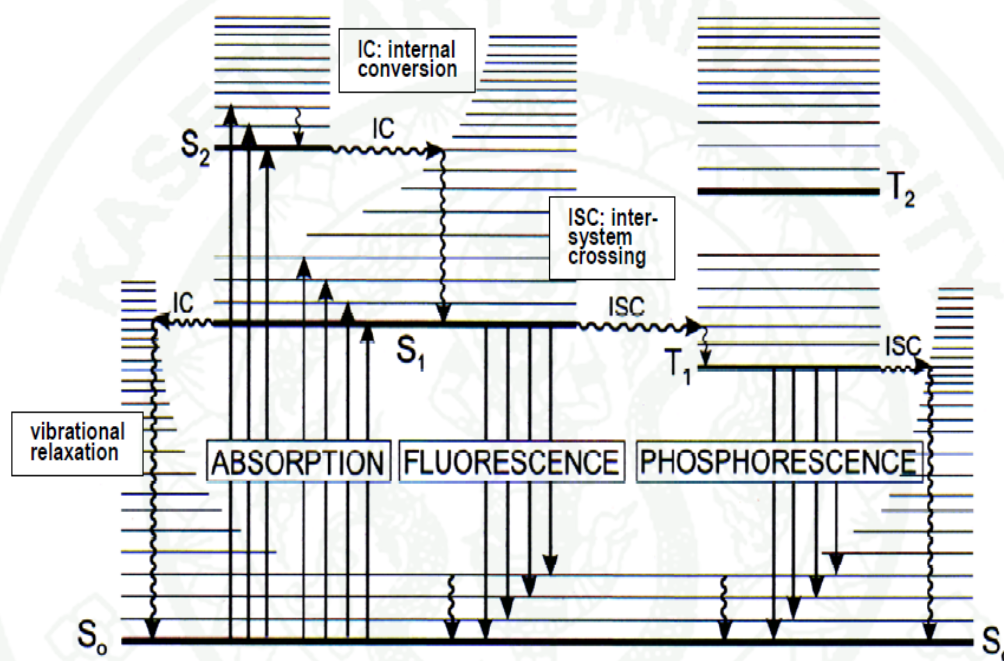


Figure 1 A simplified Jablonski diagram with absorbance, internal conversion, fluorescence, vibrational relaxation, intersystem crossing and phosphorescence.

Source: Valeur *et al.* (2002)

3.1 Singlet and triplet excited states

A molecular electronic state in which all electron spins are paired is called a singlet state, and no splitting of energy level occurs when the molecule is exposed to a magnetic field. The ground state for a free radical, on the other hand, is

a doublet state, because the odd electron can assume two orientations in a magnetic field, which imparts slightly different energies to the system.

When one of a pair of electrons of a molecule is excited to a higher energy level, a singlet or a triplet state is permitted. In the excited singlet state, the spin of the promoted electron is still paired with the ground state electron; in the triplet state, however, the spins of the two electrons have become unpaired and are thus parallel. These states can be represented as follows, where the arrows represent the direction of spin. In addition, the excited triplet state is less energetic than the corresponding excited singlet state.

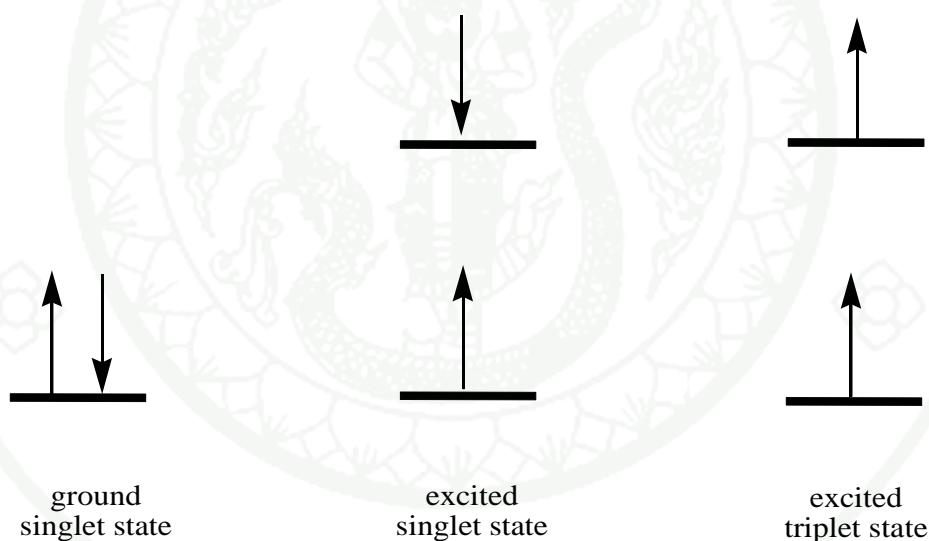


Figure 2 Electron spins in singlet and triplet excited states

Source: Skoog (1992)

2.2 Absorption ($\sim 10^{-15}$ s)

At room temperature, the vast majority of molecules are in the lowest vibrational level of the ground state. Absorption of a photon of sufficient energy will

excite the molecule from the ground state (S_0) to an excited state (S_1 , S_2 , etc.). Generally, the excitation will be to a higher vibrational level of the excited state.

3.3 Vibrational relaxation ($\sim 10^{-14}$ - 10^{-11} s)

This occurs within a given electronic state. When a molecule reaches a higher vibrational level of an electronic state, it will quickly relax to the lowest vibrational level of that state. The energy is released as heat to the surrounding solvent molecules.

3.4 Internal conversion (IC, $\sim 10^{-13}$ to 10^{-9} s)

This is a transition between two electronic states with the same energy (horizontal transition) and the same spin multiplicity (i.e. singlet-singlet or triplet-triplet). The rate will depend on the initial and final states of the transition.

(1) A molecule is excited to a higher vibrational level of the state S_2 . Vibrational relaxation occurs quickly to the lowest vibrational level of S_2 , then it undergoes internal conversion from S_2 to S_1 , followed by vibrational relaxation to the lowest vibrational level of S_1 . The overall rate is $\sim 10^{-13}$ to 10^{-11} s.

(2) The molecule can transit from the lowest vibrational level of S_1 to a higher vibrational level of S_0 . This would be followed by rapid relaxation to the lowest vibrational level of the ground state. This mechanism is one of the non-radiative transitions that can occur during de-excitation. The time scale for S_1 to S_0 internal conversion is $\sim 10^{-11}$ to 10^{-9} s. The difference in rates for these processes is related to the greater energy difference between the initial and final states (i.e. S_0 - S_1 energy difference is greater than S_1 - S_2).

3.5 Fluorescence ($\sim 10^{-10}$ to 10^{-8} s)

Fluorescence is emission of light from singlet-excited states, in which the electron in the excited orbital is paired (of opposite sign) to the second electron in the ground state orbital. Return to the ground state is spin-allowed and occurs rapidly by emission of a photon. This emission rates of fluorescence are typically 10^8 s, so that a typical fluorescence lifetime is near 10 ns. Fluorescence spectral data are generally presented as emission spectra. Emission spectra are dependent on the chemical structure of the fluorophore and the solvent in which it is dissolved.

3.6 Intersystem crossing (ISC, $\sim 10^{-10}$ to 10^{-4} s)

This is a transition between states of different multiplicity (i.e. singlet-triplet or triplet-singlet), but the same energy. It requires an interaction leading to a change of electron spin. This can be achieved through interactions with other molecules or through spin-orbit coupling within the molecule (e.g. the heavy atom effect). For isolated or shielded molecules, it can lead to phosphorescence emission. For non-protected molecules in solution, it generally leads to non-radiative deexcitation because phosphorescence is very slow process ($\sim 10^{-6}$ to 10^{-2} s), leaving many opportunities for non-radiative decay.

3.7 Phosphorescence ($\sim 10^{-3}$ to 10^2 s)

Phosphorescence is emission of light from triplet-excited states, in which the electron in the excited state orbital has the same spin orientation as the ground-state electron. Transitions to the ground state are forbidden and the emission rates are slow, so phosphorescence lifetimes are typically milliseconds to seconds. Phosphorescence is usually not seen in fluid solutions at room temperature, but there are many deactivation processes that compete with emission, such as nonradiative decay and quenching processes.

3.8 Other processes

In addition, there are other de-excitation processes that are dependent upon the local environment (e.g. interactions with other solute molecules). These include processes such as proton transfer, electron transfer, dynamic quenching, resonance energy transfer, photo-induced chemical reactions, structural changes, excimer and exciplex formation.

4. Characteristics of fluorescence emission

4.1 Mirror image rule

The emission is the mirror image of the S_0 to S_1 absorption, not of the total absorption spectrum. This is a result of the same transitions being involved in both absorption and emission and the similarities of the vibrational levels of S_0 and S_1 . In many molecules these energy levels are not significantly altered by the different electronic distributions of S_0 and S_1 . If a particular transition probability between the first and second vibrational levels is largest in absorption, the reciprocal transition is also most probable in emission (Lakowicz *et al.*, 1999). Figure 3 shows an example of this.

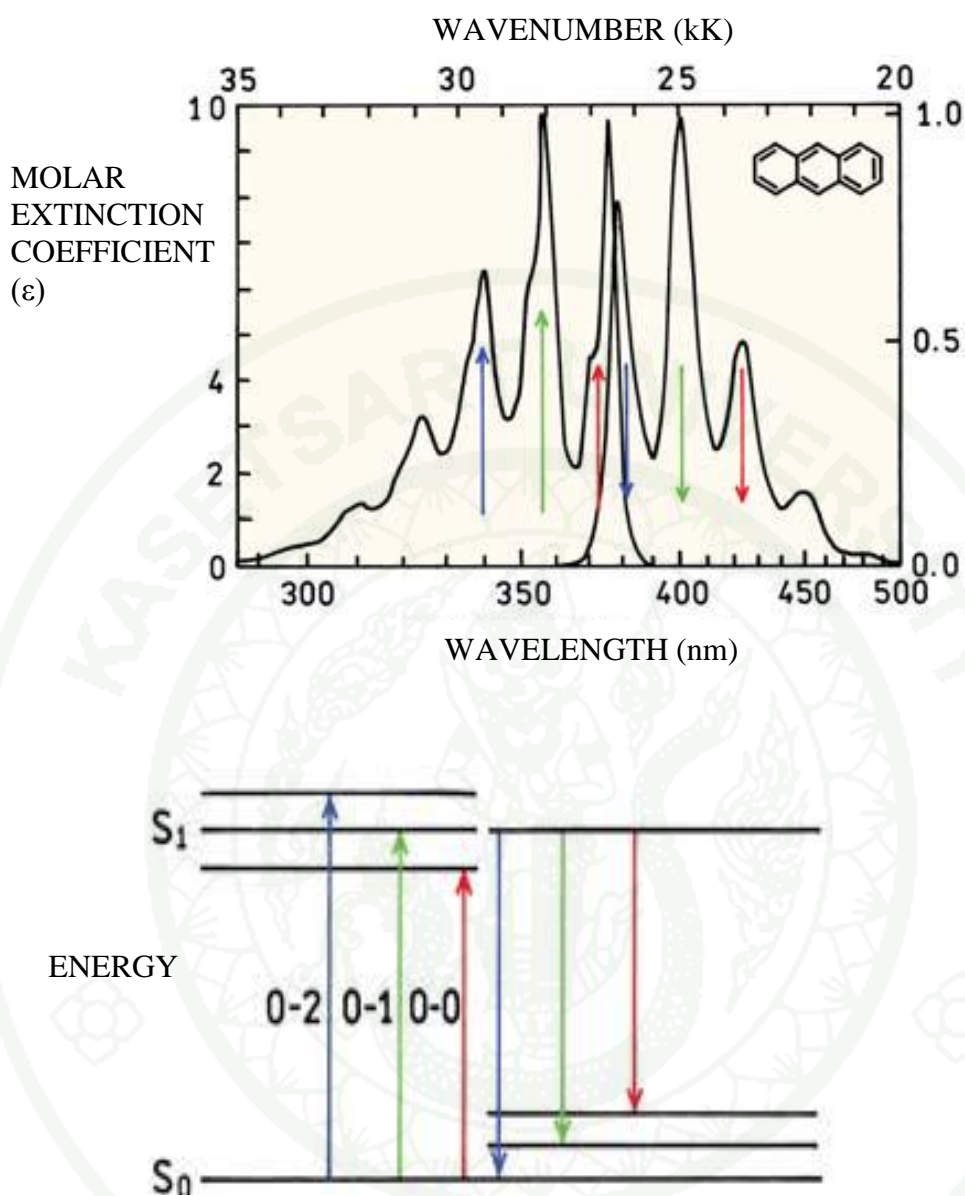


Figure 3 Mirror-image rule and Franck-Condon factors, the absorption and emission spectra are for anthracene. The numbers 0, 1 and 2 refer to vibrational energy levels.

Source: Lakowicz (1999)

4.2 Stokes shift

Stokes shift is the difference (in wavelength or frequency units) between positions of the band maxima of the absorption and emission spectra (fluorescence and Raman being two examples) of the same electronic transition. When a system (be it a molecule or atom) absorbs a photon, it gains energy and enters an excited state. One way for the system to relax is to emit a photon, thus losing its energy (another method would be the loss of heat energy). When the emitted photon has less energy than the absorbed photon, this energy difference is the Stokes shift. If the emitted photon has more energy, the energy difference is called an anti-stokes shift.

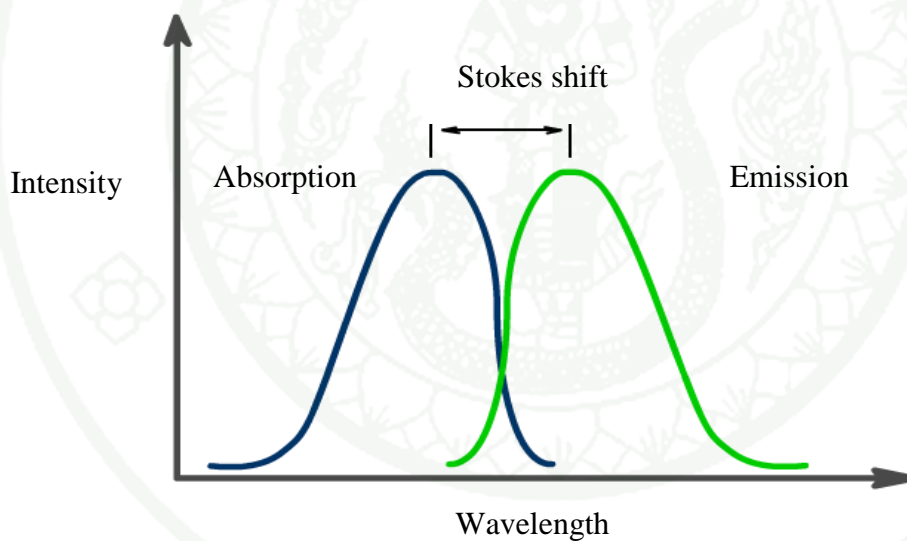


Figure 4 Stokes shift between λ_{max} of absorption and emission spectra

Source: Albani (2007)

5. Fluorophores

A fluorophore is a component of a molecule which causes a molecule to be fluorescent. It is a functional group in a molecule which will absorb energy of a specific wavelength and re-emit energy at a different wavelength. The amount

and wavelength of the emitted energy depend on both the fluorophore and the chemical environment of the fluorophore. Each fluorophore has its own specific fluorescence properties. Some typical fluorescent substances (fluorophores) are shown in Figure 5.

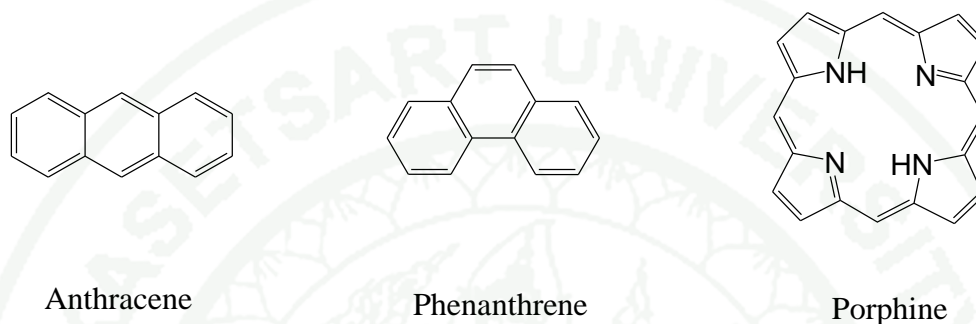


Figure 5 Structures of some typical fluorescent substance

6. Fluorescent sensor

Detecting cations is of great interest to many scientists, including chemists, biologists, clinical biochemists and environmentalists. Sodium, potassium, magnesium, calcium are involved in biological processes such as transmission of nerve impulses, muscle contraction, regulation of cell activity, etc. Moreover, various metal ions belong to metalloenzymes. In medicine, it is important to control the serum levels of lithium in patients under treatment for manic depression, and potassium in the case of high blood pressure. Regarding aluminium, its toxicity has long been recognized and there is a controversy about its possible implication in Alzheimer's disease. In chemical oceanography, it has been demonstrated that some nutrients required for the survival of microorganisms in sea water contain zinc, iron, manganese as enzyme cofactors. Finally, it is well known that mercury, lead and cadmium are toxic for organisms, and early detection in the environment is desirable.

Among the numerous analytical methods that are available for the detection of cations, flame photometry, atomic absorption spectrometry, ion sensitive electrodes, electron microprobe analysis, neutron activation analysis, etc., are expensive, often require samples of large size and do not allow continuous monitoring. In contrast, the methods based on fluorescent sensors offer distinct advantages in terms of sensitivity, selectivity, response time, local observation. Therefore, considerable efforts are being made to develop selective fluorescent sensors for cation detection. Such fluorescent sensors consists of a fluorophore linked to an ionophore and is thus called a fluoroionophore which is shown in Figure 6 (Valeur *et al.*, 2000).

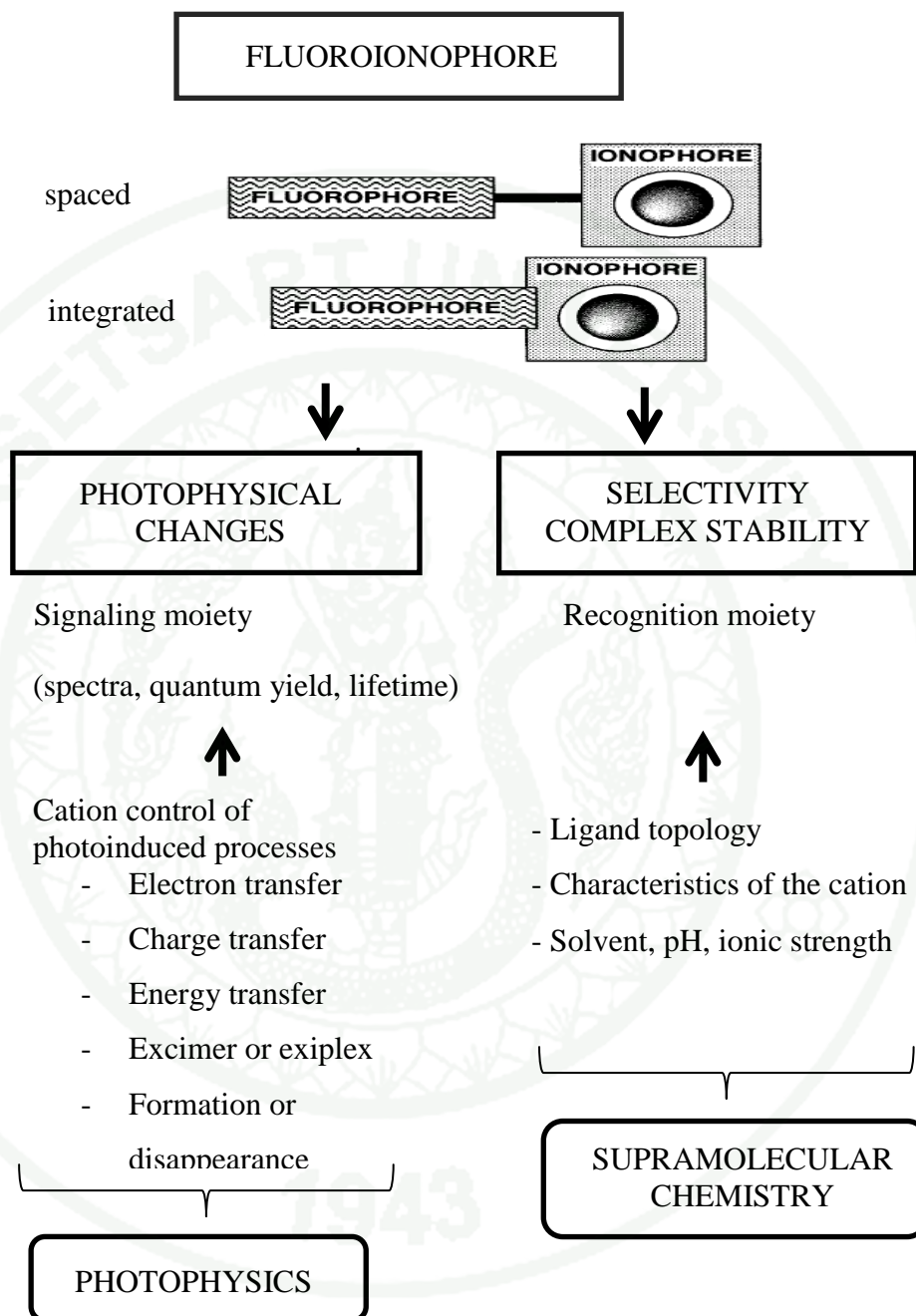


Figure 6 Main compositions of fluorescent melocular sensor for cation recognition.

Source: Valeur (2000)

In the design of such sensors, attention should be paid to both recognition and signaling moieties. The signaling moiety acts as a signal transducer, i.e. it converts the information (recognition event) into an optical signal expressed as the changes in the photophysical characteristics of the fluorophore. These changes are due to the perturbation (by the bound cation) of photoinduced processes such as electron transfer, charge transfer, energy transfer, excimer or exciplex formation or disappearance, etc. (Valeur *et al.*, 2000).

The response of selectivity and efficiency is depended on the ligand topology, the characteristics of cation (e.g. ionic radius, charge, coordination number, etc.) and the nature on solvent. In addition, it should be noted that the signaling moiety can be linked to the ionophore via spacer or they can be linked to each other without spacer unit (Figure 6).

6.1 Photoinduced electron transfer (PET)

In the PET sensors, photoinduced electron transfer makes the transfer of recognition information to fluorescence signal between receptor and fluorophore come true (Figure 7) which is shown the detailed process of how PET works in the fluorescence molecular sensor. The receptor could provide the electron to the vacated elector orbital of the excited fluorophore. The excited electron in the fluorophore could not come back the original orbital, resulting in the quenching of fluorescence emission. The coordination of receptor and guest decreased the electron donor ability of receptor reduced or even disrupted the PET process, then leading to the enhancement of intensity of fluorescence emission. Therefore, the sensors had weak or no fluorescence emission before the coordination. However, the intensity of fluorescence emission would increase rapidly after the coordination of receptor and guest.

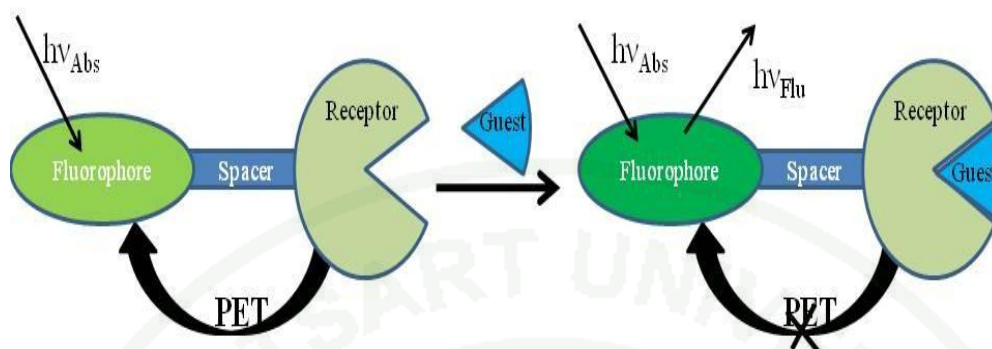


Figure 7 The general view of the principle of PET fluorescence molecular sensor.

Source: Li *et al.* (2011)

6.2 Photoinduced charge transfer (PCT)

Photoinduced charge transfer (PCT) contrasts with PET system, a fluorophore containing electron-donating group (often an amino group) conjugated to an electron-withdrawing group undergoes intramolecular charge transfer from the donor to acceptor upon excitation by light. The consequently change in dipole moment results in a Stoke shift that depends on the environment of fluorophore. It can, therefore, be anticipated that cation in close interaction with donor or acceptor will change the photophysical properties of the fluorophore because of the change in PCT system caused from the occurred complex.

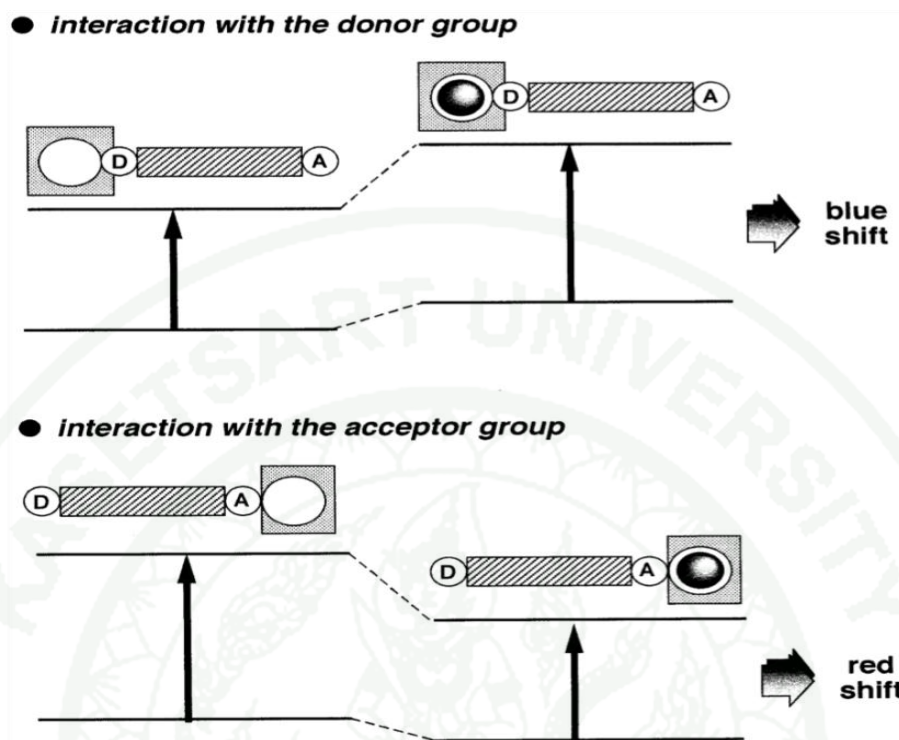


Figure 8 Interaction of a bound cation with an electron-donating or electron withdrawing group.

Source: Valeur *et al.* (2000)

From the Figure 8, when a group (like an amino group) playing the role of an electron donor within fluorophore interacts with cation, the latter reduces the electron donating character of this group, owing to the resulting reduction of conjugation, a blue shift of absorption spectrum and the decrease of the excitation coefficient are expected. Conversely, a cation interacting with acceptor group enhances the electron withdrawing character of this group. The absorption spectrum is thus red shift and the molar absorption coefficient is increased. The fluorescence spectra are in principle shifted in the same way as those of the absorption spectra.

The photophysical changes upon cation binding can also explain in term of dipole interaction change. Considering only the case where the dipole moment in the excited state is larger than that in the ground state, when the cation interacts with the

donor group, the excited state is more strongly destabilized by the cation. On the other hand, when the cation interacts with the acceptor group, the excited state is more stabilized more than ground state. The latter of these two cases lead to a blue shift and red shift respectively.

6.3 Excimer

When the two fluorophores are in the proper distance, an intermolecular excimer can be formed between the excited state and ground state. The fluorescence emission of the excimer is different with the monomer and mainly in the form of new, broad, strong, and long wavelength emission without fine structures. The proper distance determines the formation of excimer, therefore modulation of the distance between the two fluorophores becomes crucial in the design of the sensors based on this mechanism. The fluorophores have long lifetime in the singlet state to be easily forming the excimers. They are often used in such sensors (Li *et al.*, 2011).

6.4 Fluorescence resonance energy transfer (FRET)

FRET is a popular principle in the design of the fluorescence molecular sensor. In one system, there are two different fluorophores, in which one acts as a donor of excited state energy to the receptor of the other. As shown in Figure 9, the receptor accepts the energy from the excited state of the donor and gives the fluorescence emission, while the donor will return back to the electronic ground state. There are three factors affecting the performance of FRET. They are the distance between the donor and the acceptor, the proper orientation between the donor emission dipole moment and acceptor absorption moment, and the extent of spectral overlap between the donor emission and acceptor absorption spectrum (Figure 10).

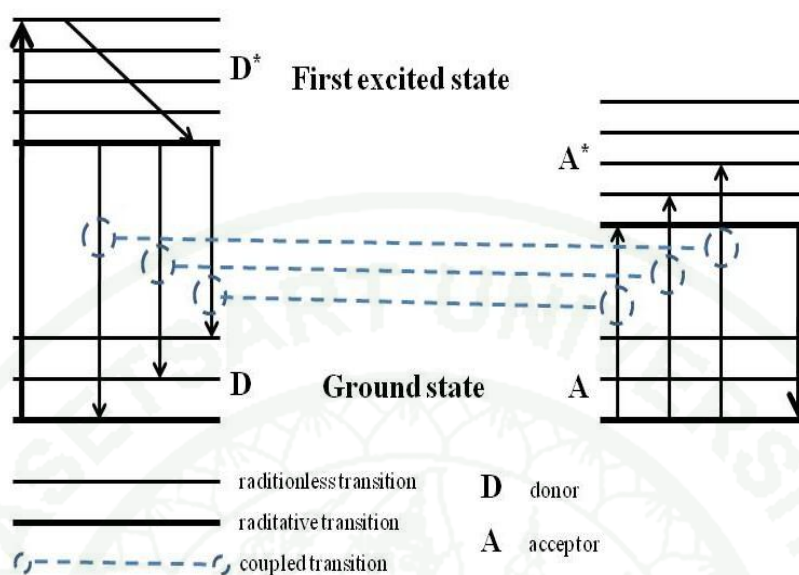


Figure 9 A schematic fluorescence resonance energy transfer system.

Source: Li *et al.* (2011)

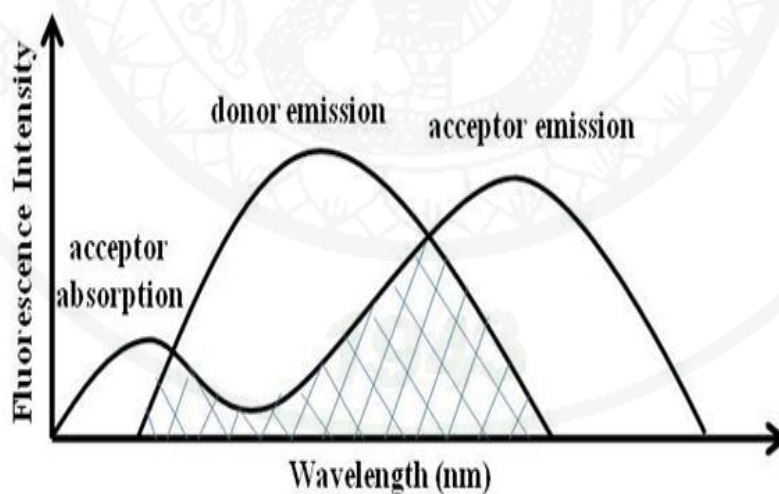


Figure 10 Diagram showing the spectral overlap for fluorescence resonance energy transfer system.

Source: Li *et al.* (2011)

7. Porphyrin

7.1 Structure and properties of porphyrin

The structure of porphyrin was first suggested in 1912 by Küster, at that time it was thought that such a large ring would be unstable, and the structure was not commonly accepted until many years later. It was eventually proved by the total synthesis of haemin in 1929 by Fischer and Zeile (Falk, 1964).

The porphyrins are derived formally from porphin by substitution of some or all of hydrogen atom by various side-chains. The studies of infrared spectroscopy have supplied strong evidence that the NH groups of porphyrins are occupied in intramolecular hydrogen bonding. Furthermore, the infrared data and calculations of orbital overlap have led to the conclusion that the most stable form of porphin and porphyrins are those in which the two hydrogen atoms are attached to the opposite nitrogens and hydrogen-bonded to the neighboring hydrogen (Figure 11). In addition, the porphin macrocycle is highly conjugated, and a number of resonance forms can be written; the porphyrins and their derivatives are intensely colored; their main absorption bands have very high molar extinction coefficients in the order of 2×10^5 (Falk, 1964).

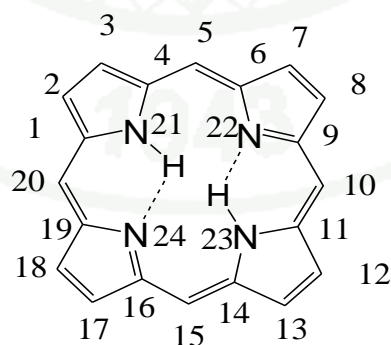


Figure 11 Molecular structure of porphin which showed a position of each atom and hydrogen bonding.

Source: Moss (1988)

The 1-24 numbering system upon which the numbering system for corrinoids is based is adopted for the porphyrin nucleus and is shown in Figure 11. The 2,3,7,8,12,13,17 and 18 positions have commonly been referred to generically as *beta*-positions (i.e. of the pyrrole rings). Similarly, positions at 1,4,6,9,11,14,16 and 19 have been referred to generically as *alpha*-positions, while those at 5,10,15 and 20 are referred to generically as *meso*-positions. However, in order to avoid possible ambiguity with stereochemical designations the use of these generic terms is discouraged (Moss, 1988).

The porphyrin macrocycle is an aromatic system which contains 22 π electrons, but only 18 electrons of them are involved in a delocalization pathway. Porphyrin, therefore, obeys Huchel's rule of aromaticity ($4n+2 \pi$ electrons, $n = 4$) (Wade L.G., 1999). The aromatic character can also be confirmed by NMR spectroscopy. Due to the anisotropic effect from the porphyrin ring current, the NMR signals for the deshielded meso protons appear at low field (8 to 10 ppm), whereas the signals for the shielded protons (on the inner nitrogen atoms) appear at very high field (-2 to -4 ppm) (Engelen, 2006).

The porphyrin ring is very stable to concentrated acid, for example, sulphuric acid. It can also function both as acid and base. The two protons in the inner nitrogen atoms of porphyrin can be removed by strong base such as alkoxides whereas acids such as trifluoroacetic acid can give protons to the two free pyrrolic nitrogen atoms easily. Moreover, porphyrin can undergo a number of chemical reactions typical of aromatic compounds. For example, electrophilic substitution reactions are often performed on porphyrin molecules which are mainly occurred on the *meso*-carbons and the β -pyrrolic carbons. In addition, certain substituents on porphyrin molecule can be modified and lead to the variety moieties of the different porphyrins.

7.2 Porphyrin in biological processes

Porphyrin system is present in well-known biological material, such as heme b, chlorophyll and vitamin B₁₂ due to the knowledge of chemistry of the porphyrins which has been accumulated since the first third of the twentieth century. Porphyrins and their derivatives are importance model compounds of great biological and technological significance in different field of sciences owing to their attractive potential, for example, high absorption coefficient at 400-450 nm, tunable fluorescence emission with a concomitant modification of molecular structure, large Stokes shifts etc. They are used as photosensitizer in photodynamic therapy (PDT) of tumor, molecular-based multi-bit memory storage, electron-donor parts in artificial photosynthetic models and also application in determination of metal ion in solution (Ostrowski, 2004).

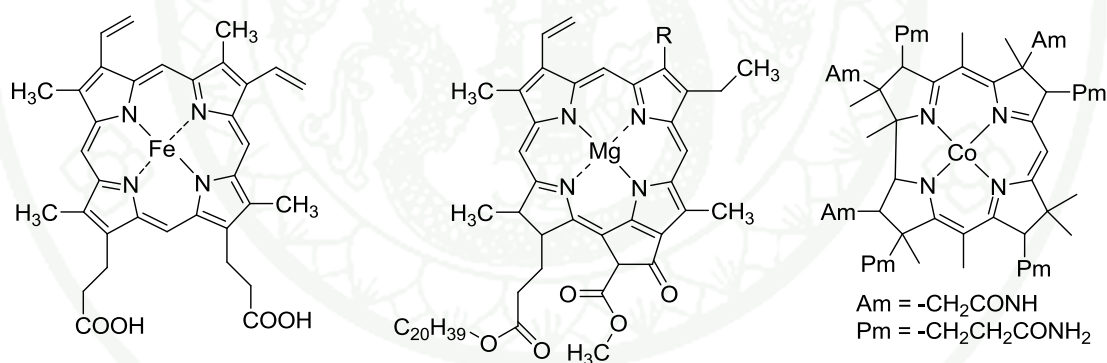


Figure 12 Structure of heme b, chlorophyll and vitamin B₁₂.

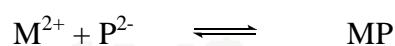
7.3 Metalloporphyrins

Metalloporphyrins are in the form of metal complexes. They exert their most important in biological activities such as iron complexes in heamoprotein, magnesium complexes in chlorophyll and cobalts complexes in vitamin B₁₂. There are widely studies on complexes of many metals, with many porphyrins as a basis

for understanding biosynthetic formations and biological activities of them.

The porphyrin nucleus is a tetradentate ligand, in which the space availability for a coordinated metal has a maximum diameter for approximately 3.7 Å (Falk, 1964). Upon coordination, two protons on the pyrrolic nitrogen atoms are lost, leaving two negative charges distributed equally about the whole inner ring. Almost metal ions form 1:1 complexes with porphyrin, only Na⁺, K⁺ and Li⁺ are known to form 2:1 complexes which the metal cation sits slightly above, and another slightly below the plane of porphyrin ring. The geometry of the porphyrin-metal complexes and the presence or not of additional ligands depends on the metal ion. For example, when Cu²⁺ and Ni²⁺ are incorporating into porphyrin ring, they display a tetra coordinate square planar complexes and show a low affinity for additional ligands forming. Nevertheless, complexes of Mg²⁺, Cd²⁺ and Zn²⁺ readily combine with outer ligand which is often corresponding to a solvent molecule to form a square based pyramidal structure, due to the large size of metal ion to fit into porphyrin hole perfectly. They are, therefore, positioned slightly out of their equatorial plane. Furthermore, porphyrin complexes of Fe²⁺, Co²⁺ or Mn²⁺ can form distorted octahedral structures with two extra ligands.

The stability constant (K_s) for a metalloporphyrin may be represented by the general expression:



$$K_s = [MP] / [M^{2+}][P^{2-}]$$

Where MP, M²⁺ and P²⁻ are the activity of the complex, the metal ions and the dianionic porphyrin species respectively (Falk, 1964).

7.4 Spectra of porphyrins

7.4.1 Absorption spectra

The absorption spectra of highly conjugated porphyrins show an intense absorption band about 400 nm which was firstly discovered in haemoglobin by Soret 1983 and was observed in porphyrins by Gamgee in 1987 (Falk, 1964). This band (usually called Soret band) is the most intense absorption band (excitation coefficient $> 10^5$) in the porphyrins and their compounds. Soret band does not have in porphyrinogen because the conjugation around the macrocyclic porphyrin is interrupted. However, porphyrin complexes which the conjugation around macrocycle is interrupted can present the Soret band because the conjugation pathway is maintained through the metal atom. Moreover, there are several weaker absorption bands following the Soret band called Q bands or β - α bands. These bands correspond to the lowest π - π^* transition and to the vibronic envelope. Variation of the peripheral substituents on the porphyrin ring can be changed in the intensity and wavelength of the absorption by certain substituents.

Upon the formation of metalloporphyrin, two pyrrolic nitrogen atoms are lost. As a result, the absorption spectrum of metalloporphyrin usually displays only two bands in Q bands, whereas porphyrin ligands have four bands in Q bands. The Soret band can remain at its original position or shift to higher or lower energy. Furthermore, the insertion of metal into porphyrin ring may cause new bands.

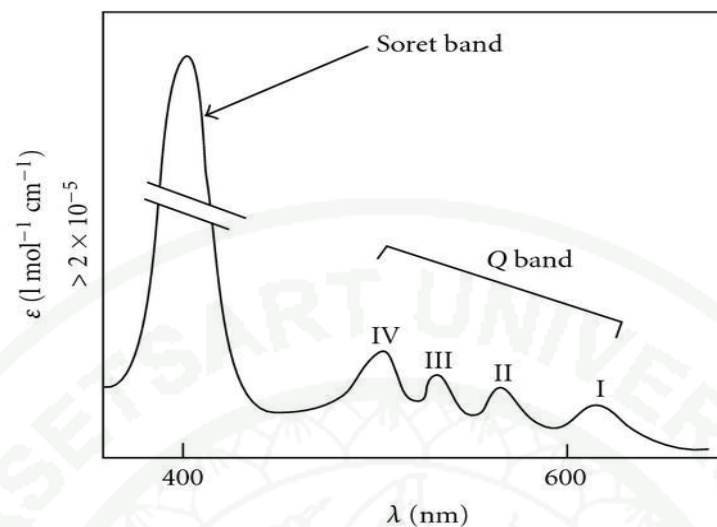


Figure 13 Typical UV-VIS absorption spectrum of porphyrins.

Source: Engelen (2006)

7.4.2 Fluorescence spectra

The fluorescence of porphyrins when irradiated with ultraviolet light provides a very sensitive method for their detection and determination. However, porphyrins do not fluoresce when colloiddally dispersed in aqueous media, and do not usually fluoresce in the solid state, though the fluorescence can be observed when porphyrins are adsorbed on talc, alumina or cellulose, in the bones and marrow cells of porphyric subjects. The fluorescence is best observed in dilute HCl solutions, but high concentrations of HCl and of NaCl and other salts can cause quenching of the fluorescence. Thus when fluorimetry is used for quantitative determinations, the procedure must be carefully standardized. An unusual case has been found in which a porphyrin-protein complex fluoresced in alkaline, but not in acid condition. The Zn complexes of bile pigments fluoresce, the color being much more orange than usually found with porphyrins. Free bile pigments do not fluoresce, but fluorescence is found in the algal chromoproteins, phycocyanin and phycoerythrin, in which the bile-pigment prosthetic groups are covalently bound to

protein. The intensity of fluorescence varies with pH, and is greatly influenced by impurities, even by inorganic ions.

7.5 Application of porphyrins

There are many applications of porphyrin molecules, such as interaction with DNA, supra molecular assembly, using as a template in de novo design and molecular recognition (Engelen, 2006). In this thesis, only application of porphyrin as sensor for molecular recognition is focused.

Molecular recognition is a key element in current research area, including drug design and synthesis, molecular catalysis, development of biomaterial and analytical sensors. A striking feature of these processes is the high selectivity between host and guest molecules. Porphyrins are such very attractive molecules as potential sensors, due to the binding of an analyte (metal) to a porphyrin center usually results in a detectable optical change, thus allowing a rapid synthesis. In addition, the introduction of polar groups on the hydrophobic surface of the porphyrin allows a use of porphyrin receptors in organic media as well as aqueous media. One of the researches in this area has been focused on synthetic porphyrins and metalloporphyrins for use as solution and as phase sensing. Considering the well-understood ability of heme to bind a variety of gases, for example NO CO₂ and O₂, porphyrins are suitable choice for the detection of gaseous species. Other application of porphyrins is the use of porphyrins as chemical sensors for recognition of metal ions. Besides this application, the recognition of small biomolecules such as amino acid, oligopeptides, nucleotides and other small organic compounds is also studied as well.

8. Complexation and stability constant

The complex formation between TBTPP and TNPP with Hg²⁺ are determined by using mole ratiometric for studying the ratio between TBTPP and TNPP with Hg²⁺ complexes. To predict the molecular geometry of the complex,

the quantum chemical calculation is used to calculate the energies of complexes formation between Hg^{2+} with TBTPP and TNPP. The determination of stability constants were performed by Benesi-Hildebrand equation (Benesi, 1949).

The determination of equilibrium constant, K , the Benesi-Hildebrand equation was applied from equilibrium reaction of complex.



The equilibrium constant for the above reaction is defined by the equation

$$K = \frac{[\text{ML}]}{([\text{M}] - [\text{ML}])([\text{L}] - [\text{ML}])} \quad \text{----- (2)}$$

Where $[\text{ML}]$ is molar concentration of the complex, $[\text{M}] - [\text{ML}]$ is molar concentration of free metal ion and $[\text{L}] - [\text{ML}]$ is molar concentration of free ligand. From Beer's law, the true molar extinction coefficient, ϵ_0 , of the complex at the wavelength of maximum absorption will then be given by the equation

$$\epsilon_0 = \frac{A}{cb} = \frac{A}{[\text{ML}]b}$$

$$[\text{ML}] = \frac{A}{\epsilon_0 b} \quad \text{----- (3)}$$

In this reaction, ligand is added in excess. Therefore, $[\text{L}]$ is much more than $[\text{ML}]$. The $[\text{ML}]$ can be eliminated and the equation (2) can be rearranged and obtained as the relationship;

$$K = \frac{[\text{ML}]}{([\text{M}] - [\text{ML}])([\text{L}] - [\text{ML}])}$$

$$K = \frac{A/\varepsilon_0 b}{([M]-A/\varepsilon_0 b)[L]}$$

$$K = \frac{A}{\varepsilon_0 b[M][L]-[L]A}$$

$$A = K\varepsilon_0 b[M][L] - K[L]A$$

$$K\varepsilon_0 b[M][L] = A + K[L]A$$

$$K\varepsilon_0 b[M][L] = A(1 + K[L])$$

$$\frac{[M]b}{A} = \frac{1}{K\varepsilon[L]} + \frac{1}{\varepsilon_0} \quad \text{-----(4)}$$

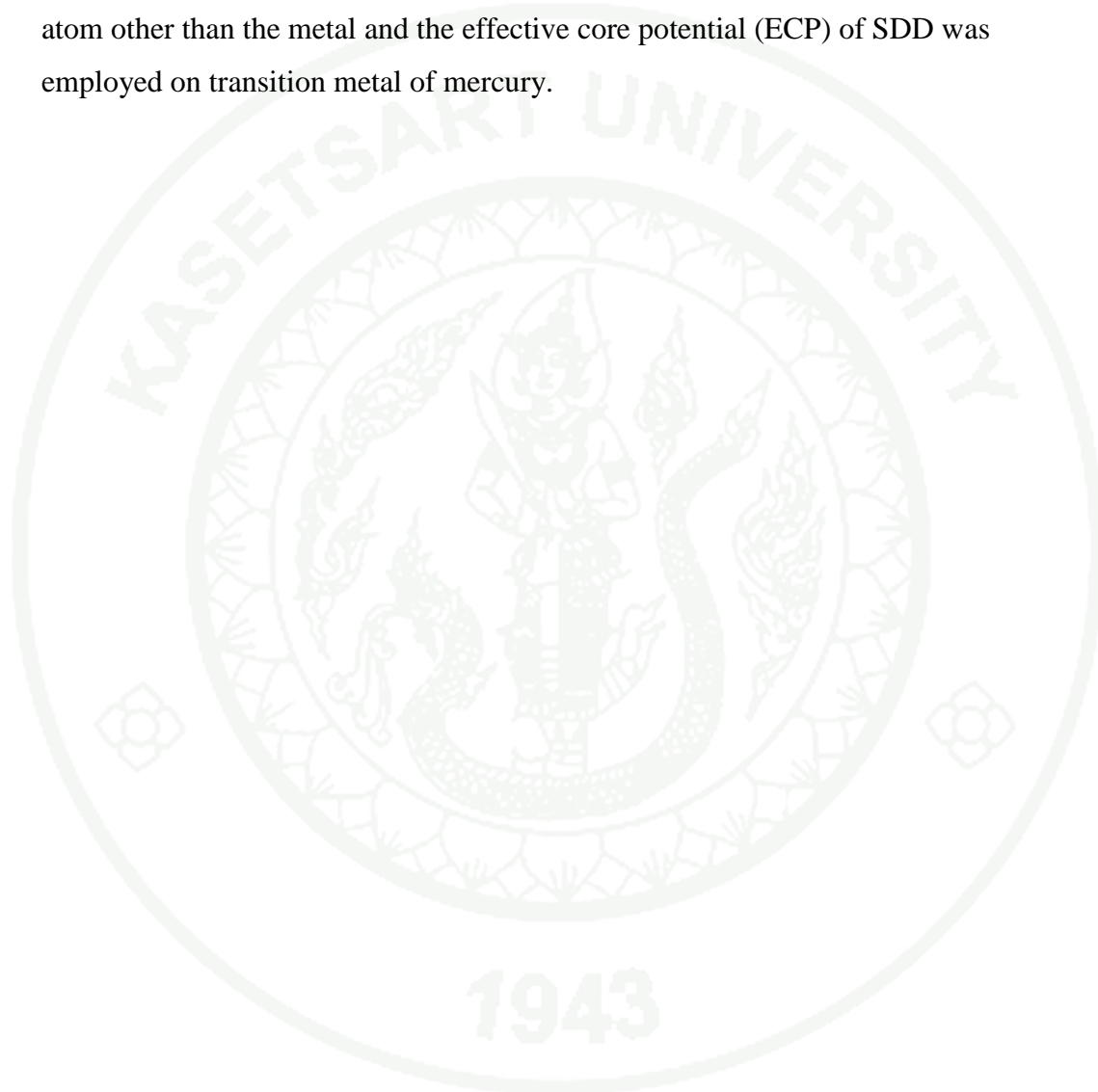
The equation (4) is “Benesi-Hildebrand equation” which is in the form of the linear equation, $y = mx + c$.

For the experiment, the concentration of Hg^{2+} is fixed while the concentrations of ligand are varied. The relationship between $[M]/A$ and $1/[L]$ are plotted, the equilibrium constant is obtained from the slope.

9. Quantum chemical calculation

Computational calculation has a potential role in the molecular modeling development. Molecular structure can be created in the virtual model on computer by bonding the elements into 3-dimension structure. The thermodynamic parameters and some physical properties can be calculated.

The study of molecular structure of complex between Hg^{2+} and porphyrins were investigated. Therefore, the stabilization energy of the complex was theoretically calculated to predict the possible structure by using the Density Functional Theory (DFT) at B3LYP level of theory using 6-31 G* basis set for each atom other than the metal and the effective core potential (ECP) of SDD was employed on transition metal of mercury.



OBJECTIVES

There are three main objectives that this work focuses on;

1. To synthesize and characterize 5,10,15,20-Tetra(*p*-bromophenyl)porphyrin and 5,10,15,20-Tetra(*p*-nitrophenyl)porphyrin to use as fluorescent sensor
2. To study the optimum conditions, parameters and the fluorescent sensing properties of prepared porphyrins for sensing Hg^{2+} .
3. To study interactions between porphyrins and Hg^{2+} by using computational method.

LITERATURE REVIEW

This section mentioned a review of works done by some previous researchers on the preparation of 5,10,15,20-Tetra(*p*-bromophenyl)porphyrin and 5,10,15,20-Tetra(*p*-nitrophenyl)porphyrin. The studies on fluorescent sensing properties for the porphyrins derivatives are also reviewed.

1. Synthesis of porphyrin derivatives.

The porphyrin derivatives are presented in well-known biological materials. They are widely diffused in nature and play various important roles in biological processes. In addition the porphyrin derivatives have been widely used in biochemistry applications for years. These reviews have been focused on synthesis, characterization and some applications of the porphyrin derivatives.

Rothmund (1936) synthesized porphyrin and five *meso*-substituted porphyrin in which pyrrole was used as a component and reacted with aldehydic functions, which were formaldehyde, acetaldehyde, propionaldehyde, *n*-butyl aldehyde, benzaldehyde and α -furaldehyde. All synthesized porphyrins were characterized by spectrochemical techniques. In this report, it described the fundamental structure of the physiologically pigment from pyrrole and formaldehyde in detail as example of the reaction.

Alder *et al.* (1967) synthesized *meso*-tetraphenylporphyrin by the condensation of pyrrole and benzaldehyde. The experiment was performed by refluxing benzaldehyde and freshly distilled pyrrole in the propionic acid. After refluxing, the solution was treated by methanol and hot water. The purple crystal of *meso*-tetraphenylporphyrin was obtained from this procedure. Combustion analysis and electronic absorption spectrum of the solution *meso*-tetraphenylporphyrin gave a good agreement with the theoretical calculation.

Kim *et al.* (1971) synthesized 11 new derivatives of *meso*-tetraphenylporphin which are substituted on the phenyl groups. For the preparation of 11 new derivatives of *meso*-tetraphenylporphin, they were synthesized by refluxing between the substituted benzaldehyde with pyrrole in propionic acid by the Rothmund reaction and characterized by ^1H NMR and ESI-MS spectroscopy. Moreover, the researcher studied the rate of porphyrin formation and of oxygen consumption lead them to conclude that oxygen oxidation is the rate –determining step under ordinary synthetic conditions. In addition, the researchers have also determined the extinction coefficients and the relative fluorescence intensities of these compounds.

Quimby and Longo (1974) synthesized several tetraarylporphins and their zinc derivatives. All the substituted tetraphenylporphins were prepared by refluxing between the substituted benzaldehyde with pyrrole in propionic acid by the Rothmund reaction and characterized by ^1H NMR and ESI-MS spectroscopy. Moreover, the Zn derivatives were prepared by reaction of the free base porphyrin and a fourfold molar excess of ZnCl_2 . In addition, the researchers determined the fluorescence spectra and quantum yields of the free base tetraarylporphins and their Zn derivatives in benzene. These porphins were substituted on positions 2, 3 and 4 of the phenyl rings. The heavy atom halogen substituents were found to quench fluorescence, especially when substituted at the 2-phenyl position. The quenching of the fluorescence was interpreted in term of a heavy atom induced increase in intersystem crossing from singlet to triplet state. The absorption and fluorescence (0-0) band intensities of the Zn derivatives were found to be reduced by the presence of an ortho substituent. A similar ortho substituent effect has previously been observed for base tetraphenylporphins. Moreover, the researchers have identified a weak emission from the Zn tetraarylporphins at 560 nm as a fluorescence hot band. The phosphorescence spectra and relative quantum yields of phosphorescence were also determined for a number of the Zn derivatives in methylcyclohexane - isopentane glass at 77 °K. Phosphorescent emission could not be detected from the free base tetraarylporphins.

Lindsey *et al.* (1987) presented a synthetic strategy for preparing *meso*-tetraphenylporphyrin and its derivatives. The porphyrins were prepared by the reaction of pyrrole and desired benzaldehyde at room temperature using acid catalyzed in order to form cyclic tetraphenylporphyrinogen. An oxidant was then added to convert the porphyrinogen to porphyrin (Figure 14). This methodology was compared with Alder-Longo reaction (Alder *et al.*, 1967). It was found that the presented methodology was complementary to the Alder-Longo procedure, allowing small quantities of porphyrins to be prepared from sensitive aldehyde in 30-40% yield without difficult purification problem. This methodology was also extended to the preparation of *meso*- tetraalkylporphyrins and one hybrid porphyrins containing both aryl and alkyl substituents.

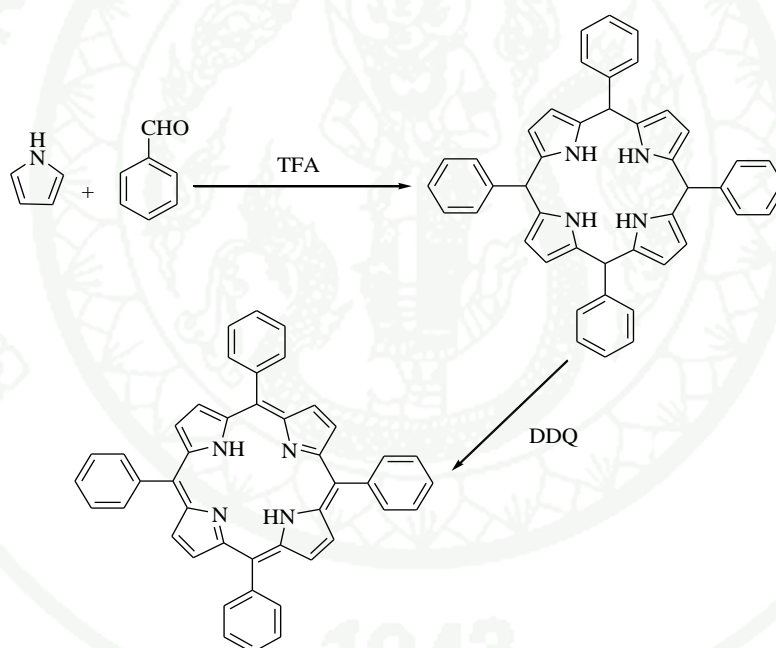


Figure 14 Reaction scheme of *meso*-tetraphenylporphyrin synthesis by Lindsey *et al.*, (1987).

Kruper (1989) developed an attractive synthesis of mono-(nitrophenyl)-triphenyl porphyrin by reaction of tetraphenylporphyrin (TPP) in chloroform with excess fuming nitric acid. The selective and stepwise nitration of the aryl group at the *p*-position was found to occur. Fuming nitric acid of two different densities was examined in the nitration of tetraphenylporphyrin and no different was noted in

required stoichiometry to achieve mononitration. The researchers summarized that their developed method was found to be controllable and highly regiospecific.

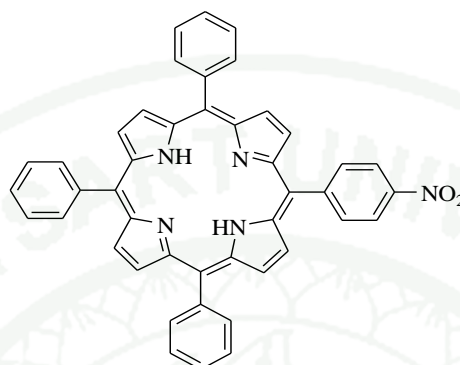


Figure 15 Mono(nitrophenyl)triphenyl porphyrin.

Chatterjee *et al.* (1997) synthesis *meso*-Tetrakis[4-(carboxymethyleneoxy)phenyl]porphyrin (H_2T4CPP). It was prepared by refluxing of 4-hydroxybenzaldehyde and ethyl chloroacetate in dry acetone in presence of K_2CO_3 for 8 hours to obtain 4-carboethoxymethyleneoxybenzaldehyde. Subsequent refluxing of 4-carboethoxymethyleneoxybenzaldehyde and pyrrole in propionic acid-nitrobenzene for 1 hour yielded the ester of the free base porphyrin and it was characterized by UV-Vis and 1H -NMR spectroscopy. For the application of H_2T4CPP , it could cleave Pbr322 plasmid DNA to single strand broken in the presence of molecular oxygen and visible light. The above photocleavage was much efficient in D_2O buffer than H_2O buffer. In addition, this photocleavag of plasmid DNA was inhibited in the presence of sodium azide, lipoic acid, tert-butanol or mannitol suggesting the involvement of 1O_2 and $\cdot OH$ in the photocleavage of plasmid DNA. The photocleavage was observed to be more efficient in the presence of H_2T4CPP than in the presence of H_2CPP [*meso*-Tetrakis[4-(carboxyphenyl)porphyrin]. The researchers studied spectrum of porphyrin derivatives by using UV-visible, fluorescence and circular dichroism techniques suggest that H_2T4CPP binded to DNA while H_2CPP did not. Thus, the difference in

photocleavage may be caused by the nonbinding of H₂CPP and by the binding of H₂T4CPP to calf thymus (CT) DNA.

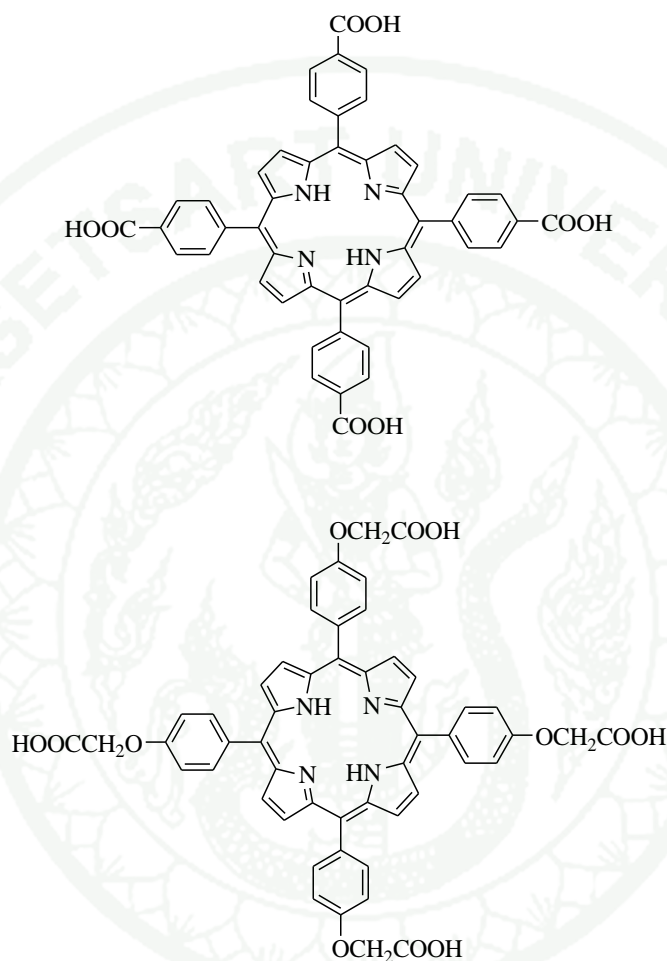


Figure 16 The structure of *meso*-Tetrakis[4-(carboxy-phenyl)porphyrin] (H₂CPP) and *meso*-Tetrakis[4-(carboxymethyleneoxy)phenyl]porphyrin (H₂T4CPP).

Shi and Wheelhouse (2002) studied the synthesis of *meso*-substituted porphyrin. They used a direct substitution of 5,10,15,20-tetrabromoporphin magnesium complex by using aryl or hetero aryl boronic acid in the presence of Pd(PPh₃)₄ (Figure 17). Due to an aromatic character of porphyrin, the researchers could change bromo-substitution to aryl or hetero aryl group on the *meso*-position in yield up to 70%. The observation that the *meso* position of unsubstituted porphyrin **1** show

more aromatic than olefinic character in their reactions led them to investigate the direct substitution of porphine, **3**, could undergo a Suzuki cross-coupling reaction with arylboronic acids in the presence of a palladium(0) catalyst to yield 5,10,15,20-tetra aryl—or tetra heteroaryl—porphines, **4** (Figure 17).

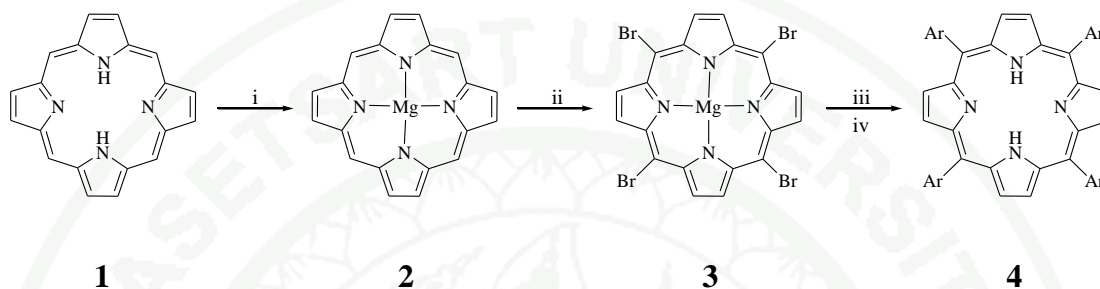


Figure 17 Synthetic scheme of Shi D. F. developed method.

i = $\text{MgBr}_2 \cdot \text{OEt}_2$, Et_3N , CH_2Cl_2 , 60°C

ii = CH_3CONHBr , CHCl_3 , 0°C

iii = $\text{ArB}(\text{OH})_2$, $\text{Pd}(\text{PPh}_3)_4$, Na_2CO_3 , PhCH_3 , MeOH , 70°C

iv = HCl

Luguya *et al.* (2004) improved the regioselective nitration of the phenyl group of *meso*-tetraphenylporphyrin. They used NaNO_2 and trifluoroacetic acid in reaction. The preparation was performed by adding an equivalent amount of NaNO_2 into *meso*-tetraphenylporphyrin to obtain nitroporphyrin 5-(4-nitroaryl)-10,15,20-triarylporphyrin, 5,10-bis(4-nitroaryl)-15,20-diarylporphyrin and 5,10,15-tris(4-nitroaryl)-20-arylporphyrin. Then, nitroporphyrins were reduced to the corresponding aminoporphyrin under SnCl_2/HCl condition (Figure 18a-18c). Reaction of tri-aminoporphyrin (Figure 18c) with 1-formyl-o-carborane followed by reduction using NaBH_4 gave novel tri-carboranylporphyrin (Figure 18d) bearing amine linkages between the porphyrin and the carborane groups.

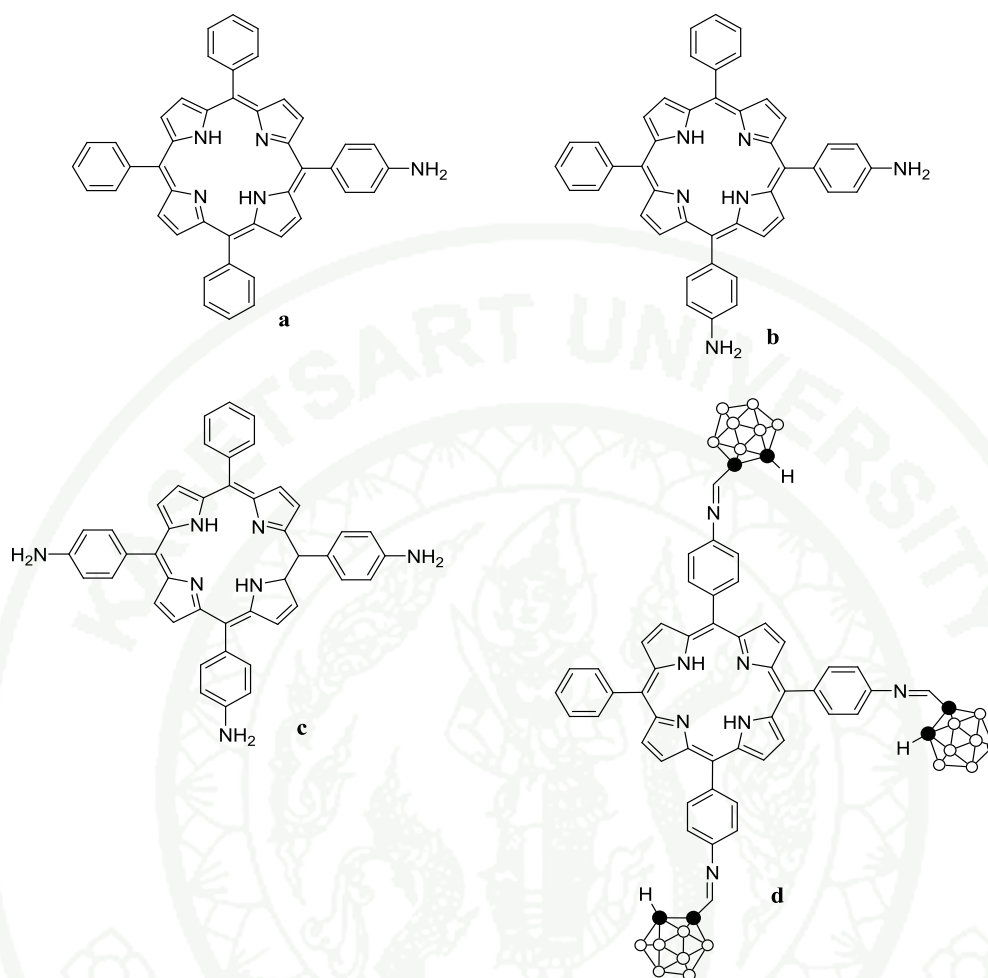


Figure 18 The structures of 5-(4-nitroaryl)-10,15,20-triarylporphyrin (**a**), 5,10-bis(4 nitroaryl)-15,20-diarylporphyrin (**b**), 5,10,15-tris(4-nitroaryl)-20-arylporphyrin (**c**) and tri-carboranylporphyrin (**d**).

Ostrowski *et al.* (2004) synthesized substituted *meso*-tetraphenylporphyrin by the reaction of *meso*-tetraphenylporphyrin (TPP) and its derivatives with fuming yellow nitric acid to form either 5-(4-nitroaryl)-10,15,20-triarylporphyrin, 5,10-bis(4-nitroaryl)-15,20-diarylporphyrin, or 5,10,15-tris(4-nitroaryl)-20-arylporphyrin (Figure 19). This reaction depended on reaction temperature (0-20 °C), amount of the acid used and reaction time. The above porphyrins were reacted with carbanion ($\text{CH}(\text{Cl})\text{SO}_2\text{Tol}$, $\text{CH}(\text{Br})\text{SO}_2\text{Tol}$ and $\text{CH}(\text{Cl})\text{SO}_2\text{NMe}_2$) in the presence of base (*t*-BuOK) to prepare highly substituted porphyrins. The synthesized porphyrins were

purified by column chromatography and determined by ^1H NMR, UV-Vis spectroscopy and mass spectrometry.

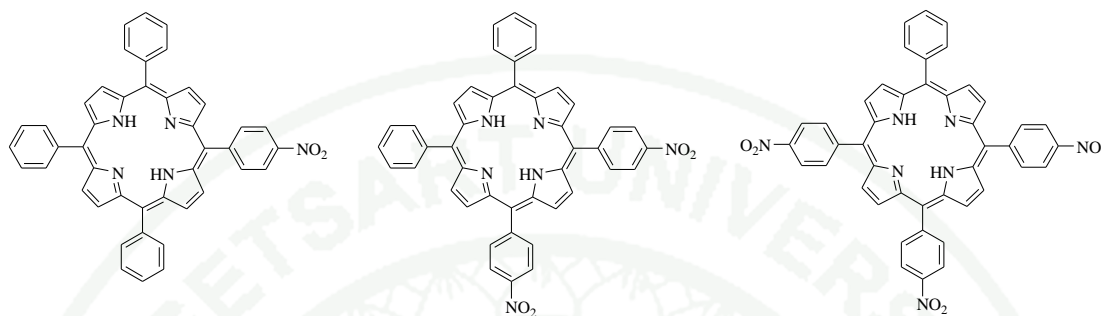


Figure 19 The structures of 5-(4-nitroaryl)-10,15,20-triarylporphyrin, 5,10-bis(4-nitroaryl)-15,20-diarylporphyrin, and 5,10,15-tris(4-nitroaryl)-20-arylporphyrin respectively.

Jaung *et al.* (2007) synthesized 5,10,15,20-Tetra[5-{2-(4-alkoxyphenyl)-ethenyl}-6-{2-phenyl-ethenyl}-2,3-dicyano-porphyrin (**20b**) by the condensation reaction of pyrrole and a bis-styryl derivative (**20a**) containing 2,3-dicyanopyrazine. The existence of a strong intramolecular charge-transfer chromophoric system was confirmed for dyes (**20b**), and its large Stokes shift of over 200 nm resulted in the emission of red fluorescence. The chromophoric systems of these dyes were studied from the viewpoint of the protonation and deprotonation effects on their absorption and fluorescence spectra in solution.

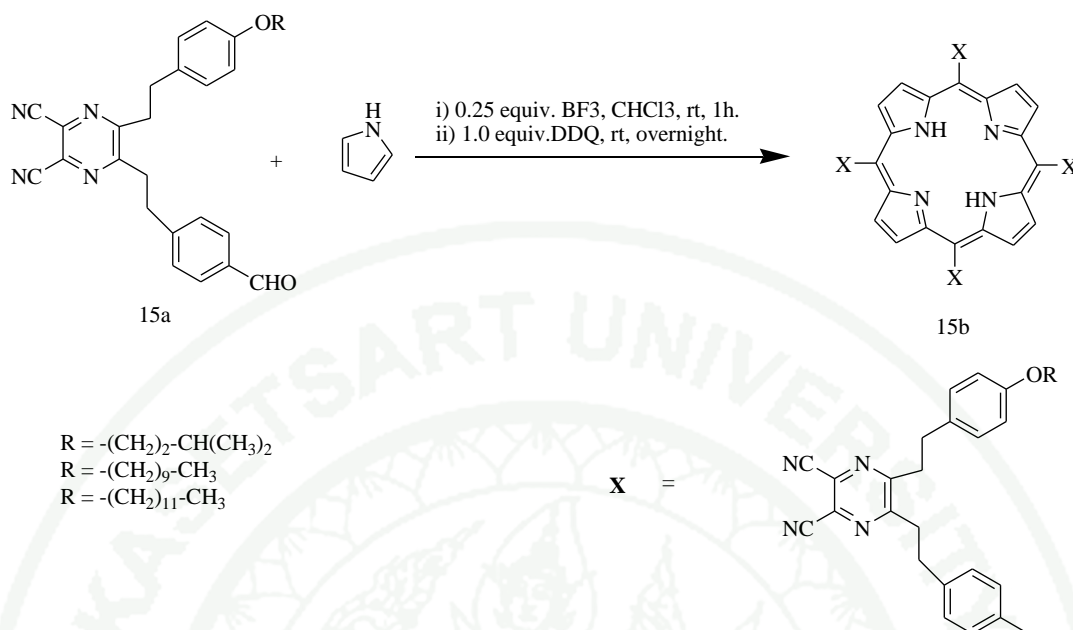


Figure 20 The synthesis of 5,10,15,20-Tetra[5-{2-(4-alkoxyphenyl)-ethenyl}-6-{2-phenyl-ethenyl}-2,3-dicyano-porphyrin.

Temelli *et al.* (2009) synthesized 5,10,15,20-tetraphenylporphyrin, it has been developed based on the reaction of 5-substituted dipyrrromethanes with N-tosyl imines in the presence of a metal triflate catalyst. *Meso*-substituted tetraphenyl porphyrins were synthesized in a two-step process (Figure 21). The first step of the method was the metal triflate-catalyzed condensation of 5-substituted dipyrrromethanes with N-tosyl imines to form a porphyrinogen intermediate and the second step was the oxidation of the porphyrinogen to porphyrin. The method was applied to the synthesis of trans-A₂B₂-tetraarylporphyrins (Figure 22) and the products were obtained with only a trace amount of one scrambling product. The synthesis of two important building blocks for porphyrin synthesis, mono and di-sulfonamide alkylated 5-substituted dipyrrromethanes to N-tosyl imine. Moreover, mono and di-sulfonamide alkylated 5-substituted dipyrrromethanes were applied in 2+2 porphyrin formation reactions.

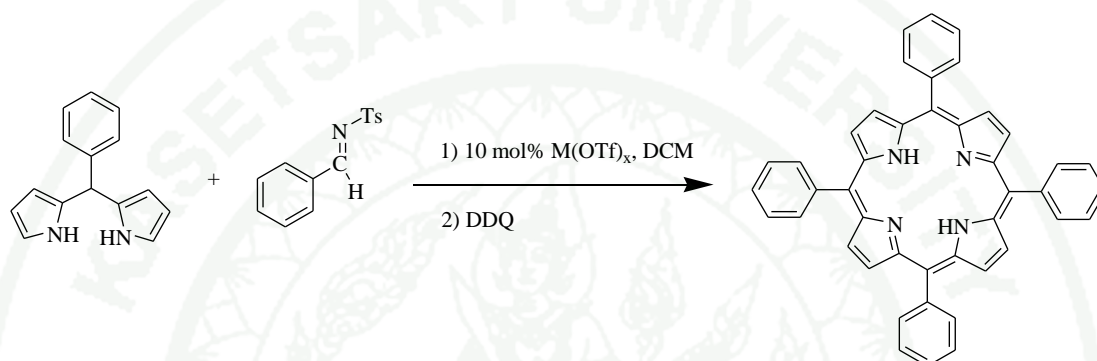
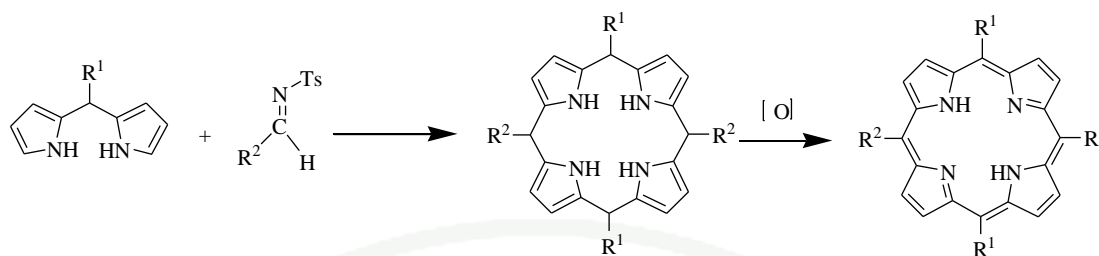
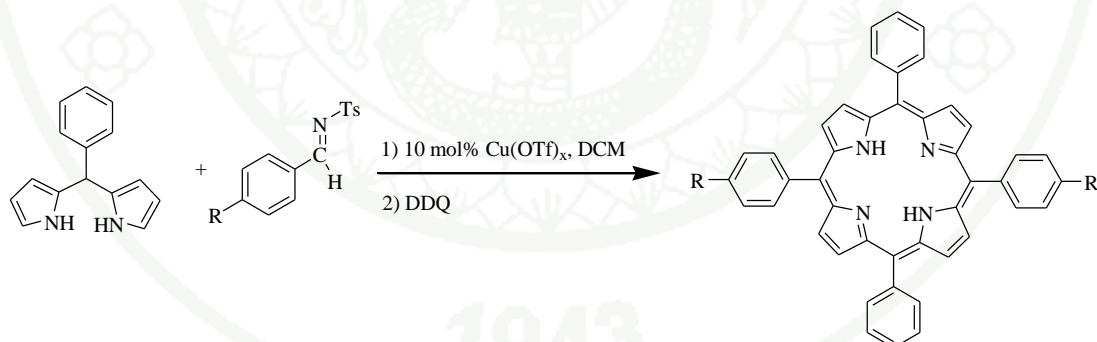


Figure 21 The synthesis of 5,10,15,20-tetraphenylporphyrin in two-step process.



R = OCH₃, CH₃, NO₂, Cl and Br

Figure 22 The synthesis of trans-A₂B₂-tetraarylporphyrins.

2. Using of porphyrin as fluorescent sensor

Recently, there are increasing interests in the development of fluorescent chemosensors for determining of many ions or compounds, for example metal cation, anion and oxygen gas, porphyrin derivatives are one of choices for using as

fluorescent chemosensor because of their high fluorescent quantum yields and large Stokes shifts. In this thesis, it focuses on using porphyrin derivatives such as 5,10,15,20-Tetra(*p*-bromophenyl)porphyrin and 5,10,15,20-Tetra(*p*-nitrophenyl)porphyrin as chemosensor.

Plaschke *et al.* (1995) studied the fluorimetric determination of mercury ions with 5,10,15,20-tetra(*p*-sulfonatophenyl)porphyrin (TPPS) in aqueous solutions and in porphyrin doped sol-gel films. Moreover, optimization of complexation conditions such as buffer components, pH range and temperature resulted in a method which enabled the determination of mercury ions in aqueous solutions within 15 minutes with a detection limit of 1.4 $\mu\text{g}/1 \text{ Hg(II)}$. In addition, the main interfering ions were found to be Cd, Zn and Pb. The researchers developed an optochemical sensing device the porphyrin derivatives was immobilized in sol-gel thin films (thickness of about 600 nm) and studied the properties of sensor. The kind of catalyst used (acid or base) was found to influence the stability and sensitivity. Moreover, sensing films prepared with acid were stable and insensitive to mercury. Preparation of the films with alkaline catalysis resulted in mercury sensitive layers with a limited stability. Stability could be improved by covalent binding of the reagent dye.

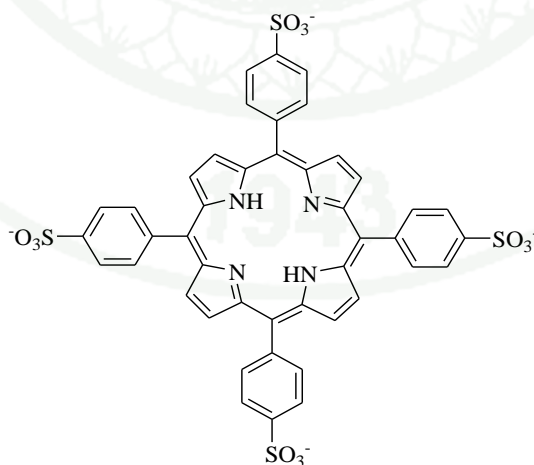


Figure 23 The structure of compound 5, 10, 15, 20-tetra(*p*-sulfonatophenyl)porphyrin (TPPS).

Lee *et al.* (2001) synthesized the porphyrin derivatives (Figure 24a-24d) with H-bond donors and color-reporting chromophoric unit, their application as anion-binding receptors. **24a** and **24b** exhibited binding selectivity in the order of $\text{AcO}^- > \text{H}_2\text{SO}_4^- \gg \text{Cl}^- > \text{Br}^- > \text{I}^-$ in DMSO-d_6 . Moreover, the porphyrin derivatives (Figure 17c-17d) were studied about colorimetric anion sensors, the color change tests with several different anions resulted in selectivities for F^- , AcO^- and H_2SO_4^- in organic solution. While **24c** and **24d** exhibited good selectivities for AcO^- and H_2SO_4^- , **24c** and **24d** showed a dramatic color change for F^- due to increased interaction with a nitrophenylazo phenolic OH group.

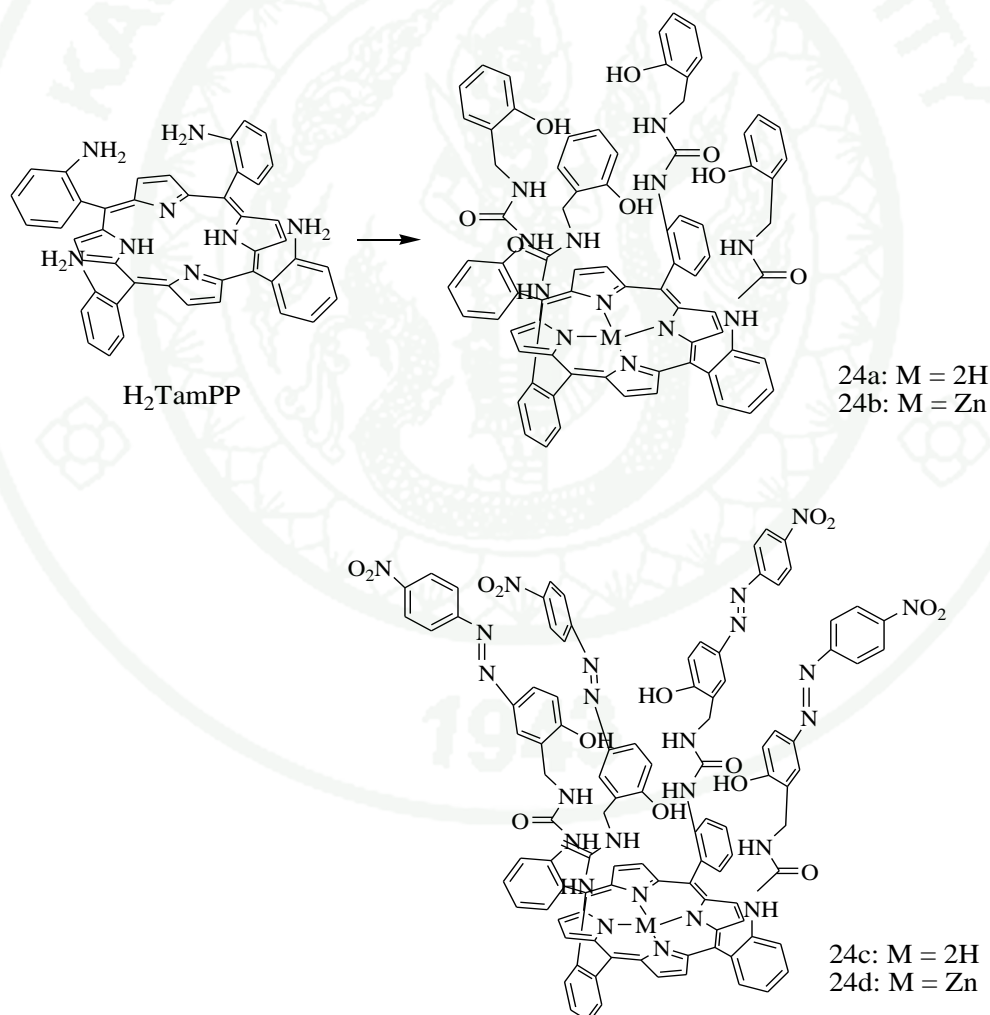


Figure 24 The structure of the porphyrin derivatives (**24a-24d**).

Starnes (2002) synthesized a disulfonamide appended porphyrin receptor (**25a**) for anionic guests such as F^- , $H_2SO_4^-$, $CH_3CO_2^-$, Cl^- , HSO_4^- , Br^- and I^- . The distinct attribute of the receptor, compared to other porphyrin based receptors, centers on the attachment of the anion binding site to the porphyrin chromophore's β -positions through a polycyclic conjugated linkage. Moreover, the strength of the binding between anions with (**25a**) have been determined by UV-Vis and 1H NMR spectroscopy, resulting the selectivity of the binding between anions with (**25a**) was in the order of $F^- > H_2SO_4^- > CH_3CO_2^- > Cl^- > HSO_4^- > Br^- > I^-$.

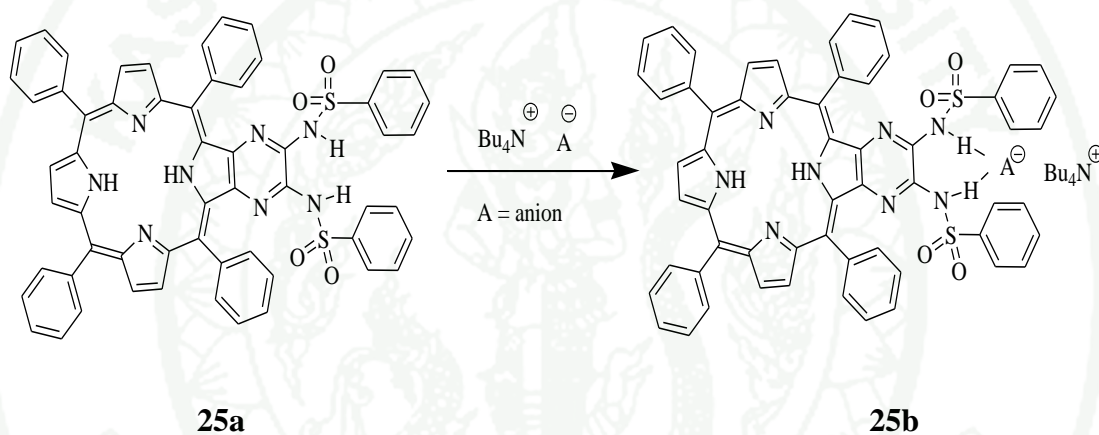


Figure 25 A disulfonamide appended porphyrin receptor (**25a**) and its anion complex (**25b**).

Itagaki *et al.* (2005) studied the detection of toxic gases such as HCl, NO_2 and SO_2 by the porphyrin dyes in ethylcellulose (EC) matrix. Toxic gases were examined using a photo-reflection spectrum technique. The intensity of the characteristic solet- band and Q-bands of the porphyrins sensitively changed with the concentration of the gasses. Introducing electron-donating— OCH_3 and —OH groups to the phenyl-group in the tetraphenylporphyrin (TPPH₂) molecule enhanced the sensitivity and that was in the order of $TP(4-OH)_4PH_2 > TP(3,5-OCH_3)_4PH_2 > TPPH_2$ to HCl. In contrast, electron-withdrawing —COOH group decreased in the sensitivity. It was interpreted that the electron density at the pyrrole nitrogen increased with the electron-donating groups. Doping of dioctylphthalate (DOP) as

a plasticizer to the porphyrin-EC composites remarkably modified their sensitivity and response behavior. The sensitivity to NO₂ was extremely high and sub-ppm level of detection was possible for all the composites. In the case of SO₂, the sensitivity was lower than NO₂, but the composite of TP(4-OH)₄PH₂ exhibited enough sensitivity to detect the concentration of 0.5 ppm. The sensing performance was strongly dependent on the humidity.

Guo *et al.* (2006) prepared an optical sensor membrane for sensing of Hg²⁺ ion in aqueous solution by using meso-tetraphenylporphyrin (TPP) as an indicator. The membrane was fabricated by sol-gel process and added an appropriate amount of TPP to the sol and mixed it. The prepared sol-gel membrane was tested by spectrofluorometer. The fluorescence quenching of the sol-gel membrane by Hg²⁺ showed the linear response over the Hg²⁺ concentration range of 5.0×10⁻⁶ M to 1.0×10⁻⁴ M with a detection limit of 3.6×10⁻⁶ M the good stability, reversibility, long lifetime and short response time could be obtained.

Luo *et al.* (2007) synthesized porphyrin-appended terpyridine, 5-(4-([2,2':6',2'']-terpyridin-4-yl-carboxyamidyl)phenyl)-10,15,20-triphenylporphyrin (H₂TPPTPy) (Figure 26), as a fluorescent chemosensor for determination Cd²⁺ ion in aqueous solution. For the preparation of fluorophore, H₂TPPPy was synthesized by refluxing between 2,2':6',2'']-terpyridine-4'-carboxylic acid and 5-(4-aminophenyl)-10,15,20-triphenylporphyrin in DMF and characterized by ¹H NMR. H₂TPPPy showed chelation-enhanced fluorescence with Cd²⁺ via photoinduced electron transfer (PET) process. The analytical performance characteristic of Cd²⁺ sensitive chemosensor showed a linear response over the range of 3.2×10⁻⁶ M to 3.2×10⁻⁴ M with a detection limit of 1.2×10⁻⁶ M. The sensor could be used for determination of Cd²⁺ ion in water samples with satisfactory recoveries.

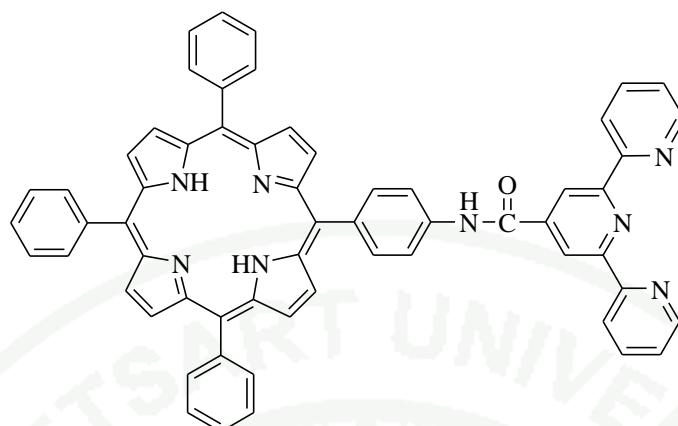


Figure 26 The structure of 5-(4-([2, 2':6', 2'']-terpyridin-4-ylcarboxamidyl)phenyl)-10,15,20-triphenylporphyrin ($H_2TPPTPy$).

Weng *et al.* (2007) synthesized 5-(*p*- N,N' -bis(2-pyridyl)amino)phenyl-10,15,20-tris(*p*-methoxyphenyl)porphyrin Zinc (Figure 27), as a fluorescent chemosensor for determination Cu^{2+} ion in aqueous solution. For the preparation of fluorophore, 5-(*p*- N,N' -bis(2-pyridyl)amino)phenyl-10,15,20-tris(*p*-methoxyphenyl)porphyrin Zinc was synthesized by refluxing between methoxyporphyrin zinc with 2,2'-dipyridylamine (dpa) under Cu-powder as catalyst and K_2CO_3 as base in DMF solution by the Ullmann-type condensation and characterized by 1H NMR and ESI-MS spectroscopy. 5-(*p*- N,N' -bis(2-pyridyl)amino)phenyl-10,15,20-tris(*p*-methoxyphenyl)porphyrin Zinc showed high selectivity for Cu^{2+} ion and exhibited fluorescence quenching upon binding of Cu^{2+} ion with an “on-off” type fluoroionophoric switching property and its fluorescence could be revived by addition of EDTA disodium solution.

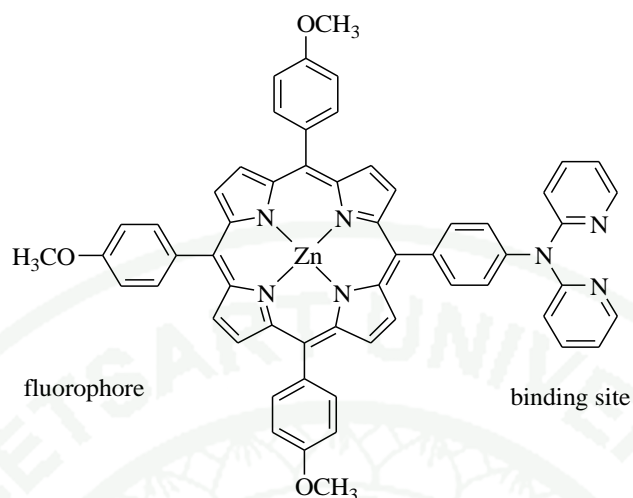


Figure 27 The structure of 5-(*p*-N,N'-bis(2-pyridyl)amino)phenyl-10,15,20-tris(*p*- methoxyphenyl)porphyrin Zinc.

Weng *et al.* (2007) designed and synthesized fluorescence sensor by the Ullmann-type condensation of bromoporphyrin zinc with 2,2'-dipyridylamine (dpa) under Cu-powder as catalyst and K_2CO_3 as base in DMF solution. This compound displayed the high selectivity for Cu^{2+} ion among the metal ions examined and showed fluorescence quenching upon binding of the Cu^{2+} ion with the fluorophore. Then, copper(II) fluorescent sensor 5,10,15,20-tetra(*p*-N,N-bis(2-pyridyl)amino)phenyl)porphyrin zinc was also synthesized by the same method of previous compound. The synthesized compound exhibited a high selectivity for Cu^{2+} ion with the detection limit of 3.3×10^{-7} M. The fluorescence of both compounds could be revived by the addition of EDTA disodium solution.

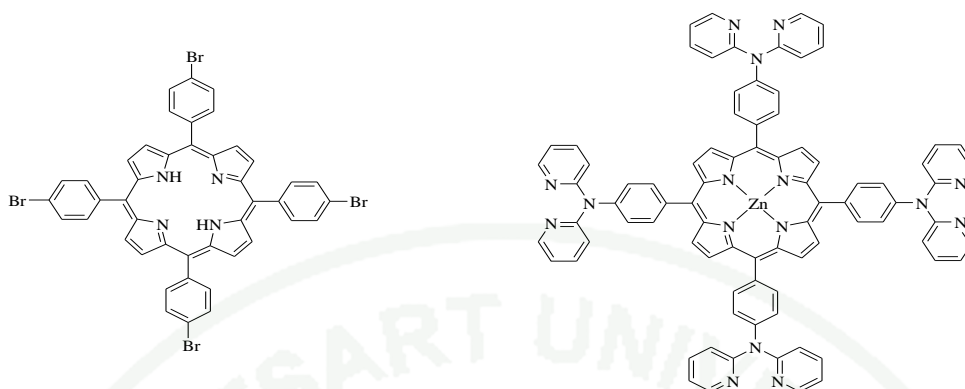


Figure 28 The structure of compound 5,10,15,20-tetra(*p*-bromophenyl)porphyrin and 5,10,15,20-tetra(*p*-*N,N*-bis(2-pyridyl)amino)phenyl)porphyrin zinc.

Li *et al.* (2008) synthesized *meso*-tetraphenylporphyrin derivative (Figure 29), containing two 2-(oxymethyl) pyridine units as a sensor for recognition of Zn^{2+} ion. This compound was synthesized by reaction between *meso*-tetraphenylporphyrin derivative, containing hydroxyl groups and 2-chloromethylpyridine hydrochloride. The synthesized chemosensor exhibited ratiometric fluorescence response to Zn^{2+} ion with high selectivity. The response of the chemosensor to Zn^{2+} ion was based on the porphyrin metallation with cooperating effect of 2-(oxymethyl) pyridine units. The analytical performance of this chemosensor showed a linear range over the range of 3.2×10^{-7} M to 1.8×10^{-4} M with a detection limit of 5.5×10^{-8} M. The experimental results showed the pH independence in 4.8–8.0 and excellent selectivity for Zn^{2+} over transition metal cation.

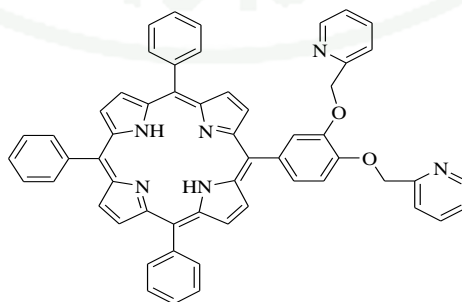


Figure 29 The structure of compound of *meso*-tetraphenylporphyrin derivative, containing two 2-(oxymethyl) pyridine units.

Bozkurt *et al.* (2009) synthesized 5,10,15,20-tetra-(3-bromo-4-hydroxyphenyl)porphyrin (TBHPP), its application as potential fluoroionophore for recognition of Pb^{2+} in immobilized medium (PVC film) ethanol medium. The analytical performance characteristics of the proposed Pb^{2+} -sensitive chemosensor were investigated. It showed a linear response toward Pb^{2+} in the concentration range of 5×10^{-6} to $4 \times 10^{-4} \text{ molL}^{-1}$ in PVC film and 5×10^{-6} to $3 \times 10^{-4} \text{ molL}^{-1}$ in ethanol medium, with a working pH 7. The researchers determined the detection limit, it was 2×10^{-8} and $4 \times 10^{-8} \text{ molL}^{-1}$ for Pb^{2+} in PVC film and ethanol medium respectively. The response time of Pb^{2+} was found as 4 minutes for PVC film and 2 minutes for ethanol medium. The sensor developed in two different mediums was used for lead determination in standard soil sample with satisfactory results.

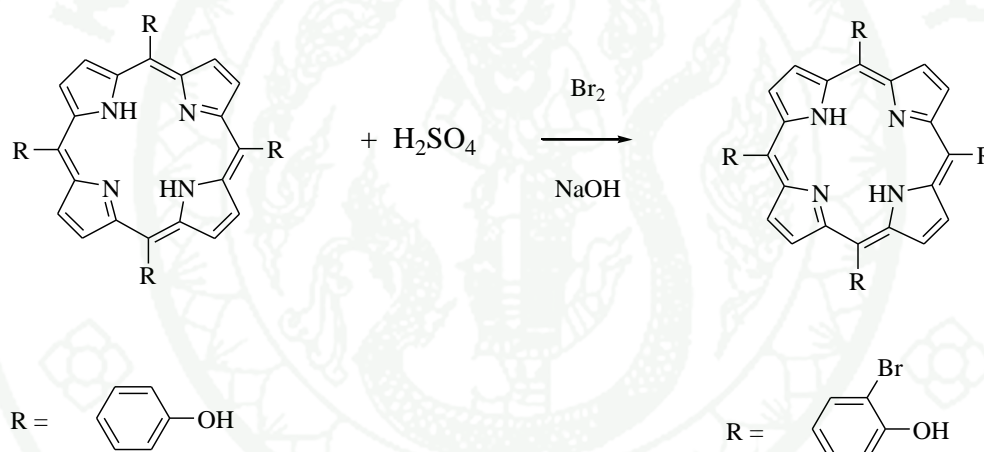


Figure 30 Preparation of 5,10,15,20-tetra-(3-bromo-4-hydroxyphenyl)porphyrin (TBHPP).

Hu *et al.* (2009) synthesized *meso*-tetra(4-*N,N,N*-trimethylanilinium) porphyrin-Pd (Pd-TAPP), its applications as optical sensing of heavy metal ions in anionic micellar solution. Pd-TAPP emits strong and stable room temperature phosphorescence (RTP) in sodium dodecyl sulfate (SDS) micellar solution. Heavy metal ions in anionic micellar solution, including Fe^{2+} , Co^{2+} , Ni^{2+} and Cu^{2+} , could efficiently quench the phosphorescence of Pd-TAPP. Moreover, the stern-volmer constants were determined from this equation: $\tau_0/\tau = 1 + kq\tau_0[Q]$ where τ_0 is the lifetime of the excited state in the absence of the quencher

Q, they increased in the order $\text{Fe}^{2+} < \text{Co}^{2+} < \text{Cu}^{2+} < \text{Ni}^{2+}$, directly reflecting the relative sensitivity of the method for these ions. In addition, the researchers calculated the detection limits following the 3σ IUPAC criteria are 2.3×10^{-7} mol/L for Cu^{2+} , 3.4×10^{-7} mol/L for Co^{2+} , 1.2×10^{-7} mol/L for Ni^{2+} and 2.1×10^{-6} mol/L for Fe^{2+} . The addition of these ions also resulted in reduction of the lifetime (τ) of Pd-TAPP, so the linear relationship between the concentration of Fe^{2+} , Co^{2+} , Ni^{2+} or Cu^{2+} ions and τ_0/τ indicated the dynamic quenching mechanism.

Yang *et al.* (2009) prepared an optical sensor for Hg^{2+} ion by using porphyrin immobilized in plasticized poly(vinylchloride) (PVC) membrane and compared the response to Hg^{2+} ion with three porphyrins including *meso*-tetraphenylporphyrin, tetra(*p*-dimethylaminophenyl) porphyrin (TDMAPP) and tetra(*n*-phenylpyrazole) porphyrin (TPPP) as shown in Figure 31. Among them, TDMAPP showed the most remarkable response to Hg^{2+} ion. The fluorescence quenching of TDMAPP was attributed to the complexation between Hg^{2+} and TDMAPP. The analytical performance of the prepared sensor showed a linear range covering from 4.0×10^{-8} M to 4.0×10^{-6} M with a detection limit of 8.0×10^{-9} M. The prepared sensor displayed excellent reproducibility, reversibility, and selectivity for the determination of Hg^{2+} ion in environmental waste water.

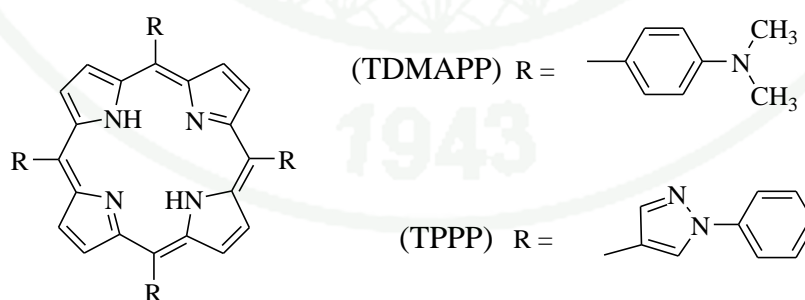


Figure 31 The structure of compounds tetra(*p*-dimethylaminophenyl) porphyrin (TDMAPP) and tetra(*n*-phenylpyrazole) porphyrin (TPPP).

Li *et al.* (2010) synthesized *meso*-tetra(*p*-methoxyphenyl)porphyrin T(*p*-OCH₃)PPH₂ and its application in fluorescent detections of Ag(I) in aqueous solution. The fluorescence quenching of T(*p*-OCH₃)PPH₂ was attributed to the formation of a complex between T(*p*-OCH₃)PPH₂ and Ag(I) by 1:1 complex ratio ($K = 3.7 \times 10^5$), which had been utilized as the basis of the fabrication of the Ag(I)-sensitive fluorescent chemosensor. The analytical performance characteristics of the proposed Ag(I)-sensitive chemosensor were investigated. The chemosensor could be applied to the quantification of Ag(I) with a linear range covering from 1.0×10^{-7} to 5.0×10^{-5} M with a detection limit of 2.5×10^{-8} M. The experimental results showed the pH independent in medium condition (pH 4.0-8.0) and the sensor has a better selectivity for Ag(I) over other metal ions tested under the same conditions.

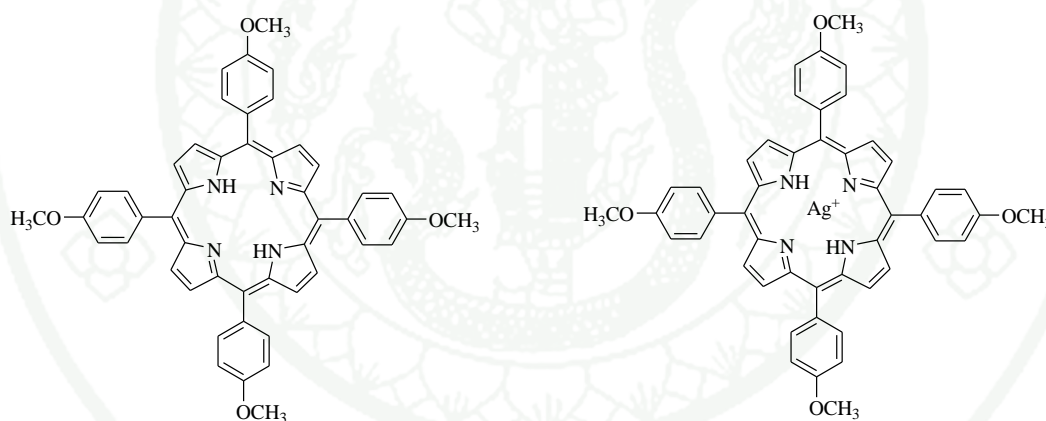


Figure 32 The structure of compound *meso*-tetra(*p*-methoxyphenyl)porphyrin T(*p*-OCH₃)PPH₂ and *meso*-tetra(*p*-methoxyphenyl)porphyrin T(*p*-OCH₃)PPH₂ - Ag(I) complex.

Kim *et al.* (2011) determined the concentration of ammonia by a porphyrin cobalt(II)-dansyl complex [Co(TPP)(Ds-pip)] sensor. [Co(TPP)(Ds-pip)] or the sensor molecule containing dansyl as so called fluorophore. When dansyl formed complex with a porphyrin cobalt(II) complex made to the photoinduced intramolecular electron transfer (PET), resulting fluorescence quenching in the

MATERIALS AND METHODS

Materials

1. Apparatus

Fluorescence measurements and absorbance measurements were carried out on a Varian Cary Eclipse Fluorescence Spectrophotometer and a Perkin Elmer Lambda 35 UV-Vis spectrophotometer respectively. Infrared spectra ($4000\text{--}400\text{ cm}^{-1}$) were obtained by a Perkin Elmer system 2000 Fourier transform infrared spectrometer and were reported in wavenumber (cm^{-1}). Nuclear magnetic resonance spectra were recorded at 400 MHz on an INNOVA VARION NMR spectrometer 400 MHz. Mass spectra of the porphyrin were recorded from Bruker micrOTOF mass spectrometer. Quantum chemical calculation was calculated using Gaussian 03 program on a Linux PC 2.4 GHz and a windows XP (home edition) operating system laptop.

2. Reagents

- 2.1 Pyrrole ($\text{C}_4\text{H}_5\text{N}$, A.R. grade, Aldrich, Steinheim, Germany)
- 2.2 4-bromobenzaldehyde ($\text{BrC}_6\text{H}_4\text{CHO}$, Lab. grade, Aldrich, Steinheim, Germany)
- 2.3 4-nitrobenzaldehyde ($\text{O}_2\text{NC}_6\text{H}_4\text{CHO}$, Lab. grade, Aldrich, Steinheim, Germany)
- 2.4 Propionic acid ($\text{C}_3\text{H}_6\text{O}_2$, Lab. grade, Sigma-Aldrich, Steinheim, Germany)
- 2.5 Methyl alcohol (CH_3OH , A.R. grade, Mallinckrodt, St. Louis, Missouri, USA.)
- 2.6 Ethyl alcohol ($\text{C}_2\text{H}_5\text{OH}$, A.R. grade, Mallinckrodt, St. Louis, Missouri, USA.)

- 2.7 Propyl alcohol (C_3H_7OH , A.R. grade, Mallinckrodt, St. Louis, Missouri, USA.)
- 2.8 Pyridine (C_5H_5N , A.R. grade, Merck, Darmstadt, Germany)
- 2.9 *N,N*-dimethylformamide (C_3H_7NO , A.R. grade, Merck, Darmstadt, Germany)
- 2.10 Tetrahydrofuran (C_4H_8O , A.R. grade, Lab Scan, Bangkok, Thailand)
- 2.11 Tetrahydrofuran (C_4H_8O , HPLC grade, Scharlau, Port Adelaide, Australia)
- 2.12 Acetic anhydride ($(CH_3CO)_2O$, Lab. grade, Fluka, Buchs, Switzerland)
- 2.13 Thin layer chromatography (TLC): aluminium sheet Silica gel 60 F₂₅₄ (Merck, Darmstadt, Germany)
- 2.14 Chloroform-*d* ($CDCl_3$ -*d*) TMS(1 vol%) : for NMR spectroscopy (Merck, Darmstadt, Germany)
- 2.15 Acetone, D-6 (CD_3COCD_3 , A.R. grade, Merck, Darmstadt, Germany)
- 2.16 Potassium bromide (KBr, A.R. grade, Merck, Darmstadt, Germany)
- 2.17 Mercuric(II)chloride ($HgCl_2$, A.R. grade, Analar, Poole, England)
- 2.18 Methylmercury(I)chloride (CH_3ClHg , A.R. grade, Aldrich, steinheim, Germany)
- 2.19 Cobalt standard for atomic absorption 1000 mg/L ($Co(NO_3)_2$, A.R. grade, Merck, Darmstadt, Germany)
- 2.20 Silver standard for atomic absorption 1000 mg/L ($AgNO_3$, A.R. grade, Carlo Erba, Milan, Italy)
- 2.21 Nickel standard for atomic absorption 1000 mg/L ($NiCl_2 \cdot 6H_2O$, A.R. grade, Carlo Erba, Milan, Italy)
- 2.22 Chromium standard for atomic absorption 1000 mg/L ($CrCl_3 \cdot 6H_2O$, A.R. grade, Carlo Erba, Milan, Italy)

- 2.23 Iron standard for atomic absorption 1000 mg/L ($\text{FeCl}_3 \cdot 6\text{H}_2\text{O}$, A.R. grade, Carlo Erba, Milan, Italy)
- 2.24 Copper standard for atomic absorption 1000 mg/L ($\text{CuCl}_2 \cdot 2\text{H}_2\text{O}$, A.R. grade, Carlo Erba, Milan, Italy)
- 2.25 Zinc standard for atomic absorption 1000 mg/L (ZnCl_2 , A.R. grade, Carlo Erba, Milan, Italy)
- 2.26 Cadmium standard for atomic absorption 1000 mg/L ($\text{Cd}(\text{NO}_3)_2$, A.R. grade, Fischer Scientific, Leicestershire, England)
- 2.27 Ruthenium standard for atomic absorption 1000 mg/L (RuCl_3 , A.R. grade, Fluka, Steinhiem, Germany)
- 2.28 Potassium nitrate (KNO_3 , A.R. grade, Carlo Erba, Milan, Italy)
- 2.29 Potassium thiocyanate (KSCN , J.T. Baker, Phillipsburg, New Jersey, U.S.A.)
- 2.30 Potassium chloride (KCl , A.R. grade, Univar, Seven Hills, Australia)
- 2.31 Potassium sulphate (K_2SO_4 , A.R. grade, Univar, Seven Hills, Australia)
- 2.32 Sodium carbonate (Na_2CO_3 , A.R. grade, Univar, Seven Hills, Australia)
- 2.33 Potassium hydrogen phosphate (K_2HPO_4 , A.R. grade, Merck, Darmstadt, Germany)
- 2.34 Sodium nitrite (NaNO_2 , A.R. grade, Merck, Darmstadt, Germany)

Methods

1. Synthesis of 5,10,15,20-Tetra(*p*-bromophenyl)porphyrin and 5,10,15,20-Tetra(*p*-nitrophenyl)porphyrin.

For synthesizing 5,10,15,20-Tetra(*p*-bromophenyl)porphyrin (TBTPP), 1.4 mL (0.02 mol) of pyrrole and 3.7004 g (0.02 mol) of 4-bromobenzaldehyde were added (by slowly pouring down the reflux condenser) to 75 mL of refluxing propionic acid. The mixture was refluxed for 30 minutes and allowed the flask to cool for a few minutes. The dark brown mixture, obtained after refluxing, was filtered and washed thoroughly with methanol. After hot water washing, the obtained purple crystals were air dried to get the product of TBTPP. Then, the product was characterized by Fourier transform infrared (FTIR) and Nuclear magnetic resonance spectroscopy (NMR) to confirm its structure.

For the synthesis of 5,10,15,20-Tetra(*p*-nitrophenyl)porphyrin (TNPP), 0.7 mL (0.01 mol) of pyrrole and 1.8502 g (0.01 mol) of 4-nitrobenzaldehyde were added to 75 mL of stirring propionic acid, then the mixture was refluxed for 30 minutes with stirring. After refluxing, the obtained tarry solution was allowed to cool and stand for a few minutes. The dark solid was collected by filtration, and then the dark solid was washed by methanol. After hot water washing, the obtained dark crystals were air dried to get the product of TNPP. Then, the product was characterized by Fourier transform infrared (FTIR) and Nuclear magnetic resonance spectroscopy (NMR) to confirm its structure.

2. Preparation of solutions

2.1 Preparation of 1 mM and 0.1 mM TBTPP solution

For the preparation of 1 mM TBTPP solution, 93 mg amount of prepared TBTPP was dissolved and made up to 100 mL by tetrahydrofuran (THF) in

volumetric flask. The solution of 0.1 mM TBTPP was prepared by diluted from 1 mM TBTPP.

2.2 Preparation of 1 mM and 0.1 mM TNPP solution

For the preparation of 1 mM TNPP solution, 80 mg of prepared TNPP was dissolved and made up to 100 mL by THF in a volumetric flask. The solution of 0.1 mM TNPP was prepared by diluted from 1 mM TNPP.

2.3 Preparation of 1 mM of metal standard

Almost cation standards used in this work were diluted from liquid 1000 ppm atomic absorption spectroscopy (AAS) grade except mercury ion (Hg^{2+}) which was used from solid chloride salt. All metal ions were dissolved and made up to 100 mL by ethanol in volumetric flask. The amounts of all metal ions were stated in Table 2.

Table 2 The amount of metal ion solutions and metal ion salt for the preparation of 1 mM standard metal cation in ethanol. To explore the utility of TBTPP and TNPP as Hg^{2+} -sensing and investigate of interfering ion in Hg^{2+} analysis by using TBTPP and TNPP.

Metal cation	Amount of each metal cation
Hg^{2+} (from HgCl_2)	0.0272 g
Ru^{3+}	20.74 mL
Ag^+	16.99 mL
Co^{2+}	15.20 mL
Cd^{2+}	23.64 mL
Ni^{2+}	23.77 mL
Cr^{3+}	26.65 mL
Fe^{2+}	27.03 mL
Cu^{2+}	17.04 mL
Zn^{2+}	13.63 mL

2.4 Preparation of 0.1 M anion standard

All anion standards used in this work were prepared by dissolving of each anion salt in distilled water and making up to 100 mL in volumetric flask. The amounts of all anions were stated in Table 3.

Table 3 The amount of anion salts for the preparation of 1 M standard anion in distilled water. To investigate of interfering ion in Hg^{2+} analysis by using TBTPP and TNPP.

Anion	Amount of each anion
SCN^- (from KSCN)	0.9718 g
NO_3^- (from KNO_3)	1.0110 g
Cl^- (from KCl)	0.7456 g
CO_3^{2-} (from K_2CO_3)	1.6000 g
CN^- (from KCN)	0.6500 g

3. Application of TBTPP and TNPP as fluorescent sensing for determination of Hg^{2+}

3.1 Fluorescence quenching of TBTPP and TNPP by Hg^{2+}

To explore the utility of TBTPP and TNPP as Hg^{2+} -sensing, the fluorescence responses of TBTPP and TNPP to Hg^{2+} were tested. The tested solutions were prepared by pipetting 2.5 mL of 0.1 mM solution of TBTPP and TNPP into each 10 mL volumetric flask. After that, the solution of 0.1 mM solution of Hg^{2+} was pipetted in the volume of 2.5 mL into each volumetric flask, respectively. Then, the mixture solutions were diluted to the mark with THF. Then, TBTPP solution was recorded by fluorescence responses with excitation and emission wavelength at 424 and 650 nm respectively. Moreover, TNPP solution was recorded by fluorescence responses with excitation and emission wavelength at 424 and 653 nm respectively.

3.2 Stoichiometric determination of complexes between TBTPP and TNPP with Hg^{2+} by continuous variation method (Job's method)

From experiments, Hg^{2+} could quench fluorescence of TBTPP and TNPP with excitation and emission wavelength at 424 and 650 nm respectively for TBTPP system and excitation and emission wavelength at 424 and 653 nm respectively for TNPP system. The stoichiometric determination of complexes between TBTPP and TNPP with Hg^{2+} were studied.

The stoichiometric of the complexes were examined by pipetting 0.00, 0.10, 0.20, 0.30, 0.40, 0.50, 0.60, 0.70, 0.80, 0.90 and 1.00 mL of 0.1 mM Hg^{2+} into each of eleven 10 mL volumetric flasks. After that, 1.00, 0.90, 0.80, 0.70, 0.60, 0.50, 0.40, 0.30, 0.20 and 0.10 mL of 0.1 mM solutions of TBTPP and TNPP were pipetted into each volumetric flask, respectively. Then, the solutions were diluted to the mark with THF. The absorbance of the solutions were measured by UV-Vis

spectrophotometer at 438 nm for TBTPP system and 424 nm for TNPP system. The Job's plot of complex between TBTPP with Hg^{2+} is shown in Figure 42.

3.3 Stoichiometric determination of complexes between TBTPP and TNPP with Hg^{2+} by mole ratio method

Volume of 0.50 mL of 0.1 mM Hg^{2+} was pipetted into each of eleven 10 mL volumetric flasks. After that, 0.00, 0.10, 0.20, 0.30, 0.40, 0.50, 0.60, 0.70, 0.80, 0.90 and 1.00 mL of 0.1 mM solution of TBTPP and TNPP were pipetted into each volumetric flask, respectively. Then, the mixture solutions were diluted to the mark with THF. The absorbances of the solutions were measured by UV-Vis spectrophotometer at 438 nm for TBTPP system and 424 nm for TNPP system. The mole ratio method of complexes between TBTPP and TNPP with Hg^{2+} are shown in Figure 43 and 45 respectively.

3.4 Determination for stability constant of TBTPP and TNPP with Hg^{2+}

The stability constant of complexes could be determined by using the data from continuous variation method (Job's plot) and mole ratio method by following method of (Connors, 1987) and (Benesi, 1949) respectively. The complexes between TBTPP and TNPP with Hg^{2+} in THF solution were studied by UV-Vis spectrophotometer at 438 and 424 nm respectively. The calculation of stability constant of the complexes are shown in Appendix B and C.

3.5 Determination of linear range and detection limit of Hg^{2+} analysis by using TBTPP and TNPP

For the determination of linear range and detection limit of analysis of Hg^{2+} by TBTPP and TNPP, 10 μl aliquots of Hg^{2+} (from 0.1 mM and 1 mM Hg^{2+} in ethanol) were added to a 2.5 mL solution volume of TBTPP and TNPP (0.1 mM in THF) and made up each flask by THF. Then, TBTPP system of each flask was recorded by fluorescence spectrometer with excitation and emission wavelength at

424 and 650 nm respectively. Moreover, TNPP system of each flask was recorded by fluorescence spectrometer with excitation and emission wavelength at 424 and 653 nm respectively. The calculations of the linear range and detection limit of Hg^{2+} analysis by TBTPP and TNPP are shown in Appendix D.

3.6 Calculation for the formation energy of TBTPP and TNPP complexes

The optimized molecular structure of metal-TBTPP and metal-TNPP complexes and their energy were also studied. Quantum chemical calculation was performed using Gaussian 03 program suite of programs on a Linux PC 2.4 GHz. The formation energies of porphyrin complexes were theoretically calculated to predict the possible structure by using the Density Functional Theory (DFT) at B3LYP level of theory using 6-31G* basis set for each atom on porphyrin and the effective core potential (ECP) of LanL2DZ was employed on each transition metal. The theoretical background and example of method for quantum chemical calculation are shown in Appendix F.

3.7 Investigation of interfering ion in Hg^{2+} analysis by using TBTPP and TNPP

The degree of interfering cation and anion, effecting on complexes formation of TBTPP and TNPP with Hg^{2+} , were investigated. Series of complexes formation between TBTPP and TNPP with Hg^{2+} by mixing 2.5 mL of 0.1 mM TBTPP and 2.5 mL of 0.1 mM TNPP into each 10 mL volumetric flask with 0.15 mL of 1 mM Hg^{2+} standard for TBTPP system and 0.19 mL of 1 mM Hg^{2+} standard for TNPP system in the presence of interference ion at the various concentration ratios to Hg^{2+} , which were 0.005:1, 0.02:1, 0.1:1, 0.5:1, 1:1 and 10:1 respectively. Each solution was made up to the mark by THF in 10 mL volumetric flask. The fluorescence responses of complex solutions in presence of interference ion were measured by fluorescence spectrometer in the same condition as the above section. The presence of interference cations and anions, which caused change of the

fluorescence intensity, was accepted as non-significant interfering effect in the range of 99% confident interval.



RESULTS AND DISCUSSIONS

1. Synthesis of 5,10,15,20-Tetra(*p*-bromophenyl)porphyrin (TBTPP) and 5,10,15,20-Tetra(*p*-nitrophenyl)porphyrin (TNPP).

The synthesis pathways of TBTPP and TNPP, which were synthesized by refluxing of pyrrole with 4-bromobenzaldehyde for TBTPP and with 4-nitrobenzaldehyde for TNPP in the presence of acid catalyst are shown in Figure 34. All obtained products of TBTPP and TNPP were 22.10% and 30.19% yield respectively. All products were characterized by FT-IR and ^1H NMR. The results of the characterization are shown in the next section.

The synthesis mechanisms of both 4-bromobenzaldehydes and 4-nitrobenzaldehyde with pyrrole are very similar. The mechanism of the reaction has been interpreted in term of four important chemical steps. These include (a) an addition step to produce a carbinol (b) a condensation or chain-building step involving the carbinol and another molecule of pyrrole, leading the chains to grow (c) the closure of the open chain tetrapyrrole to form a cyclic tetrapyrrole or porphyrinogen, and (d) oxidation (Kim, 1972). Moreover, the bromo and nitro groups, which are electron-withdrawing groups, at the *para*-position of benzaldehyde should favor the initial step by making the carbonyl carbon more susceptible to nucleophilic attack by the α -carbon of the pyrrole. The reaction mechanisms of TBTPP and TNPP synthesis are proposed in Appendix A.

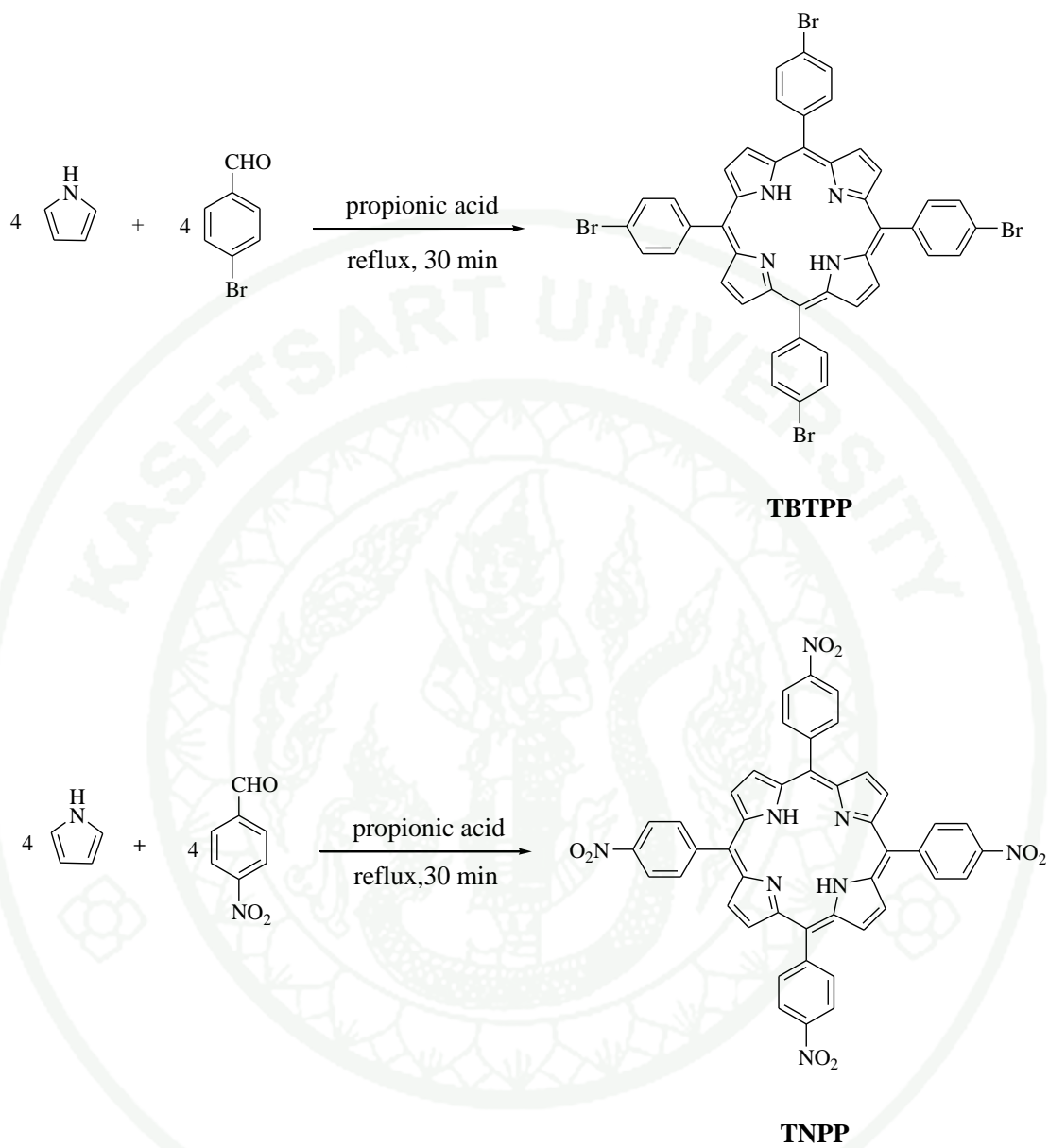


Figure 34 The synthesis pathways of TBTPP and TNPP.

2. Characterization of 5,10,15,20-Tetra(*p*-bromophenyl)porphyrin (TBTPP) and 5,10,15,20-Tetra(*p*-nitrophenyl)porphyrin (TNPP)

Before characterizing the synthesized compounds (TBTPP and TNPP), the components of synthesized porphyrins were investigated by thin layer chromatography (TLC) with various solvents as mobile phase, the best condition are ethanol: hexane = 1:1 and CH₂Cl₂: hexane = 3:1 for TBTPP and TNPP respectively. For all various solvents used as mobile phase, it was found that there was only one spot appearing on the TLC plate for each synthesized porphyrin.

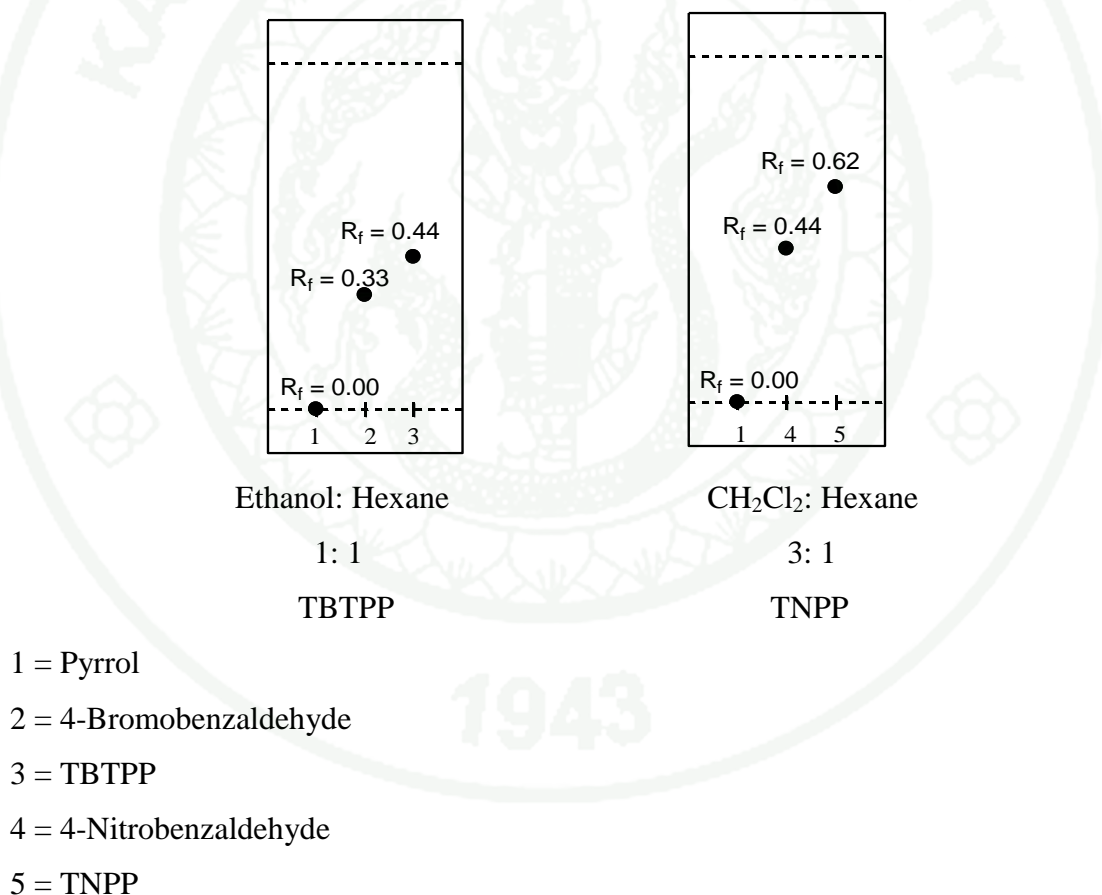


Figure 35 The components of synthesized TBTPP and TNPP with the best condition on thin layer chromatography (TLC).

2.1 5,10,15,20-Tetra(*p*-bromophenyl)porphyrin (TBTPP)

Infrared spectrum

The KBr disks of TBTPP which ground and dried at 123 °C, were prepared by mixing of these compounds with KBr. FT-IR spectra were recorded in KBr disks in the 4000-400 cm⁻¹ region. The spectra and assignment peaks of TBTPP is shown in Figure 36 and Table 4. The spectra of TBTPP is similar to the report by Weng *et al.* (2007).

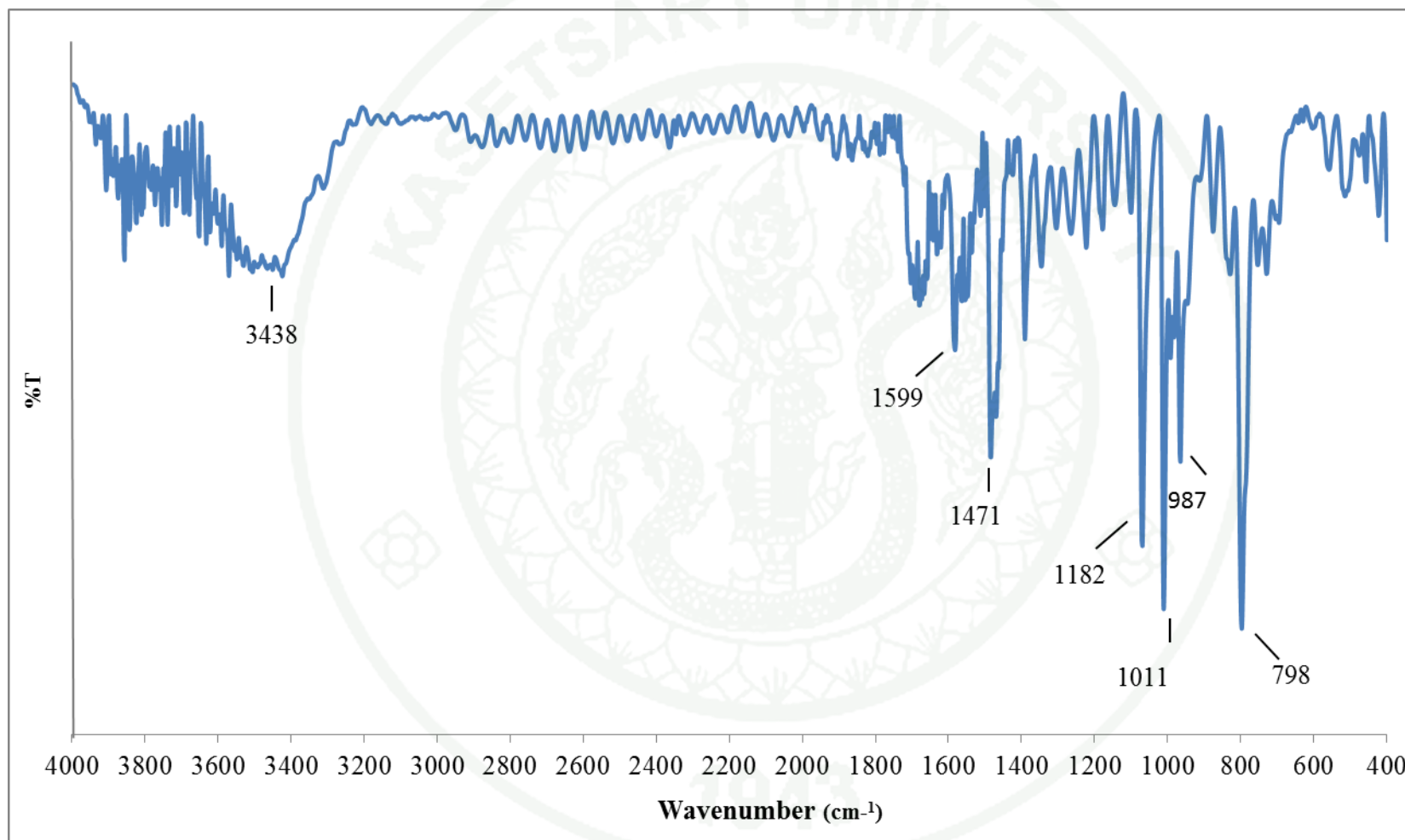


Figure 36 The FT-IR spectrum of TBTPP

Table 4 Data from the FT-IR spectra of TBTPP

Wavenumber of TBTPP(cm^{-1}) Weng <i>et al.</i> (2007)	Wavenumber of the synthesized TBTPP(cm^{-1})	Functional group
3438(s)	3438(s)	N-H stretching
3082(s)		C-H (aromatic) stretching
1584(s)		C-C stretching
1599(s)	1599(s)	N-H bending
1471(s)	1471(s)	Pyrrole stretching
1182(s)	1182(s)	C-C stretching
1011(s)	1011(s)	C-H out-of-plane bending
987(s)	987(s)	=C-H oop bending
965(s)		=C-H oop bending
848(s)		Pyrrole in-plane bending
798(s)	798(s)	C-Br stretching

¹H NMR spectrum

For ¹H NMR of TBTPP, 15 mg of TBTPP was dissolved in chloroform-*d* (CDCl₃). The ¹H NMR spectra were recorded at 400 MHz on an INNOVA VARION NMR spectrometer 400 MHz. The ¹H NMR spectra of TBTPP is shown in Figure 37. The chemical shifts of TBTPP is also shown in Table 5. The ¹H NMR spectrum of TBTPP shows 8.84 ppm for 8H (pyrrole) and 7.89-8.08 ppm for 16H (phenyl). The ¹H NMR spectra of TBTPP is similar to the report by Weng *et al.* (2007).

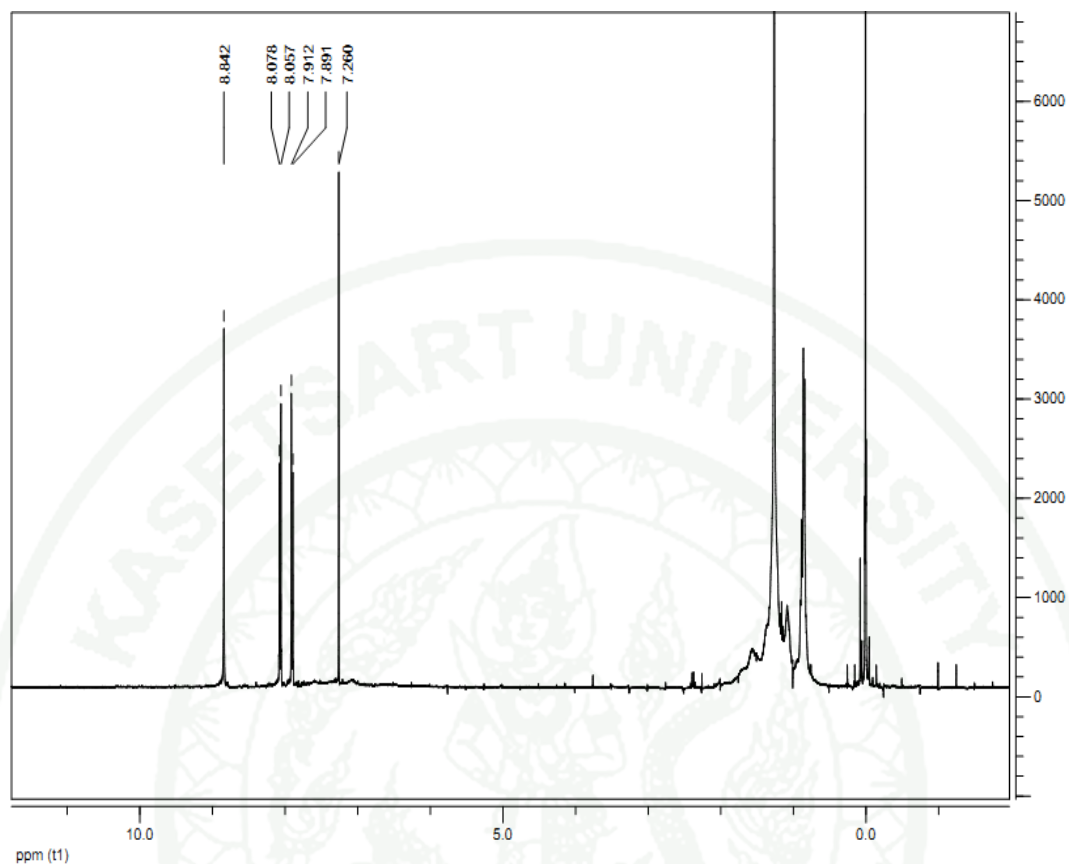


Figure 37 The ^1H NMR spectrum of TBTPP in chloroform-*d* (CDCl_3).

Table 5 Chemical shifts from ^1H NMR spectra of TBTPP.

TBTPP		
Chemical Shift (ppm) Weng <i>et al.</i> (2007)	Chemical Shift (ppm)	Proton
-2.84		N-H
7.88	7.89, 7.91	Phenyl, 8H
8.06	8.06, 8.08	Phenyl, 8H
8.82	8.84	Pyrrole, 8H

2.2 5,10,15,20-Tetra(*p*-nitrophenyl)porphyrin (TNPP)

Infrared spectrum

The KBr disks of TNPP which ground and dried at 123 °C, was prepared by mixing of this compound with KBr. FT-IR spectrum was recorded in KBr disk in the 4000-400 cm⁻¹ region. The spectrum and assignment peaks of TNPP are shown in Figure 39 and Table 6. The spectrum of TNPP is similar to the reported papers (Hu, 2003).

Table 6 Data from the FT-IR spectrum of TNPP.

Wavenumber of TNPP (cm ⁻¹) Hu (2003)	Wavenumber of the synthesized TNPP (cm ⁻¹)	Functional group
3313(w)	3313(w)	N-H stretching
1679(w), 1595(s)	1679(w), 1595(s)	C-C stretching
1516(s), 1344(s)	1344(s)	NO ₂ stretching
1400(w)	1400(w)	Pyrrole stretching
1223(w)	1223(w)	C _β -H in-plane bending
963(m), 864(m)	963(m), 864(m)	C-N stretching
846(m)	846(m)	Pyrrole in-plane bending

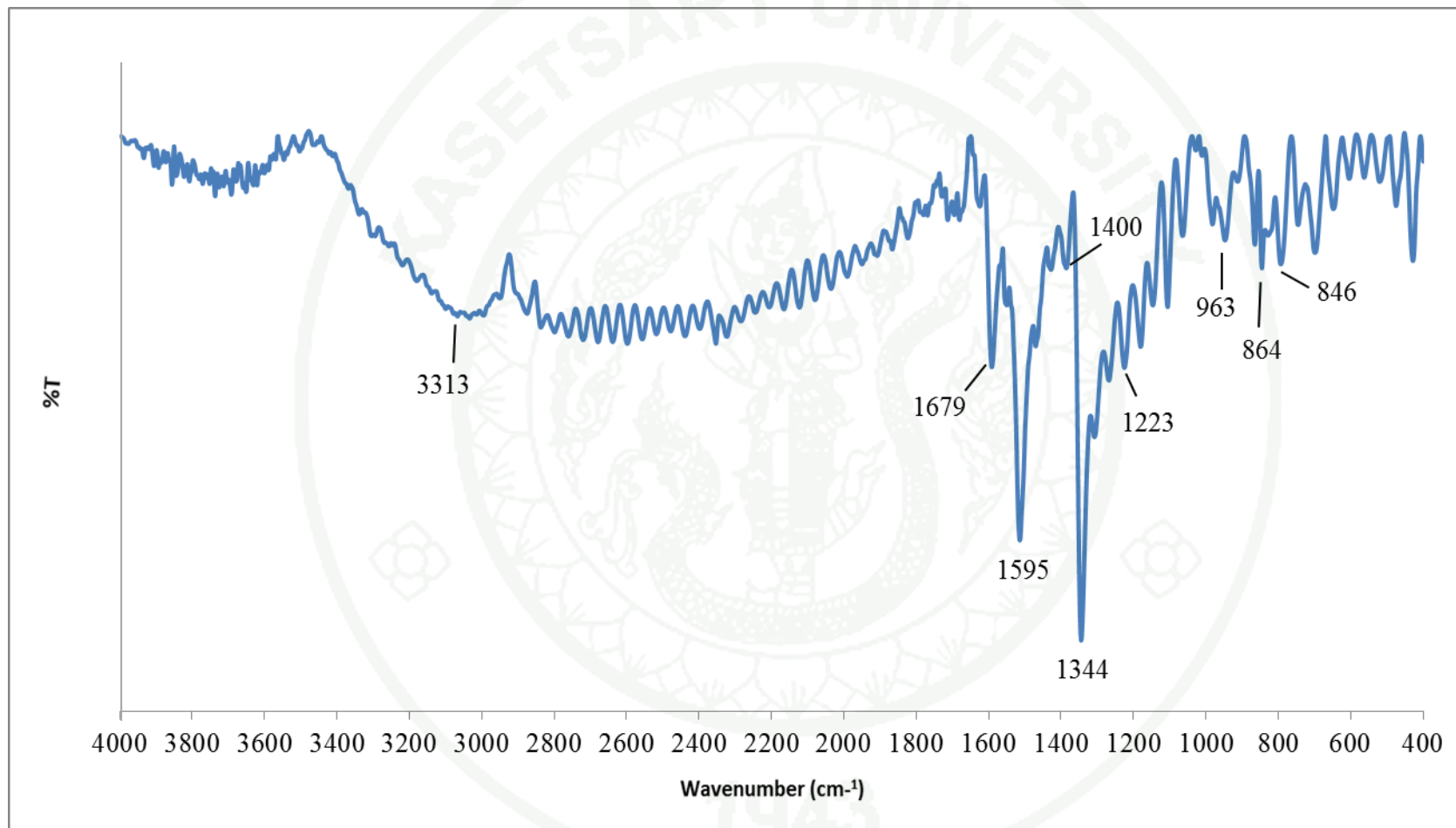


Figure 38 The FT-IR spectrum of TNPP

^1H NMR spectrum

For ^1H NMR of TNPP, 15 mg of TNPP was dissolved in chloroform-*d* (CDCl_3). The ^1H NMR spectra were recorded at 400 MHz on an INNOVA VARION NMR spectrometer 400 MHz. The ^1H NMR spectra of TNPP is shown in Figure 40. The chemical shifts of TNPP is also shown in Table 7. The ^1H NMR spectrum of TNPP shows 8.82 ppm for 8H (pyrrole) and 8.39-8.68 ppm for 16H (phenyl). The ^1H NMR spectra of TNPP is similar to the report by Luguya *et al.* (2004).

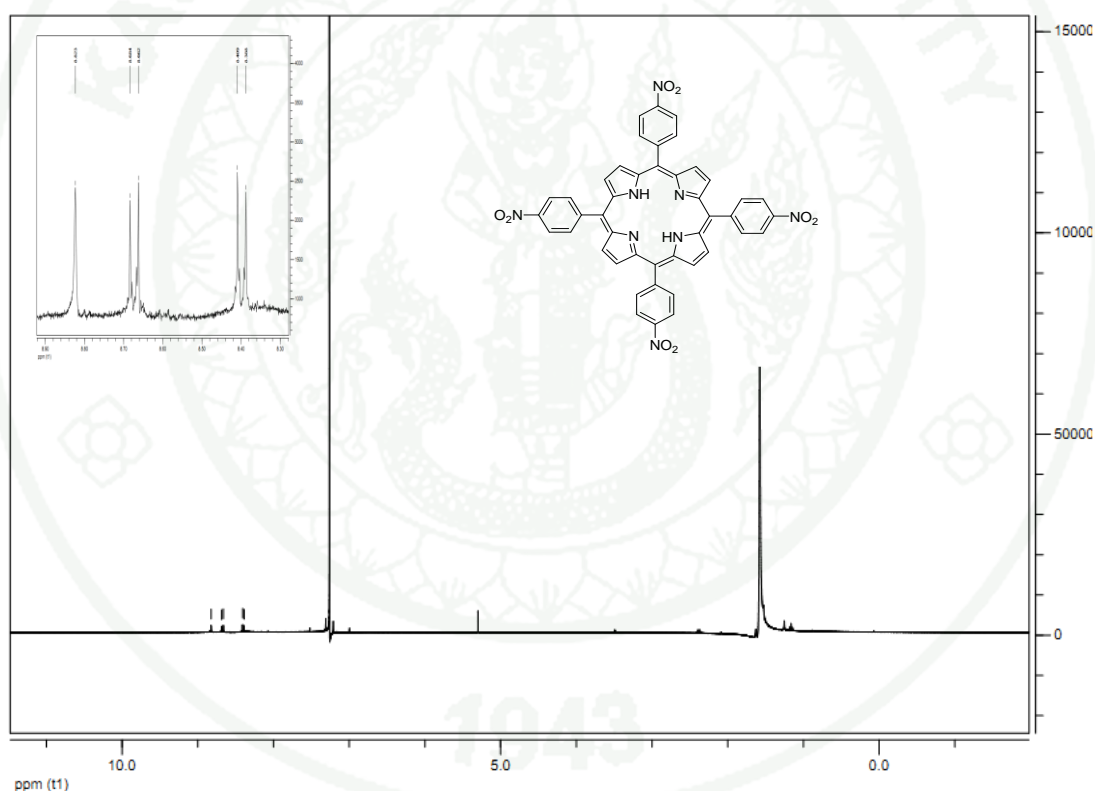


Figure 39 The ^1H NMR spectrum of TNPP in chloroform-*d* (CDCl_3).

Table 7 Chemical shifts from ^1H NMR spectra of TNPP.

TNPP		
Chemical Shift (ppm) Luguya <i>et al.</i> (2004)	Chemical Shift (ppm)	Proton
-2.80		N-H
8.40	8.39, 8.41	Phenyl, 8H
8.65	8.66, 8.68	Phenyl, 8H
8.80	8.82	Pyrrole, 8H

3. Application of TBTPP and TNPP as fluorescent sensing for the determination of Hg^{2+}

3.1 Fluorescence quenching of TBTPP and TNPP by Hg^{2+}

In this research, 5,10,15,20-Tetra(*p*-bromophenyl)porphyrin and 5,10,15,20-Tetra(*p*-nitrophenyl)porphyrin, TBTPP and TNPP respectively were initially synthesized for studying its recognition capability toward Hg^{2+} . Due to the effect from bromo and nitro groups, being electron-withdrawing groups, they would expand the binding site at the center of porphyrin ring. In the same, Hg^{2+} could coordinate with *meso*-Tetraphenylporphyrin (TPP) even it had not substituent groups (Falk, 1964). Moreover, Hg^{2+} could be introduced into the center of porphyrin ring in order to form complexes of TBTPP and TNPP with Hg^{2+} . It was found that both the synthesized TBTPP and TNPP could coordinate with Hg^{2+} . In addition, the bromo group of TBTPP act as both electron withdrawing and electron donating groups. The bromo group can donate electron by resonance effect and can accept electron by inductive effect. So, TBTPP was expected to coordinate with Hg^{2+} better than TNPP because the bromo group of TBTPP can donate electron to porphyrin ring by resonance effect better than nitro group of TNPP, which was only electron-withdrawing groups. Therefore, bromo groups of TBTPP could increase electron density of porphyrin ring better than nitro groups of TNPP. Consequently, 5,10,15,20-Tetra(*p*-bromophenyl)porphyrin (TBTPP) could coordinate to Hg^{2+} better than 5,10,15,20-Tetra(*p*-nitrophenyl)porphyrin (TNPP). In addition, the synthesized TBTPP shows ratiometric fluorescence response to Hg^{2+} better than TNPP.

In this research, THF was used as solvent to dissolve TBTPP and TNPP because TBTPP and TNPP have higher solubility than other solvents such as water, alcohol, acetone and dichloromethane.

Moreover, the use of mercury are becoming more restrictive because of its toxicity. Inorganic mercury, Hg^0 and Hg^{2+} , is released into an environment through a variety of anthropogenic and natural sources. Emitted elementary mercury

vapors are easily transported into the atmosphere and are oxidized to Hg^{2+} . Then Hg^{2+} can accumulate on plants, in topsoil and in water (Diez, 2008). In the case that, Hg^{2+} accumulates in water. Therefore, in this research, solvent polarity was used for dissolving mercury dichloride. In the experiment, TBTPP and TNPP in THF did not homogenize with Hg^{2+} in water. Consequently, alcohol solvent was used for dissolving mercury dichloride, it was solvent polarity as same as water. In addition, TBTPP and TNPP in THF homogenize with Hg^{2+} in alcohol, for this reason, this system could investigate fluorescence quenching response of TBTPP and TNPP with Hg^{2+} in alcohol.

To compare response characteristic of TBTPP with Hg^{2+} in different solution such as methanol, ethanol and propanol, fluorescence responses of TBTPP with Hg^{2+} in 3 solvents were investigated. Figure 41 shows that fluorescence quenching response of TBTPP with Hg^{2+} in ethanol is greater than any other examined solutions. Consequently, in next steps, Hg^{2+} in ethanol was investigated by TBTPP to study fluorescence titration. In addition, from results of fluorescence response of TBTPP with Hg^{2+} in different solution, it could indicate that methanol, ethanol and propanol could effect on the complexation between TBTPP and Hg^{2+} . Ethanol molecule might coordinate above or below the plane of the square planar complex to obtain octahedral or square base pyramid complex, which could effect to the fluorescence response of TBTPP.

1943

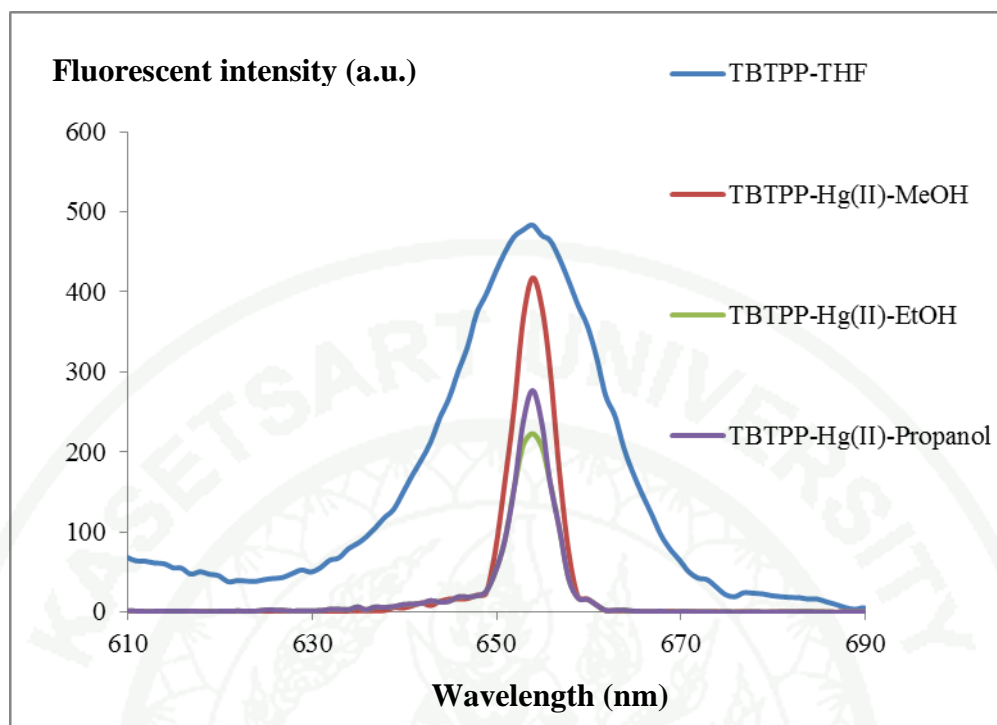


Figure 40 The fluorescence spectra of TBTPP in the presence of Hg^{2+} in methanol, ethanol and propanol. The excitation and emission wavelength are 424 and 650 nm respectively.

3.2 Stoichiometric determination of complex between TBTPP and Hg^{2+}

From the first section, the fluorescence quenching of TBTPP upon the addition of Hg^{2+} might attributed to the formation of complex between TBTPP and Hg^{2+} , so the stoichiometric of complex between TBTPP and Hg^{2+} was studied. Stoichiometric determination of TBTPP- Hg^{2+} was performed by continuous variation method (Job's method) and mole ratio.

3.2.1 Continuous variation method

The stoichiometry of TBTPP with Hg^{2+} complex was determined by continuous variation method using UV-Vis spectrophotometer. The plot between absorbance and mole fraction of TBTPP at 438 nm is shown in Figure 42. It was

found that the stoichiometric ratio between Hg^{2+} and TBTPP was 1:1. The stability constant of the complex between TBTPP and Hg^{2+} which calculated from the job's plot was 1.87×10^5 . The calculation of the stability constant of the complex between TBTPP and Hg^{2+} is shown in Appendix B.

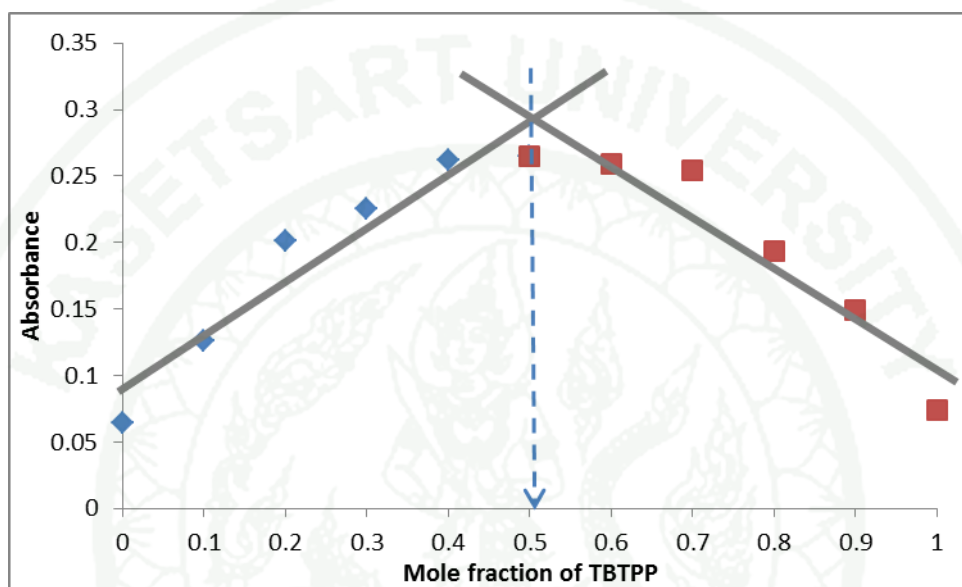


Figure 41 Continuous variation plot of complex between TBTPP and Hg^{2+} in ethanol.

3.2.2 Mole ratio method

The stoichiometry of TBTPP with Hg^{2+} complex was also determined by mole ratio method. The plot between absorbance and fraction of mole of Hg^{2+} at 438 nm is shown in Figure 43. It was found that the stoichiometric ratio between Hg^{2+} and TBTPP complex was 1:1. The stability constant of the complex between TBTPP and Hg^{2+} which determined by Benesi-Hildebrand equation was 1.00×10^6 . The calculation of the stability constant of the complex between TBTPP and Hg^{2+} is shown in Appendix C.



Figure 42 The mole ratio plot of complex between TBTPP and Hg^{2+} in ethanol.

3.3 Fluorescence quenching of TNPP by Hg^{2+}

5,10,15,20-Tetra(*p*-nitrophenyl)porphyrin, TNPP, was initially synthesized for studying its recognition capability toward Hg^{2+} . Moreover, to compare the recognition capability between Hg^{2+} with TNPP and TBTPP. Nitro group is electron-withdrawing group, it would expand the binding site at the center of porphyrin ring. Consequently, Hg^{2+} could be introduced into the center of porphyrin ring in order to form complex with TNPP. It was found that TNPP coordinated with Hg^{2+} inferior than TBTPP with Hg^{2+} .

To compare response characteristic of TNPP with Hg^{2+} in different solution such as methanol, ethanol and propanol, fluorescence responses of TNPP with Hg^{2+} in 3 solutions were investigated. Figure 44 shows that fluorescence quenching response of TNPP with Hg^{2+} in methanol is greater than any other examined solution. Moreover, the fluorescence quenching response of TNPP with Hg^{2+} in ethanol occurred at the different emission wavelength. Then, Hg^{2+} in methanol was investigated by TNPP. It was found that fluorescence response didn't change even concentration of Hg^{2+} in methanol changed. In contrast, when Hg^{2+} in

ethanol was investigated by TNPP, fluorescence response changed when concentration of Hg^{2+} in ethanol changed. Consequently, in next steps, Hg^{2+} in ethanol was investigated by TNPP to study fluorescence titration.

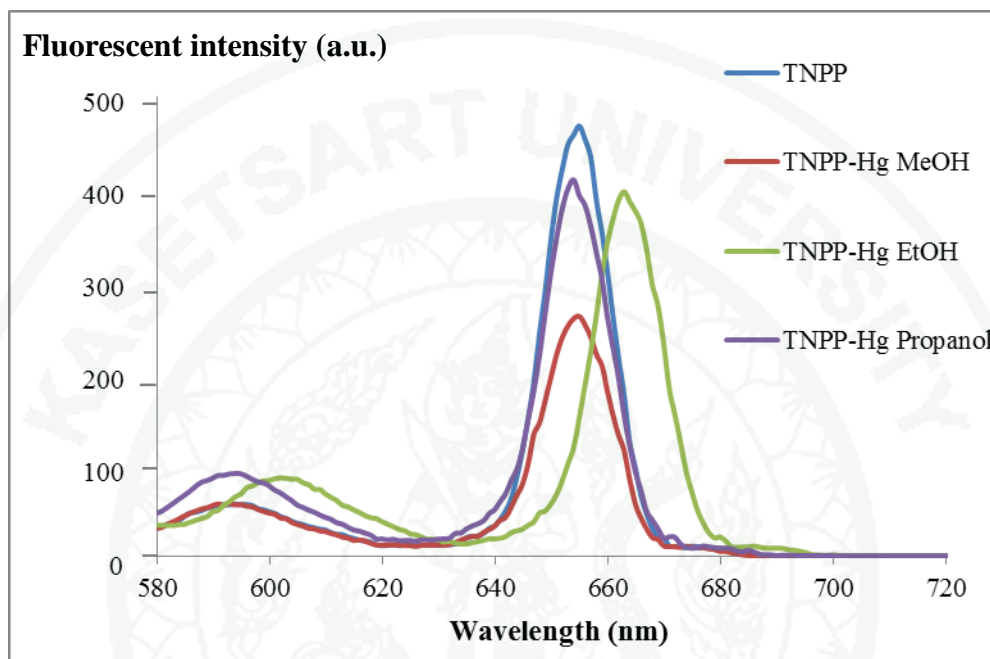


Figure 43 The fluorescence spectra of TNPP in the presence of Hg^{2+} in methanol, ethanol and propanol. The excitation and emission wavelength were 424 and 653 nm respectively.

3.4 Stoichiometric determination of complex between TNPP and Hg^{2+}

From the previous results, Hg^{2+} could quench the fluorescence of TNPP which might be from the formation of complex between TNPP and Hg^{2+} . Therefore, the stoichiometric of complex between TNPP and Hg^{2+} was studied by using continuous variation and mole ratio method. However, the continuous variation method could not identify the stoichiometry of TNPP- Hg complex. In contrast, the mole ratio method could identify the stoichiometry of TNPP- Hg complex.

3.4.1 Mole ratio method

The plot between absorbance and fraction of mole of Hg^{2+} at 424 nm is shown in Figure 45. It was found that the stoichiometric ratio between Hg^{2+} and TNPP complex was 1:1. The stability constant of the complex between TBTPP and Hg^{2+} which determined by Benesi-Hildebrand equation was 6.67×10^5 . The calculation of the stability constant of the complex between TNPP and Hg^{2+} is shown in Appendix C.

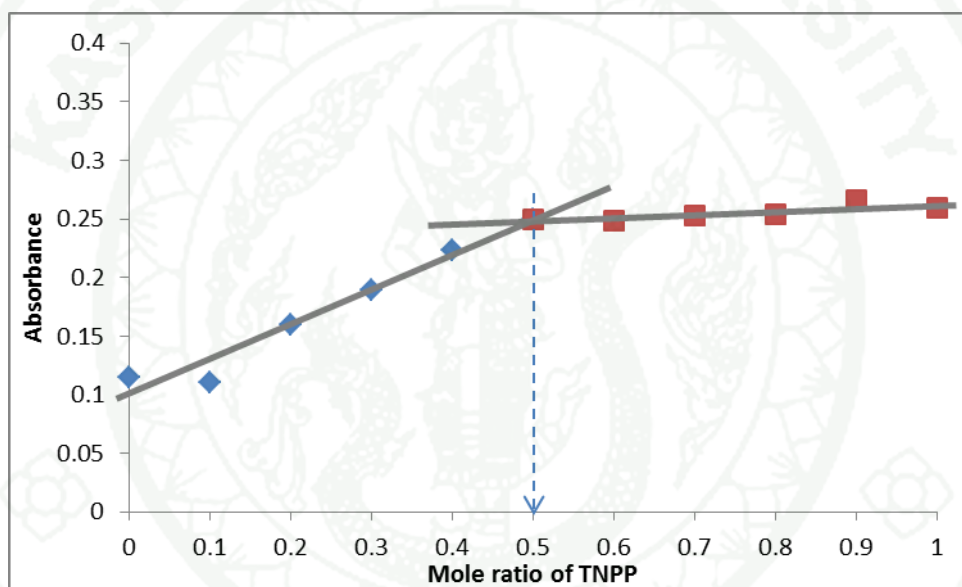


Figure 44 The mole ratio plot of complex between TNPP and Hg^{2+} in ethanol.

3.5 Determination of linear range and detection limit of Hg^{2+} analysis by using TBTPP and TNPP

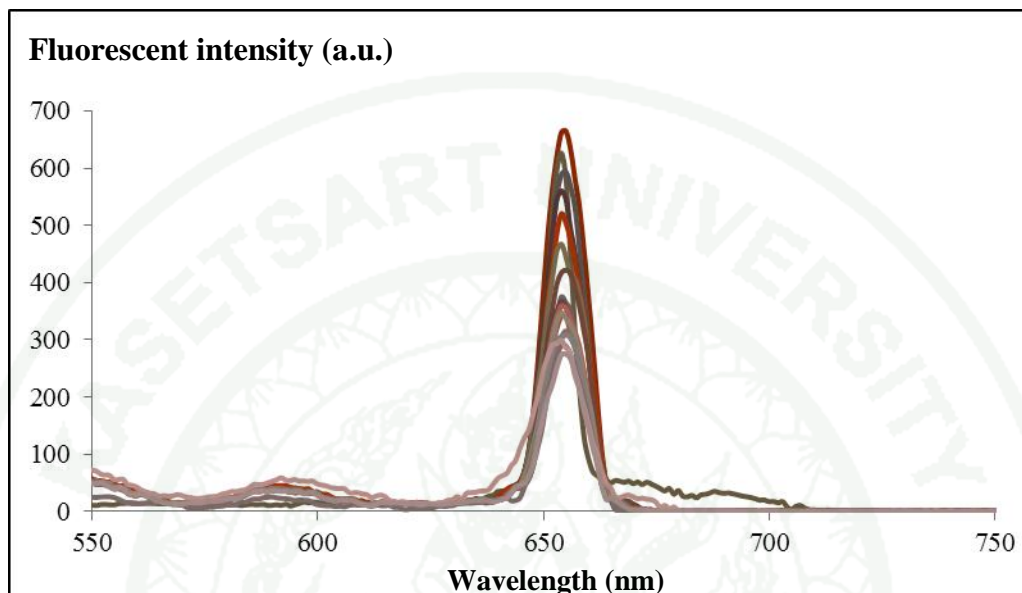


Figure 45 Fluorescent titration emission spectra of TBTPP (25 μM) upon the addition of different concentration of Hg^{2+} (0-30 μM) in ethanol solution. The excitation and emission wavelength are 424 and 650 nm respectively.

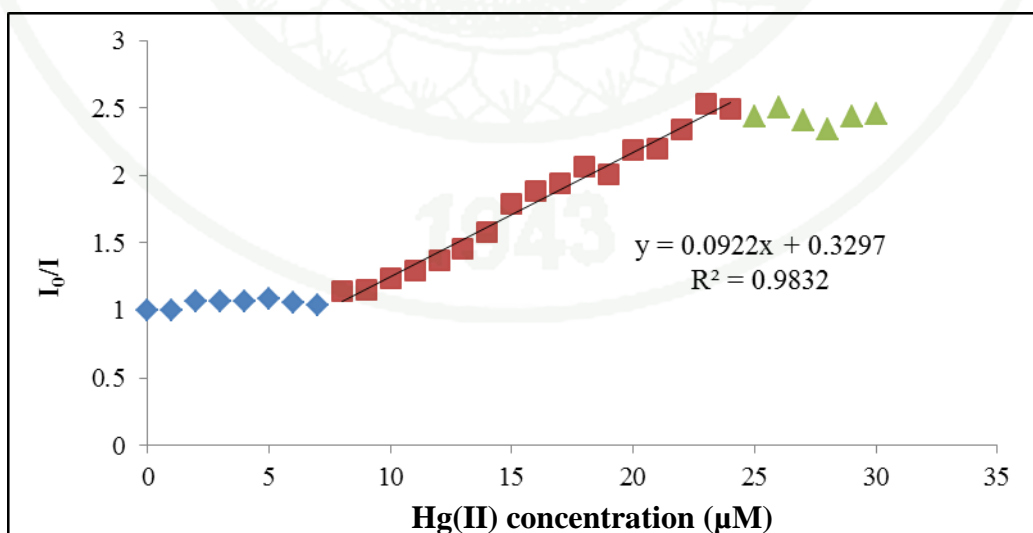


Figure 46 The plot of relative fluorescence intensity (I_0/I) as a function of Hg^{2+} concentration.

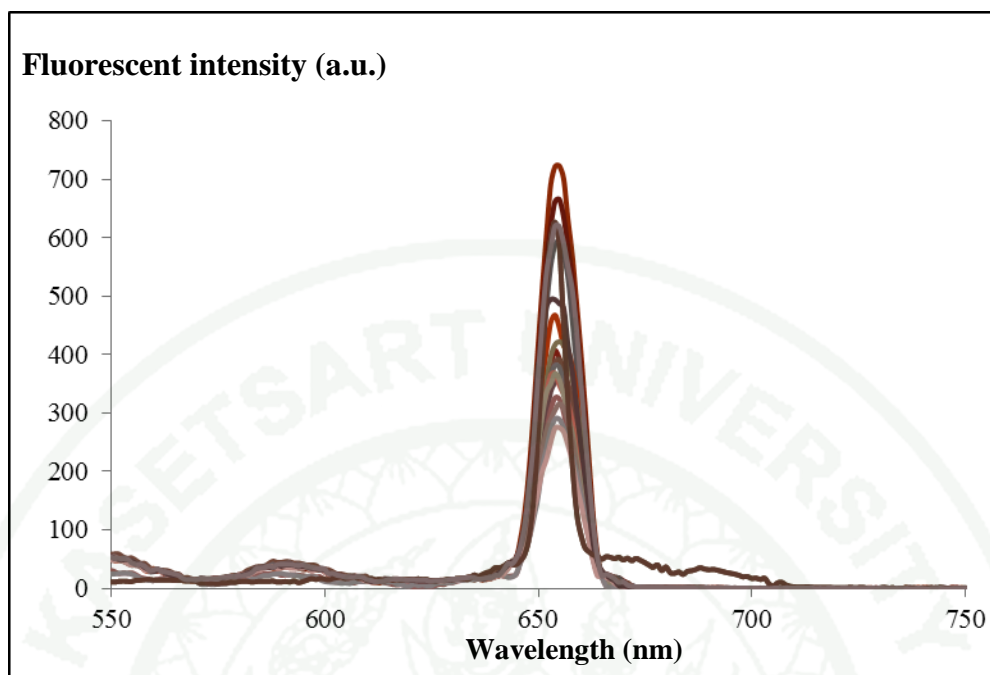


Figure 47 Fluorescent titration emission spectra of TNPP (25 μ M) upon the addition of different concentration of Hg²⁺ (0-30 μ M) in ethanol solution. The excitation and emission wavelength are 424 and 653 nm respectively.

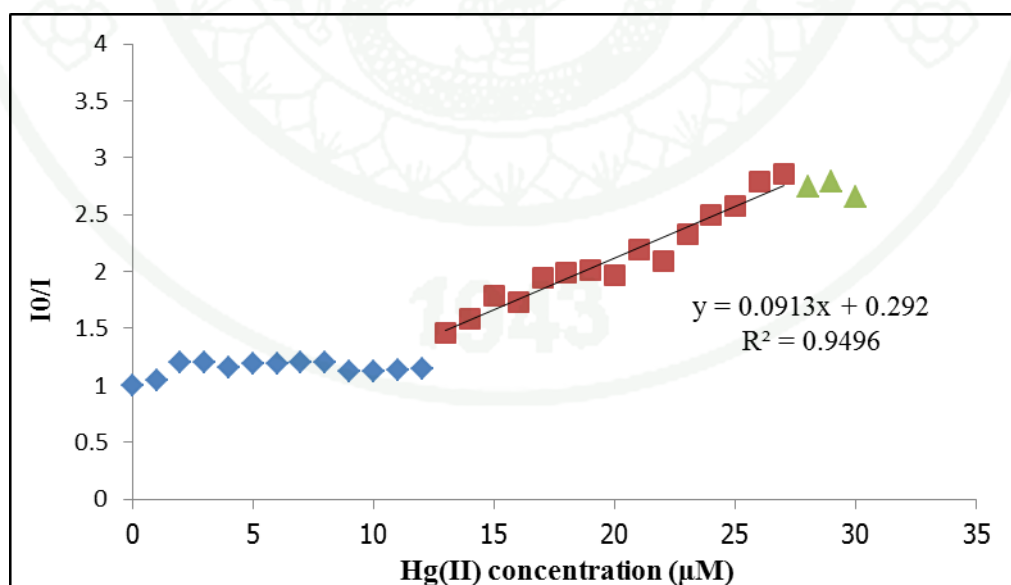


Figure 48 The plot of relative fluorescence intensity (I_0/I) as a function of Hg²⁺ concentration.

The linear range and limit of detection (L.O.D) for determining Hg^{2+} by TBTPP and TNPP were studied. From Figure 46 and 48, the fluorescent emission spectra of TBTPP and TNPP in THF showed a sharp band with a maximum at 650 nm and 653 nm respectively. When Hg^{2+} was added to the solution of TBTPP and TNPP, fluorescence quenching in TBTPP and TNPP were observed. To determine the amount of Hg^{2+} required to induce the complete fluorescence quenching from TBTPP and TNPP, fluorescent titration experiments were carried out as shown in Figure 46 and 48 respectively. When an equivalent of Hg^{2+} was added, the emission of TBTPP and TNPP were almost completely quenched, indicating the binding of Hg^{2+} to TBTPP and TNPP ring forming Hg-TBTPP and Hg-TNPP complexes as previously described. Then, the fluorescence responses of TBTPP and TNPP with various concentrations of Hg^{2+} at 650 nm and 653 nm respectively, they were plotted as shown in Figure 46 and 48. The increasing of I_0/I (where I_0 = fluorescence intensity of TBTPP and TNPP without Hg^{2+} and I = fluorescence intensity of TBTPP and TNPP in the presence of different concentrations of Hg^{2+}) in the fluorescence responses were deviated from Beer's law when the concentration of Hg^{2+} was higher and lower than 24 and 8 μM respectively for TBTPP and was higher and lower than 27 and 13 μM respectively for TNPP. Therefore, this can be concluded that the linear range for determining Hg^{2+} was in the range of 8-24 μM with the regression line $y = 0.0922x + 0.3297$ ($R^2 = 0.9832$), where y = fluorescence intensity of TBTPP in the presence of Hg^{2+} and x = concentration of Hg^{2+} . In contrast with TNPP, it can be concluded that the linear range for determining Hg^{2+} was in the range of 12-27 μM with the regression line $y = 0.0913x + 0.292$ ($R^2 = 0.9496$), where y = fluorescence intensity of TNPP in the presence of Hg^{2+} and x = concentration of Hg^{2+} .

In addition, the fluorescence titration of TNPP upon the addition of different concentrations of Hg^{2+} in methanol were also studied. It was found that fluorescence response didn't change even concentration of Hg^{2+} in methanol changed. The fluorescence responses of TNPP with various concentrations of Hg^{2+} at 653 nm, it was plotted as shown in Appendix D.

In addition, the limit of detection (L.O.D) for determining Hg^{2+} could be calculated. There is a trend to define the limit of detection as the analyte concentration giving a signal equal to the blank signal, y_B , plus three standard deviations of the blank, $3SB$: $L.O.D = y_B + 3SB$ (Miller, 2000). From the equation, L.O.D of the analysis of Hg^{2+} by TBTPP and TNPP were 1.92 and 1.94 μM , which equivalent to 1.79 and 1.54 ppm respectively. The calculation of L.O.D for the analysis of Hg^{2+} by TBTPP and TNPP are shown in Appendix D.

3.6 Interference ion of the analysis of Hg^{2+} by TBTPP and TNPP

The effect of interference cations and anions for the analysis of Hg^{2+} were studied. Some metal cations and anions were selected to use as interference ion. In this study, the fluorescence responses of TBTPP and TNPP with Hg^{2+} in the presence of each interference ion were investigated at three replicates. The average fluorescence intensity and standard deviation of three replicates of Hg^{2+} concentration were calculated. It was found that the analysis of Hg^{2+} could be accepted in the range of fluorescence intensities from 439.660 to 646.319 and 724.094 to 742.616 (99 % confidence) for the study the effect of interference on the analysis of Hg^{2+} by TBTPP and TNPP respectively.

When interfering metal cations and anions at various concentrations were added to the solution of TBTPP and TNPP with Hg^{2+} , the change in the fluorescence intensity comparing to the solution of TBTPP and TNPP respectively, which has only Hg^{2+} , could indicate the effect of interference cations and anions on the analysis of Hg^{2+} . The cations and anions will consider to have the interfering effect, when the analysis fluorescence intensity of each solution is out of the acceptable range. Table 8 and Table 9 show the results of interference metal cations and anions effecting on the analysis of Hg^{2+} .

Table 8 Fluorescent sensing of Hg^{2+} by using of TBTPP in the presence of interfering cations and anions.

Ion	Molar ratio of interference ion : Hg^{2+}					
	0.005:1	0.02:1	0.1:1	0.5:1	1:1	10:1
Ag^+	-	-	-	-	+	+
Co^{2+}	-	-	+	+	+	+
Cd^{2+}	-	-	-	-	+	+
Ni^{2+}	-	-	+	+	+	+
Cr^{2+}	-	-	+	+	+	+
Fe^{3+}	-	-	+	+	+	+
Cu^{2+}	-	-	+	+	+	+
Zn^{2+}	-	-	+	+	+	+
Ru^{3+}	-	-	-	+	+	+
CN^-	-	-	-	-	-	-
SCN^-	-	-	-	-	-	-
CO_3^{2-}	-	-	-	-	-	-
NO_3^-	-	-	-	-	-	-
Cl^-	-	-	-	-	-	-

+ = Interfere, - = Not interfere

At the high concentration level, all cations have effect on the analysis of Hg^{2+} , whereas at the low concentration level ($< 0.1:1$) they do not interfere the analysis of Hg^{2+} . Cations Co^{2+} , Ni^{2+} , Cu^{2+} and Zn^{2+} are borderline acid that can interact with borderline bases (pyrrolic nitrogens of TBTPP), for this reason, they can effect on the analysis of Hg^{2+} more than other cations and anions used in this experiment. In addition, Cr^{2+} and Fe^{3+} have small radius, they can be introduced into the center of porphyrin ring to effect on the analysis of Hg^{2+} . In contrast, Ag^+ and Cd^{2+} are soft acid, they have a bigger radius. Consequently, they have a slightly effect to the Hg^{2+} in coordinating with TBTPP. In addition, all investigated anions do

not interfere with the determination of Hg^{2+} by TBTPP even at high concentration. This may be because they cannot interact with pyrrolic nitrogens of TBTPP.

Table 9 Fluorescent sensing of Hg^{2+} by using of TNPP in the presence of interfering cations and anions.

Ion	Molar ratio of interference ion : Hg^{2+}					
	0.005:1	0.02:1	0.1:1	0.5:1	1:1	10:1
Ag^+	-	-	-	+	+	+
Co^{2+}	-	-	+	+	+	+
Cd^{2+}	-	-	-	+	+	+
Ni^{2+}	-	-	+	+	+	+
Cr^{2+}	-	-	+	+	+	+
Fe^{3+}	-	-	-	+	+	+
Cu^{2+}	-	+	+	+	+	+
Zn^{2+}	-	+	+	+	+	+
Ru^{3+}	-	+	+	+	+	+
CN^-	-	-	-	-	-	-
SCN^-	-	-	-	-	-	-
CO_3^{2-}	-	-	-	-	-	-
NO_3^-	-	-	-	-	-	-
Cl^-	-	-	-	-	-	-

+ = Interfere, - = Not interfere

At the high concentration level, all cations have effect on the analysis of Hg^{2+} , whereas at the low concentration level (< 0.02:1) they do not interfere the analysis of Hg^{2+} . Cations Cu^{2+} , Zn^{2+} and Ru^{3+} can effect on the analysis of Hg^{2+} more than other cations and anions used in this experiment. They are borderline acid that can interact with borderline bases (pyrrolic nitrogens of TNPP). Moreover, all investigated anions do not interfere with the determination of Hg^{2+} by TNPP even at

high concentration. This may be because they cannot interact with pyrrolic nitrogens of TNPP.

Table 10 The classification of Lewis acids and bases.

	Hard	Borderline	Soft
Acids	H ⁺ , Li ⁺ , Na ⁺ , K ⁺ , Be ²⁺ , Mg ²⁺ , Ca ²⁺ , Al ³⁺ , Cr ²⁺ , Co ³⁺ , Fe ³⁺ , Mn ²⁺	Fe ²⁺ , Co ²⁺ , Ni ²⁺ , Cu ²⁺ , Zn ²⁺ , Rh ³⁺ , Ir ³⁺ , Ru ³⁺ , Os ²⁺	Cu ⁺ , Ag ⁺ , Au ⁺ , Cd ²⁺ , Hg ²⁺ , Hg ²⁺ , CH ₃ Hg ⁺ , Pd ²⁺ , Pt ²⁺ , Pt ⁴⁺
Bases	F ⁻ , Cl ⁻ , H ₂ O, OH ⁻ , O ²⁻ , NH ₃ , CO ₃ ²⁻ , NO ₃ ⁻ , ClO ₄ ⁻ , SO ₄ ²⁻ , PO ₄ ³⁻	Br ⁻ , NO ₂ ⁻ , N ₃ ⁻ , N ₂ , SO ₃ ²⁻ , C ₆ H ₅ NH ₂ , C ₅ H ₅ N	H ⁻ , I ⁻ , H ₂ S, HS ⁻ , S ²⁻ , SCN ⁻ , CN ⁻ , S ₂ O ₃ ²⁻ , C ₂ H ₄ , C ₆ H ₆

Source: Miessler (2004)

3.7 Investigation of structure of TBTPP complexes and TNPP complexes by computational calculation

According to the experimental results, the stability constant of the Hg-TBTPP complex was higher than Hg-TNPP complex. Therefore, the quantum chemical calculation of these complexes have been studied and compared to the other TBTPP complexes (Pb-TBTPP and Cd-TBTPP) for Hg-TBTPP complex. Moreover, the quantum chemical calculation of Hg-TNPP complex has been studied and compared to the other TNPP complexes (Pb-TNPP and Cd-TNPP). TBTPP and TNPP are tetradentate ligand which can form complexes with metal cations by using pyrrolic nitrogen as donor atoms. The optimized geometries of possible complexes (Figure 54 to Figure 58) were calculated by using the Density Functional Theory (DFT) at B3LYP level of theory with 6-31G* basis set for each atom on porphyrin and the effective core potential (ECP) of LanL2DZ for each metal cation. The

stabilization energies of the possible complex structures were determined by these equations

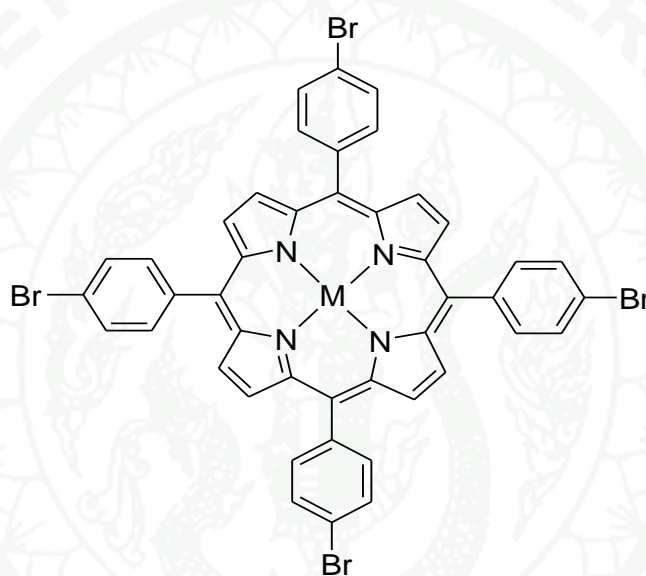


Figure 49 Postulated structure of Metal-TBTPP complex, where M= Hg, Pb, Cd.

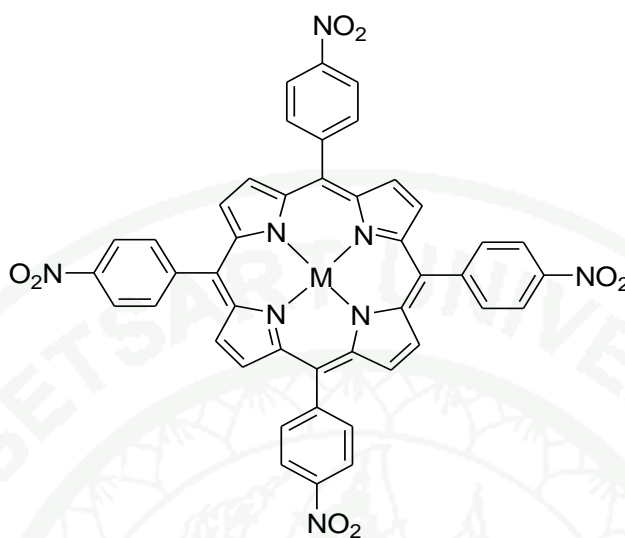


Figure 50 Postulated structure of Metal-TNPP complex, where M= Hg, Pb.

The structure of H_2TBTPP , $TBTPP^{2-}$ and H_2TNPP are shown in Figure 51-53. From the optimized structures, the holes of H_2TBTPP , H_2TNPP and $TBTPP^{2-}$ are about 4.2 Å. This confirmed that, electron-withdrawing group (-Br and $-NO_2$) caused make the larger hole of H_2TBTPP , H_2TNPP and $TBTPP^{2-}$ than *meso*-tetraphenylporphyrin (TPP), which is about 4.0 Å. The hole of TPP was calculated by the same method of H_2TBTPP , $TBTPP^{2-}$ and H_2TNPP .

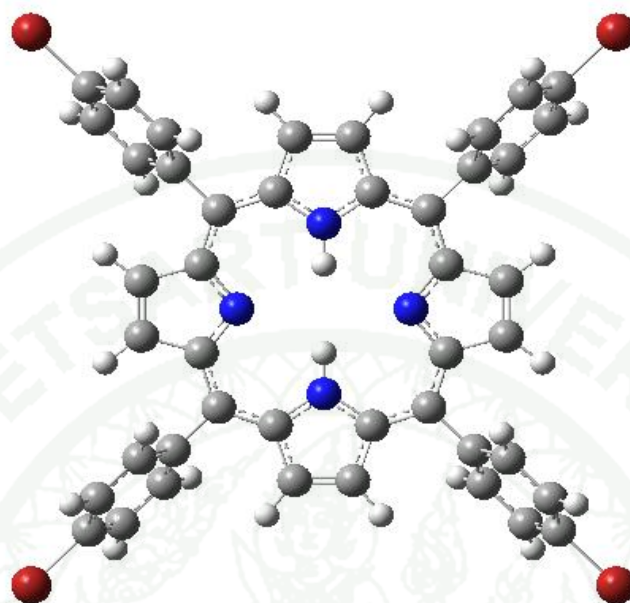


Figure 51 The optimized structure of ligand H_2TBTPP .

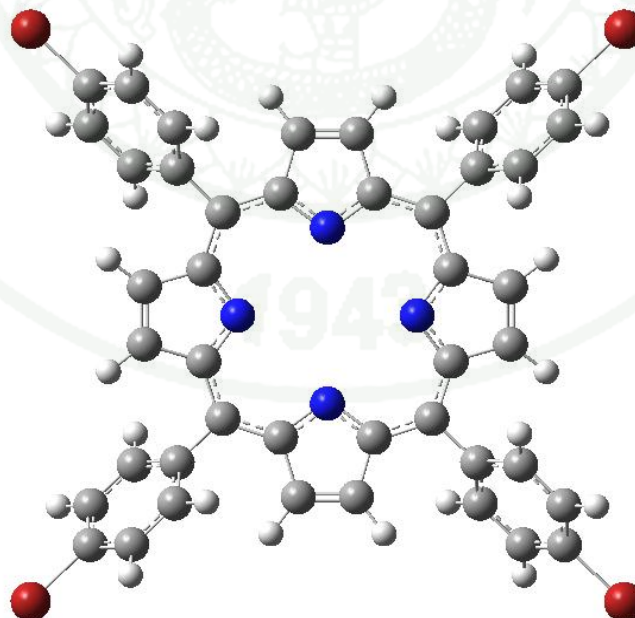


Figure 52 The optimized structure of ligand $TBTPP^{2-}$.

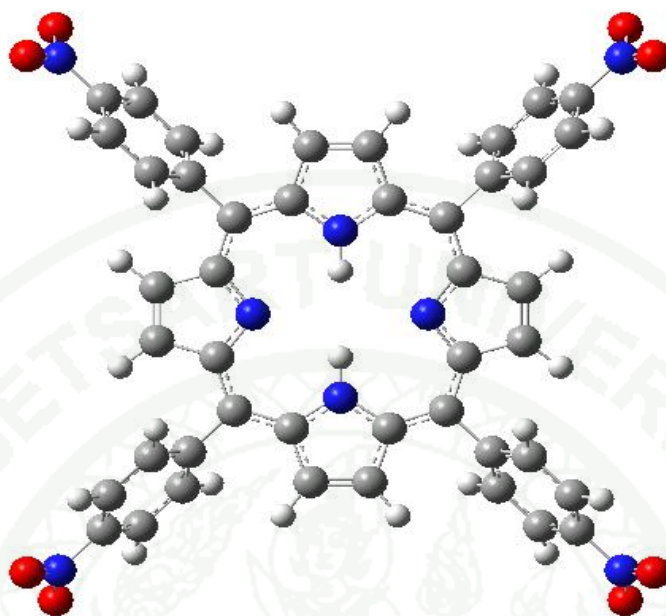


Figure 53 The optimized structure of ligand H₂TNPP.

In addition, comparing with the ionic radius of metal cations (Table 11), it can be seen that all of the cations have a size smaller than the hole of H₂TBTPP, TBTPP²⁻ and H₂TNPP, therefore, all of them might be able to coordinate with H₂TBTPP, TBTPP²⁻ and H₂TNPP ligand. From the results of optimizing the structures and the stabilization energies of complexes by computational calculation, it was found that Hg²⁺ and Pb²⁺ could form complexes with H₂TBTPP, TBTPP²⁻ and H₂TNPP. Moreover, Cd²⁺ could form complexes with H₂TBTPP and TBTPP²⁻.

Table 11 Ionic radii of some metal cations at coordination number of 6.

Ion	Ionic radii (pm)
Hg(II)	116
Ag(I)	129
Co(II)	89
Cd(II)	109
Ni(II)	83
Cr(III)	76
Fe(III)	79
Cu(II)	87
Pb(II)	175

Source: Miessler (2004)

The optimized structures of M-TBTPP and M-TNPP complexes obtained from quantum chemical calculation are displayed in Figure 54-56 and Figure 57-58, respectively. It can be seen that metals cations were fitted in the porphyrin hole.

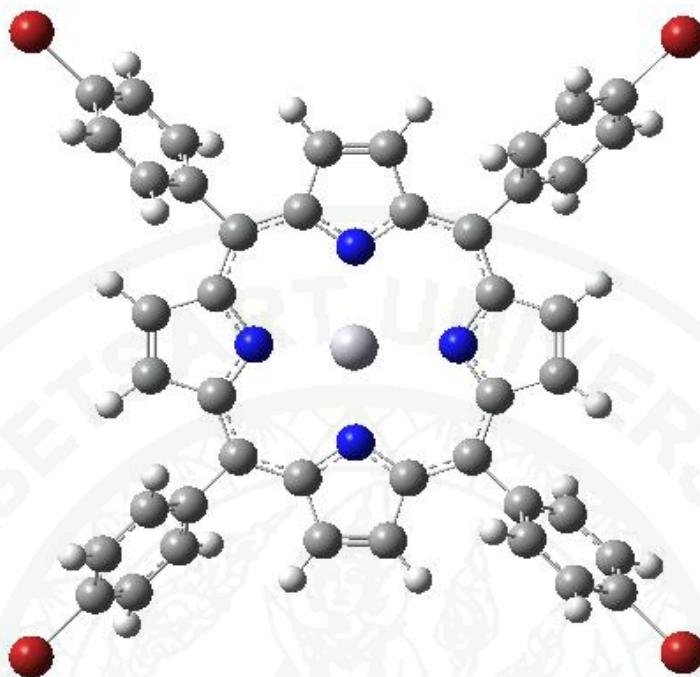


Figure 54 The optimized structure of Hg-TBTPP

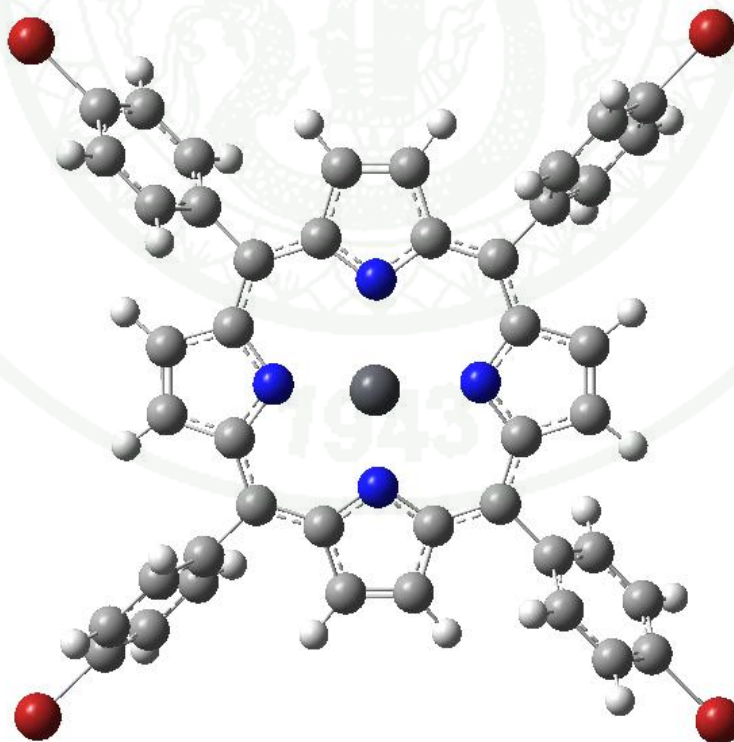


Figure 55 The optimized structure of Pb-TBTPP

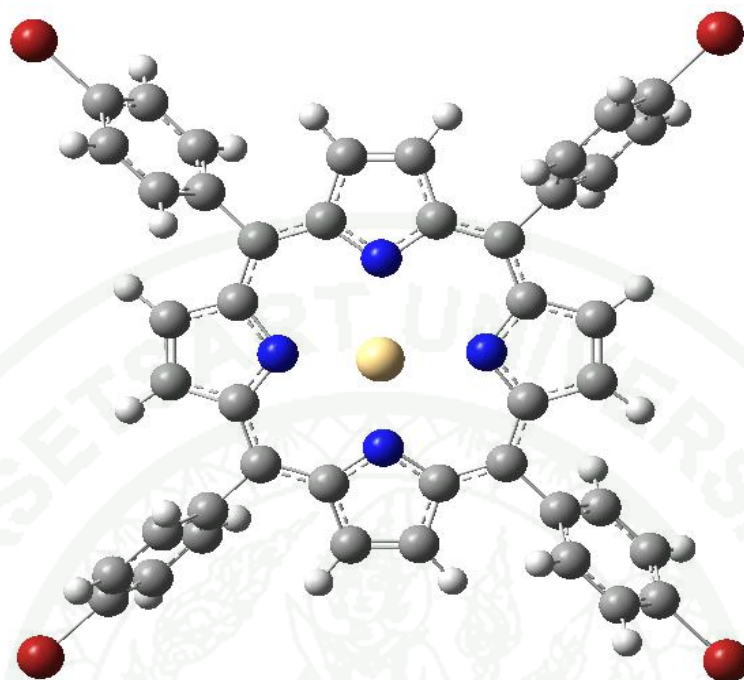


Figure 56 The optimized structure of Cd-TBTPP

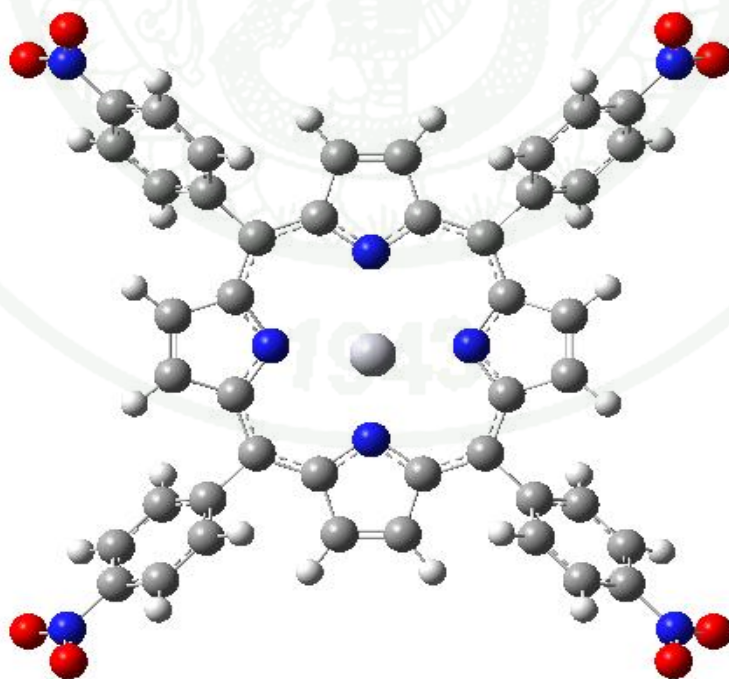


Figure 57 The optimized structure of Hg-TNPP

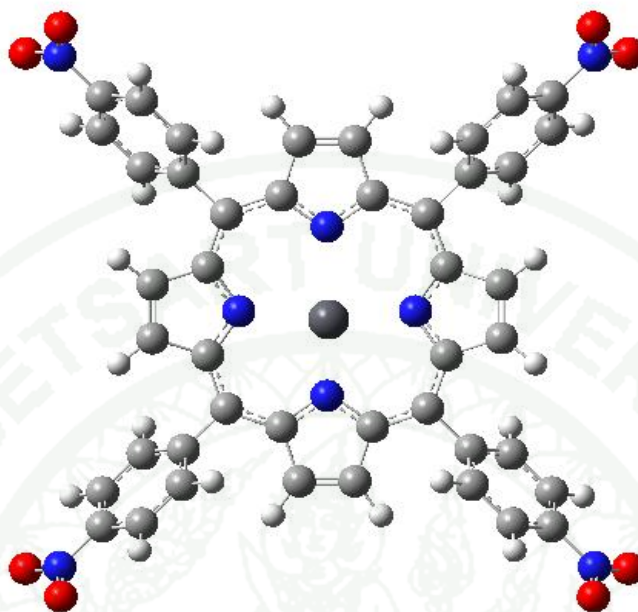


Figure 58 The optimized structure of Pb-TNPP

The possible formation routes of these complexes should be as followed:



The stabilization energies of porphyrin formation in route (a), (c) are illustrated in Table 12 and route (b) is also illustrated in Table 13, Examples of the calculations are shown in Appendix F. The stabilization energies of complexes in route (a) is more positive than stabilization energies of porphyrin complexes in route (b). It indicated that the metallation of metal into the porphyrin ring is a stepwise mechanism, which is interpreted in term of two steps including the loss of protons (route (a)) and metallation steps route (route (b)). Furthermore, the stabilization energies of Hg-TBTPP complex in route (a) and (b) are more negative than Hg-TNPP complex (route (c)). These results indicated the higher selectivity of TBTPP

for the Hg^{2+} than the selectivity of TNPP. In addition, These also indicated that the selectivity of TBTPP to the Hg^{2+} higher than Pb^{2+} and Cd^{2+} .

Table 12 Energetic data of isolated atoms, molecules and possible structure of TBTPP and TNPP complexes calculated at B3LYP level of theory using 6-31G* and LandL2DZ basis set in route (a, c).



Atoms, molecules and complexes	Figure	Total energies (a.u.)	Stabilization Energies (a.u.)	Stabilization Energies (kcal/mol)
<u>Atoms and molecules</u>				
Hg^{2+}	-	-41.79347	-	-
Pb^{2+}	-	-2.65346	-	-
Cd^{2+}	-	-47.15587	-	-
H_2TBTPP	51	-12198.16906	-	-
H_2TNPP	52	-2731.75398	-	-
<u>Complexes</u>				
Hg-TBTPP	54	-12240.99139	-1.0288573	-645.618
Pb-TBTPP	55	-12199.30282	+1.5196980	+953.626
Cd-TBTPP	56	-12243.87062	+1.4543126	+912.596
Hg-TNPP	57	-2773.97827	-0.4081800	-256.137
Pb-TNPP	58	-2733.99719	+0.4102470	+257.434

Table 13 Energetic data of isolated atoms, molecules and possible structure of TBTPP complexes calculated at B3LYP level of theory using 6-31G* and LandL2DZ basis set in route (b).



Atoms, molecules and complexes	Figure	Total energies (a.u.)	Stabilization Energies (a.u.)	Stabilization Energies (kcal/mol)
<u>Atoms and molecules</u>				
Hg ²⁺	-	-41.793473	-	-
Pb ²⁺	-	-2.653458	-	-
Cd ²⁺	-	-47.155873	-	-
TBTPP ²⁻	51	-12196.922342	-	-
H ₂ TNPP	53	-2731.753980	-	-
<u>Complexes</u>				
Hg-TBTPP	54	-12240.99139	-2.27558	-1427.930
Pb-TBTPP	55	-12199.30282	+0.27298	+171.298
Cd-TBTPP	56	-12243.87062	+0.20759	+130.265
Hg-TNPP	57	-2773.97827	-0.40818	-256.137
Pb-TNPP	58	-2733.99719	+0.41025	+257.434

CONCLUSION AND RECOMMENDATIONS

Conclusion

The porphyrins, 5,10,15,20-Tetra(*p*-bromophenyl)porphyrin and 5,10,15,20-Tetra(*p*-nitrophenyl)porphyrin were synthesized by the reaction of pyrrole with *p*-bromobenzaldehyde and *p*-nitrobenzaldehyde respectively in the presence of acid catalyst. Each compound was characterized by FT-IR and ^1H NMR spectroscopy. The results indicated that the synthesized products were TBTPP and TNPP.

TBTPP and TNPP could be applied as the ratiometric fluorescence chemosensor for the analysis of Hg^{2+} . It was found that the analysis of Hg^{2+} by using TBTPP and TNPP were attributed to the metallation of Hg^{2+} to the TBTPP and TNPP ring respectively. The stoichiometric of complex formation between TBTPP and Hg^{2+} verified by continuous variation and mole ratio methods showed that the ratio of Hg^{2+} with TBTPP was 1:1. Moreover, The stoichiometric of complex formation between TNPP and Hg^{2+} verified by mole ratio methods showed that the ratio of Hg^{2+} with TNPP was 1:1. According to Benesi-Hildebrand's equation, the stability constants of Hg-TBTPP and Hg-TNPP were 1.00×10^6 and 6.67×10^5 , respectively. The structures of complexes were studied by theoretical calculation optimized by using 6-31G* and LanL2DZ basis sets at B3LYP level theory. It was found that the diameter of TBTPP hole as same as diameter of TNPP hole, also TBTPP and TNPP can act as tetradentate ligand by using four pyrrolic nitrogen atoms to coordinate to Hg^{2+} . Moreover, TBTPP could coordinate with Hg^{2+} better than TNPP because bromo group of TBTPP act as both electron withdrawing and electron donating groups. The bromo group can accept electron by inductive effect and can donate electron by resonance effect. Therefore, bromo group of TBTPP could increase electron density of porphyrin ring better than nitro group of TNPP, which was only electron-withdrawing groups. Consequently, the coordination of TBTPP with Hg^{2+} was more stable than TNPP. These results could confirm by the stabilization energies, it was found that the stabilization energies of Hg-TBTPP was

lower than stabilization energies of Hg-TNPP, consequently, Hg-TBTTP complex was more stable than Hg-TNPP complex. Moreover, the results showed that the metallation mechanism was a stepwise mechanism which was interpreted in term of two steps including the loss of protons and metallation steps, and the metallation route may be $M^{n+} + \text{TBTTP}^{2-} \rightleftharpoons [M(\text{TBTTP})]^{n-2}$. Besides, the results indicated that the selectivity of TBTTP with Hg^{2+} higher than the selectivity of TNPP with Hg^{2+} . For the analytical performance of TBTTP and TNPP for determining Hg^{2+} , the linear range was found to be in the range of 8-24 and 12-27 μM with the detection limit of 1.92 and 1.94 μM for TBTTP and TNPP, respectively. The interfering effects on the analysis of Hg^{2+} by various ions were studied. It was found that TBTTP and TNPP had highly selective to Hg^{2+} , when the concentration of interference cations was lower than 10 and 20 folds of Hg^{2+} concentration. Anions seem not to interfere with the analysis of Hg^{2+} by both TBTTP and TNPP even at high concentration.

Moreover, the synthesized TBTTP and TNPP can be applied as chemosensor for Hg^{2+} in aqueous solution at low concentration of interference cations such as Ag^+ , Cd^{2+} , Co^{2+} , Ni^{2+} , Cr^{2+} , Fe^{3+} , Cu^{2+} , Zn^{2+} and Ru^{3+} .

Recommendations

There are some points need to be studied in order to improve this research work. Firstly, the purification processes of synthesized TBTPP and TNPP need to be improved, resulting in the better efficiency of the Hg^{2+} analysis. Besides, the quantum chemical calculations should be concerned with the solvent effect. In addition, in case of square-based pyramid complexes will be changed from square planar complexes which are used in these calculations, so it need to be concerned about spin multiplicity calculation of complexes for precisely calculating of total energies of complexes.

LITERATURE CITED

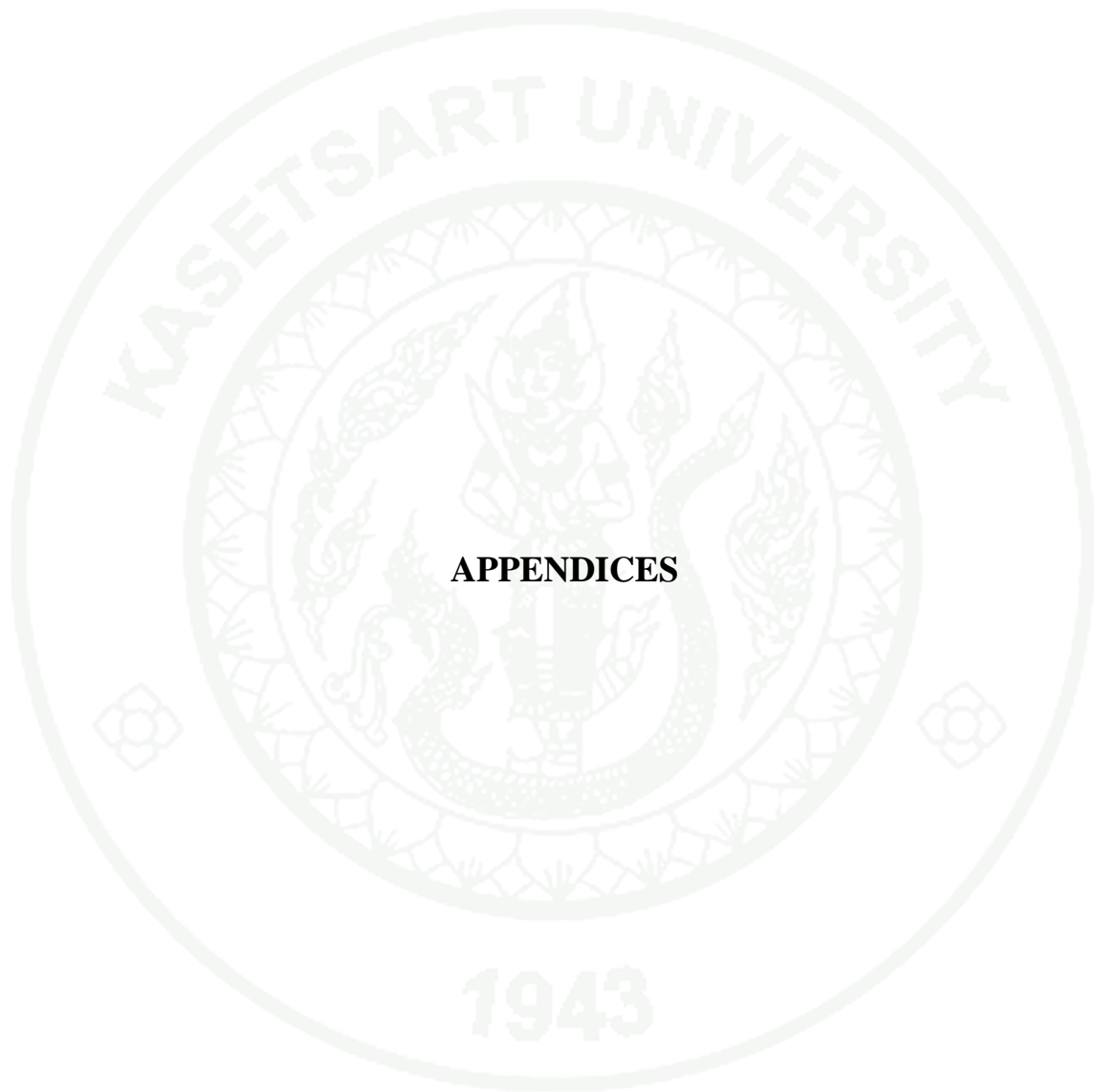
- Albani, J.R. 2004. **Structure and Dynamics of Macromolecules: Absorption and Fluorescence Studies**. Elsevier Science, Amsterdam.
- Alder, A.D., F.R. Longo, J.D. Finarelli, J. Goldmacher, J. Assour and L. Korsakoff. 1967. A simplified synthesis for meso-tetraphenylporphine. **J. Org. Chem.** 32(2): 476.
- Benesi, H.A. and J.H. Hildebrand. 1949. A spectrophotometric investigation of the interaction of iodine with aromatic hydrocarbons. *J. Am. Chem. Soc.* 70: 2703-2707.
- Bozkurt, S.S., S. Ayata and I. Kaynak. 2009. Fluorescence-based sensor for Pb(II) using tetra-(3-bromo-4-hydroxyphenyl)porphyrin in liquid and immobilized medium. **Spectrochim. Acta Part A.** 72: 880-883.
- Chatterjee, S.R., S.J. Shetty, T.P.A. Devasagayam and T.S. Srivastava. 1997. Photocleavage of plasmid DNA by the porphyrin meso-tetrakis[4-(9-carboxymethyleneoxy)phenyl]porphyrin. **J. Photochem. Photobiol. B: Biology.** 41(1-2): 128-135.
- Cornors, K.A. 1987. **Binding Constants: The measurement of molecular complex stability**. Wiley Interscience, New York.
- Díez S. 2008. Human health effects of methylmercury exposure. **Rev. Environ. Contam. Toxicol.** 198: 111-125.
- Engelen, M. 2006. **New molecular scaffolds for the construction of complex biomolecules**. Ph.D. Thesis, University of Naples.

- Falk, J.E. 1964. **Porphyrins and metalloporphyrins**. Elsevier Publishing Company. New York.
- Greenwood, N.N. and A. Earnshaw. 1997. **Chemistry of the element**. 2nd ed. Butterworth-Heinemann, Oxford.
- Guo, L., W. Zhang, Z. Xie, X. Lin and G. Chen. 2006. An organically modified sol-gel membrane for detection of mercury ions by using 5,10,15,20-tetraphenylporphyrin as a fluorescence indicator. **Sens. Actuators B**. 119: 209-214.
- Hu, J., I. Pavel, D. Moigno, M. Wumaier, W. Kiefer, Z. Chen, Y. Ye, Q. Wu, Q. Huang, S. Chen, F. Niu, Y. Gu. 2003. Fourier-transform Raman and infrared spectroscopic analysis of 2-nitro-tetraphenylporphyrin and metallo-2-nitro-tetraphenylporphyrins. **Spectrochim Acta Part A**. 59: 1929-1935.
- Hu, S., H. Mao and Y. Wang. 2009. Optical sensing of heavy metal ions in anions micellar solution using a Pd porphyrin phosphorescent probe. **J. Photochem. Photobiol. A: Chemistry**. 204: 1-6.
- Itagaki, Y., K. Deki, S.I. Nakashima and Y. Sadaoka. 2005. Toxic gas detection using porphyrin dispersed polymer composites. **Sens. Actuators B**. 108: 393-397.
- Jaung, J.Y. 2007. Synthesis of new porphyrins with dicyanopyrazine moiety and their optical properties. **Dyes Pigm.** 72: 315-321.
- Kim, L.B., J.J. Leonard and F.R. Longo. 1972. A Mechanistic Study of the Synthesis and Spectral Properties of *meso*-Tetraarylporphyrins. **J. Am. Chem. Soc.** 94(11): 3986-3992.

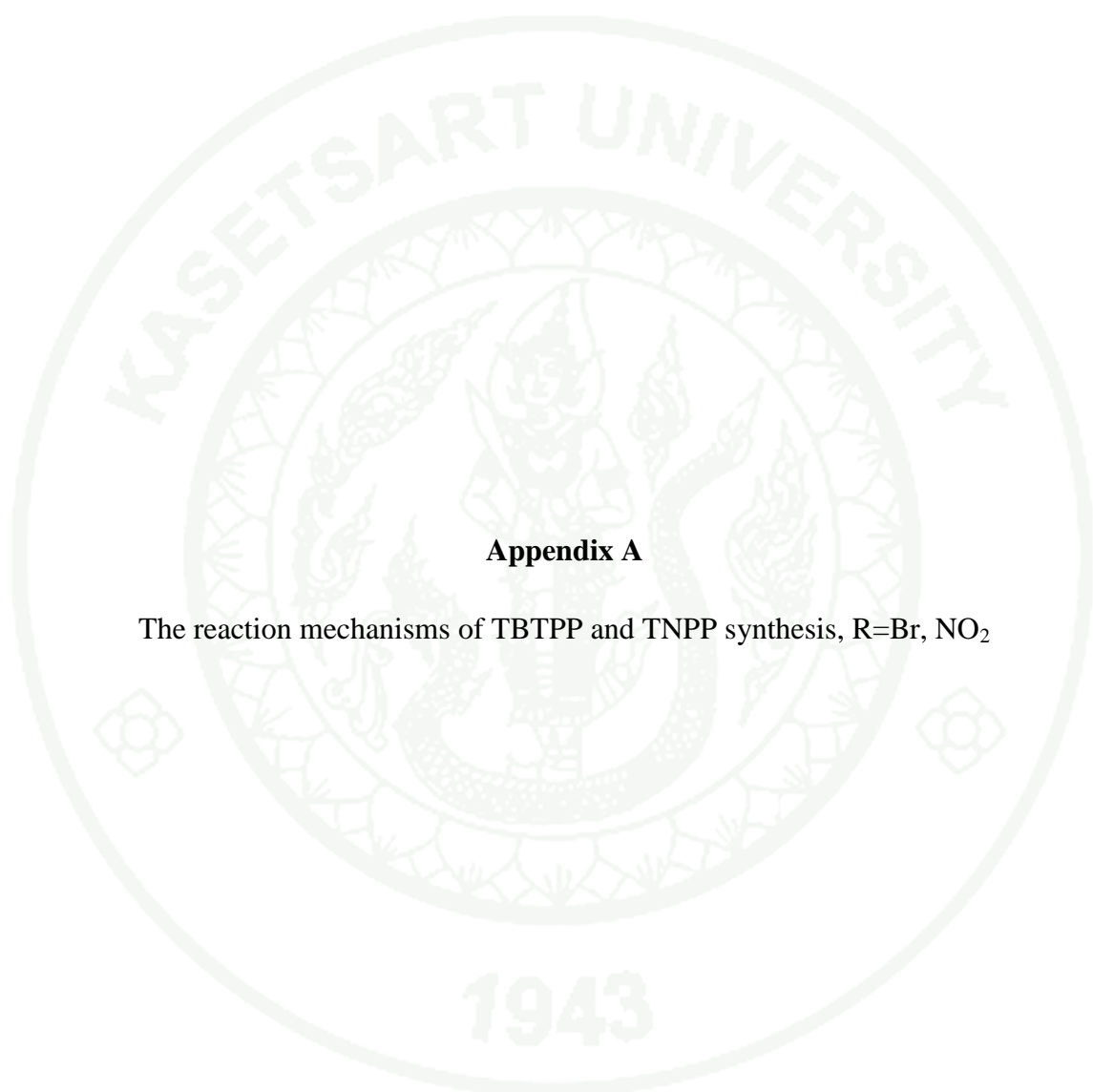
- Kim, J., S.H. Lim, Y. Yoon, T.D. Thangadurai and S. Yoon. 2011. A fluorescent ammonia sensor based on a porphyrin cobalt(II)-dansyl complex. **Tetrahedron Lett.** 52: 2645-2648.
- Kruper, W.J., T.A. Chamberlin, and M. Kochanny. 1989. Regiospecific aryl nitration of meso-substituted tetraarylporphyrins: a simple route to bifunctional porphyrins. **J. Org. Chem.** 54(11): 2753-2756.
- Lakowicz, J.R. 1999. Principles of Fluorescence Spectroscopy (2nd edⁿ). Kluwer Academic/Plenum Publishers. New York, London, Moscow, Dordrecht.
- Lee, C., D.H. Lee and J.I. Hong. 2001. Colorimetric anion sensing by porphyrin-based anion receptors. **Tetrahedron Lett.** 42: 8665-8668.
- Li, C.Y., F. Xu and Y.F. Li. 2010. A fluorescent chemosensor for silver ions based on porphyrin compound with high selectivity. **Spectrochim. Acta Part A.** 76: 197-201.
- Li, C.Y., X.B. Zhang, Y.Y. Dong, Q.J. Ma, Z.X. Han, Y. Zhao, G.L. Shen and R.Q. Yu. 2008. A porphyrin derivative containing 2-(oxymethyl)pyridine units showing unexpected ratiometric fluorescent recognition of Zn²⁺ with high selectivity. **Anal. Chim. Acta.** 616: 214–221.
- Li, L. and A.R. Barron. 2011. **Physical Methods in Inorganic and Nano Chemistry: the application of fluorescence spectroscopy in the mercury ion detection.** Rice University. New York.
- Lindsey J.S. 2010. Synthetic Routes to *meso*-Patterned Porphyrins. **Acc. Chem. Res.** 43(2): 300-311.

- Luguya R., L.Jaquinod, F.R. Fronczek, M.G.H. Vicente and K.M. Smith. 2004. Synthesis and reactions of meso-(p-nitrophenyl)porphyrins. **Tetrahedron**. 60: 2757-2763.
- Luo H.Y., J.H. Jiang, X.B. Zhang, C.Y. Li, G.L. Shen and R.Q. Yu. 2007. Synthesis of porphyrin-appended terpyridine as a chemosensor for cadmium based on fluorescent enhancement. **Talanta**. 72: 575-581.
- Miessler, G.L. and D.A. Tarr. 2004. **Inorganic Chemistry**. 3rd ed. Pearson Education International, New Jersey.
- Moss, G.P. 1988. **Nomenclature of Tetrapyrroles**. Queen Mary College. London.
- Ostrowski S., A. Mikus and B. Łopuszyńska. 2004. Synthesis of highly substituted meso-tetraarylporphyrins. **Tetrahedron**. 60: 11951-11957.
- Plaschke, M., R. Czolk and H.J. Ache. 1995. Fluorimetric determination of mercury with a water-soluble porphyrin and porphyrin-doped sol-gel films. **Anal. Chim. Acta**. 304: 107-113.
- Quimby, D.J. and F.R. Longo. 1974. Luminescence Studies on Several Tetraarylporphyrins and Their Zinc Derivatives. **J. Am. Chem. Soc.** 97: 5111-5116.
- Rothmund, P. 1936. A new porphyrin synthesis. The synthesis of porphin. **J. Am. Chem. Soc.** 58(4): 625-627.
- Shi, D.F. and R.T. Wheelhouse. 2002. A novel, high-yielding synthesis of meso-substituted porphyrins via the direct arylation of porphine. **Tetrahedron Lett.** 43: 9341-9342.

- Skoog, D.A. 1992. **Principles of instrumental analysis**. Saunders College Publishing. New York.
- Starnes, S.D., S. Arungundram and C.H. Saunders. 2002. Anion sensors based on β , β' -disubstituted porphyrin derivatives. **Tetrahedron Lett.** 43: 7785-7788.
- Temelli, B. and C. Unaleroglu. 2009. Synthesis of meso-tetraphenyl porphyrins via condensation of dipyrromethanes with N-tosyl imines. **Tetrahedron.** 65: 2043-2050.
- Valeur, B. 2002. **Molecular Fluorescence: Principles and Applications**. Wiley-VCH. Weinheim.
- Valeur, B., I. Leray. 2000. Design principles of fluorescent molecular sensors for cation recognition. **Coord. Chem. Rev.** 205: 3-40.
- Wade, L.G. 1999. **Organic Chemistry**. 4th ed. Prentice Hall International, New Jersey.
- Weng, Y.Q., F. Yue, Y.R. Zhong and B.H. Ye. 2007. A copper(II) ion-selective on-off-type fluoroionophore based on zinc porphyrin-dipyridylamino. **Inorg. Chem.** 46: 7749-7755.
- Weng, Y.Q., F. Yue, Y.R. Zhong and Y.L. Teng. 2007. A new selective fluorescent chemosensor for Cu(II) ion based on zinc porphyrin-dipyridylamino. **Inorg. Chem. Commun.** 10: 443-446.
- Yang, Y., J. Jiang, G. Shen and R. Yu. 2009. An optical sensor for mercury ion based on the fluorescence quenching of tetra(*p*-dimethylaminophenyl)porphyrin. **Anal. Chim. Acta.** 636: 83-88.

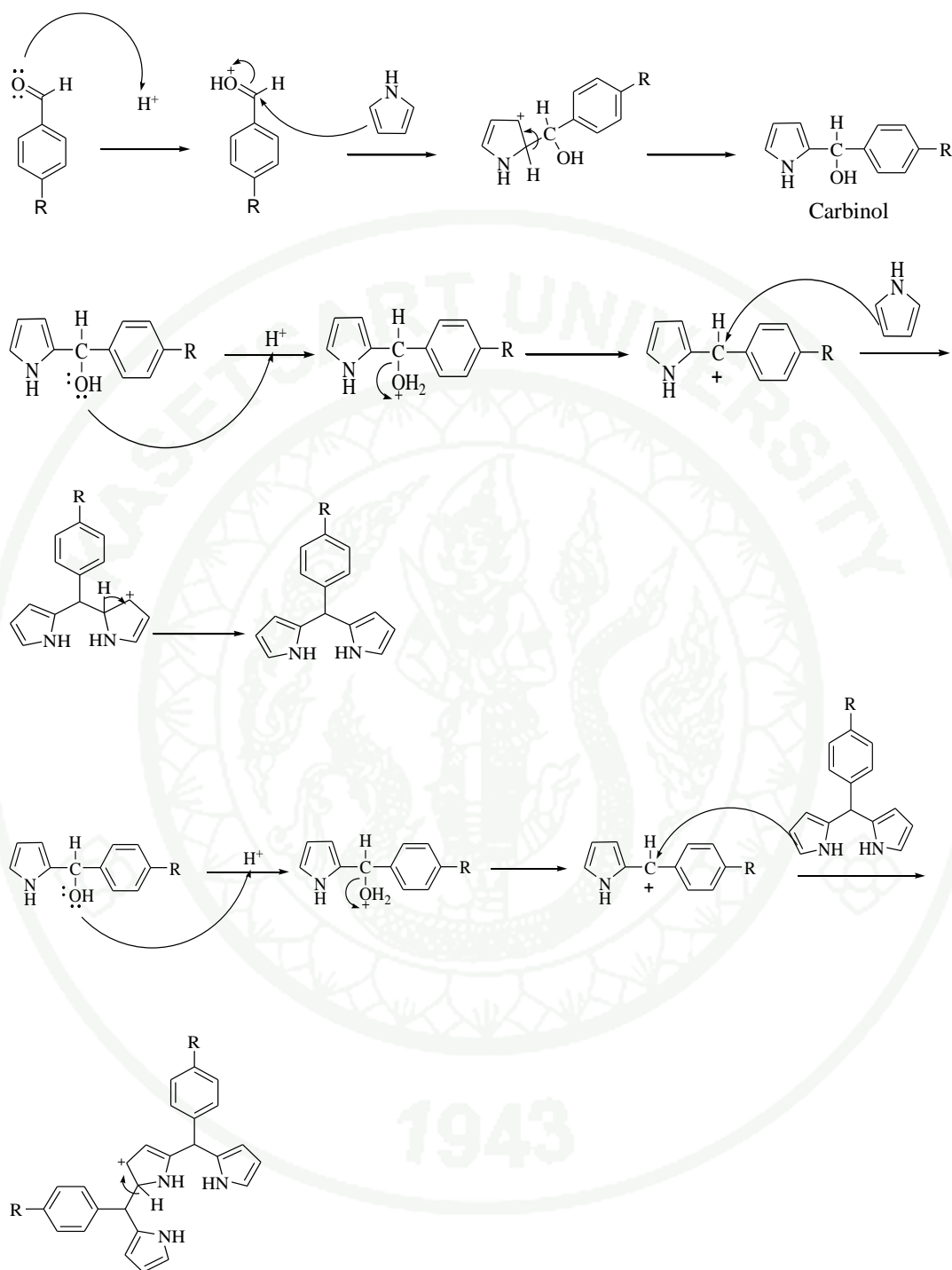


APPENDICES

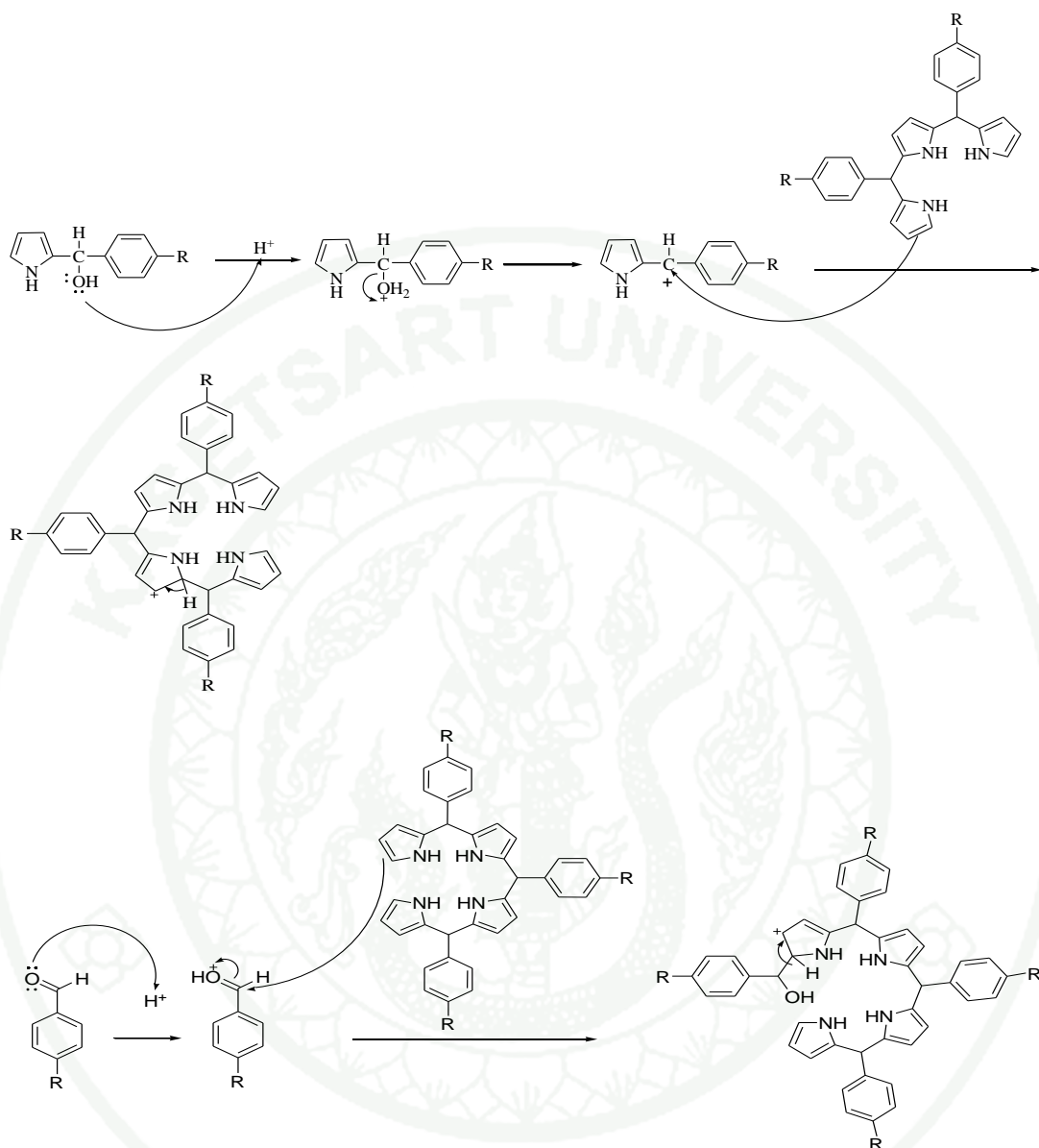


Appendix A

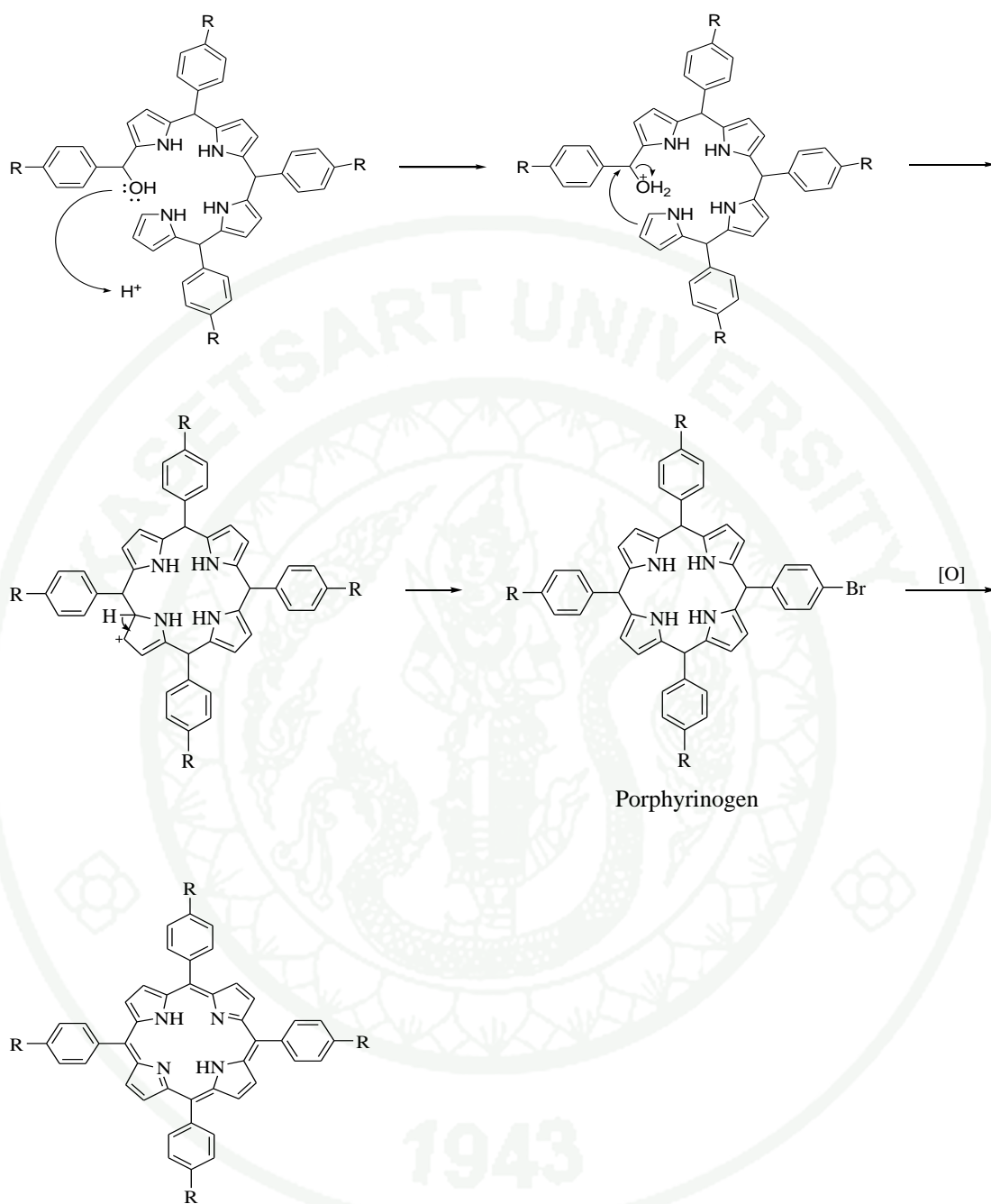
The reaction mechanisms of TBTPP and TNPP synthesis, R=Br, NO₂



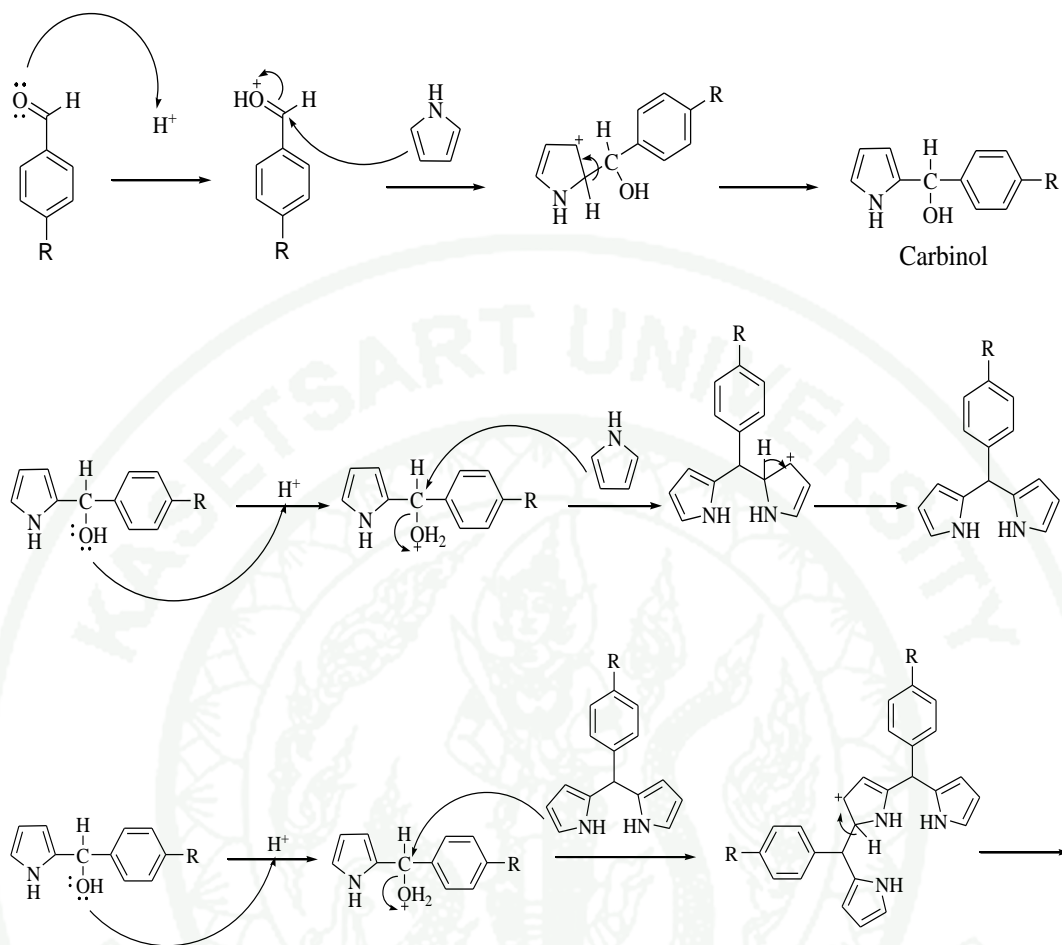
Appendix Figure A1 The S_N1 reaction mechanisms of TBTPP and TNPP synthesis, R=Br, NO_2 .



Appendix Figure A1 (Continued).

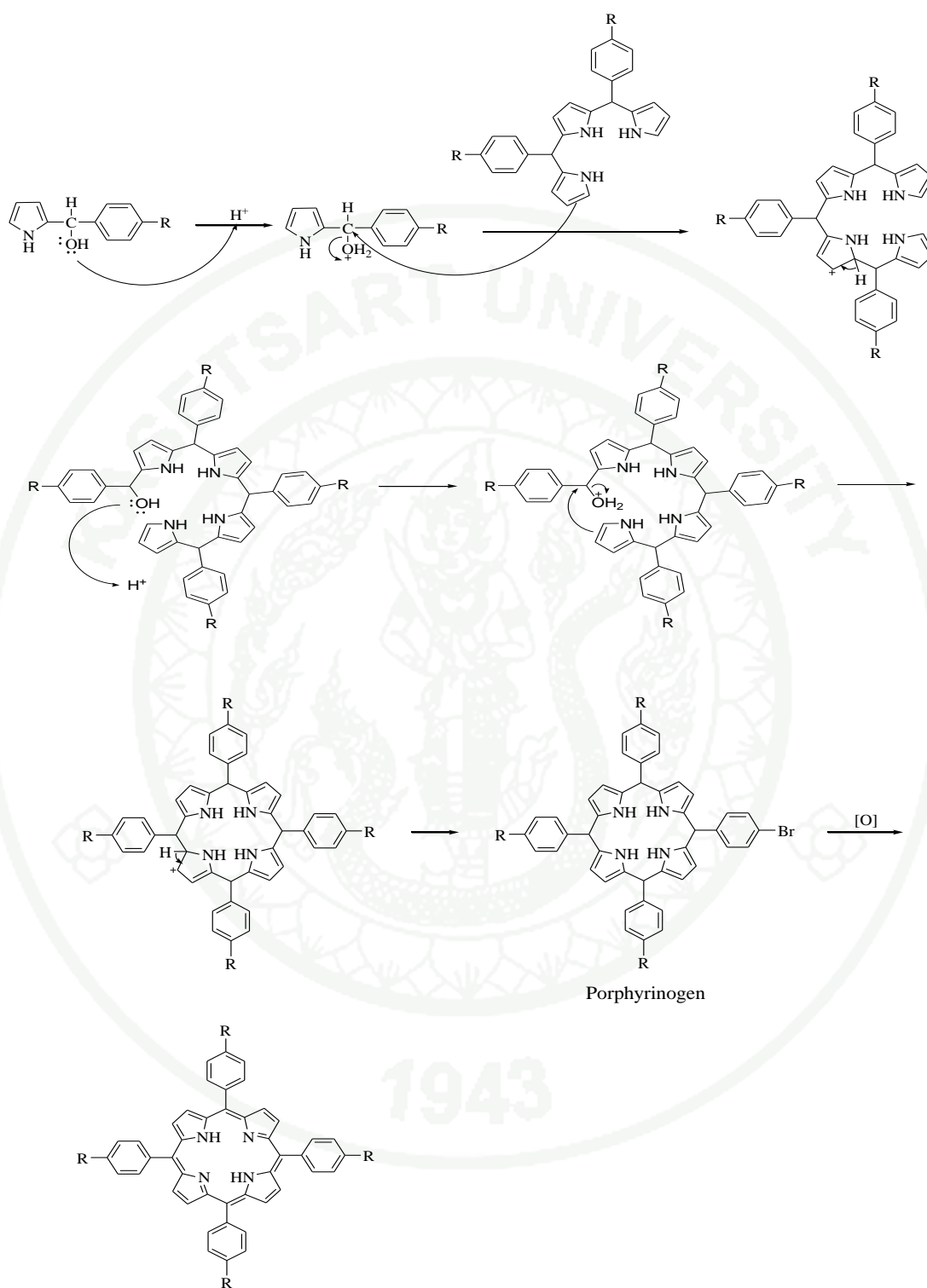


Appendix Figure A1 (Continued).

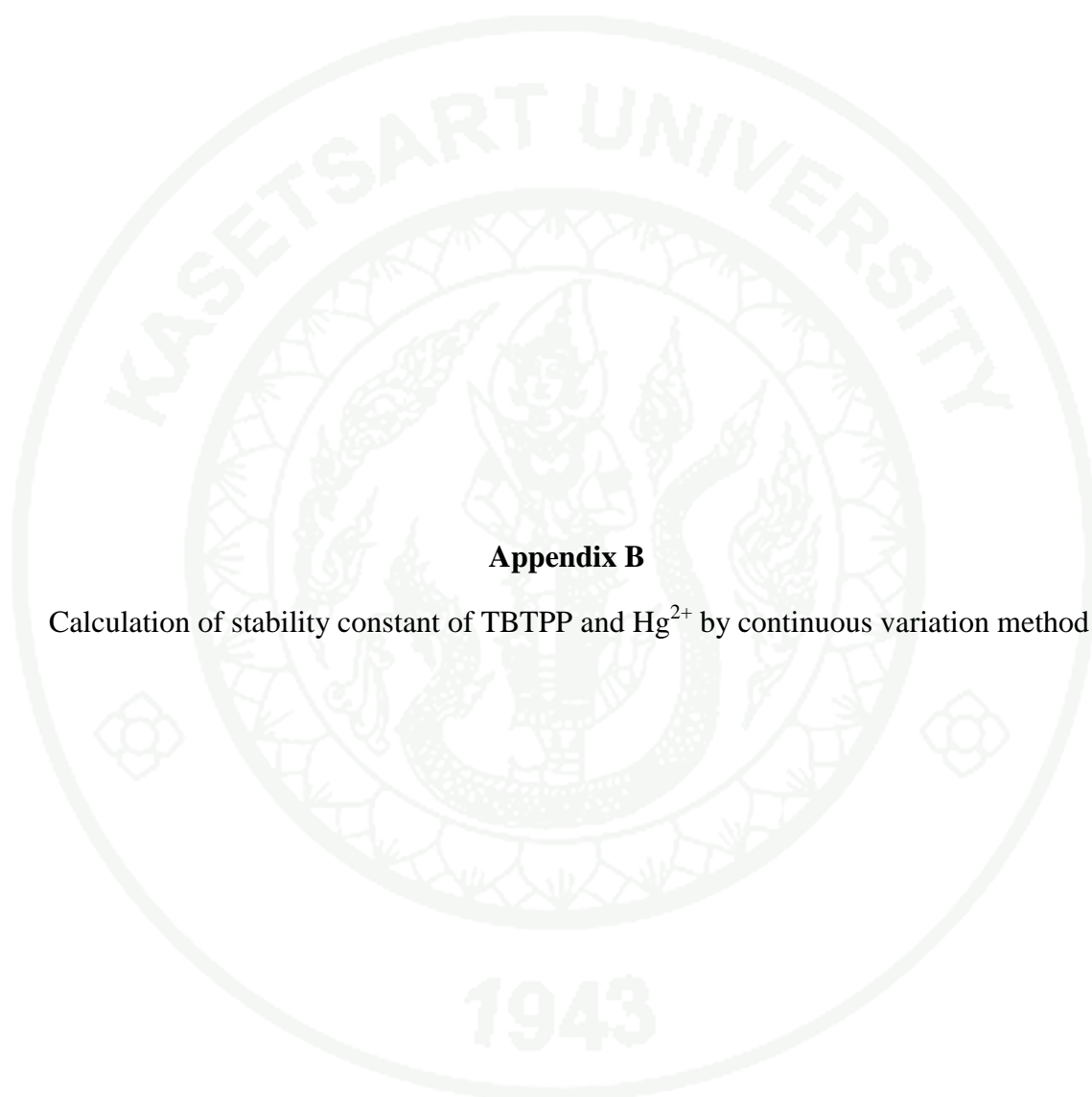


Appendix Figure A2 The S_N2 reaction mechanisms of TBTPP and TNPP synthesis, R=Br, NO_2 .

1943



Appendix Figure A2 (Continued).



Appendix B

Calculation of stability constant of TBTPP and Hg^{2+} by continuous variation method

For the continuous variation method (Connors, 1987), stability constant (K_{stab}) of the complex can be evaluated from measurements of the deviations from the theoretical straight line, which represent the curve that would result if the reaction between the ligand and the metal produced to completion.

TBTPP-Hg complex



$$K_{\text{stab}} = \frac{[\text{Hg}(\text{TBTPP})]}{[\text{Hg}^{2+}][\text{TBTPP}^{2-}]}$$

$$C_{\text{Hg}} = [\text{Hg}^{2+}] + [\text{Hg}(\text{TBTPP})]$$

$$[\text{Hg}^{2+}] = C_{\text{Hg}} - [\text{Hg}(\text{TBTPP})]$$

$$C_{\text{TBTPP}} = [\text{TBTPP}^{2-}] + [\text{Hg}(\text{TBTPP})]$$

$$[\text{TBTPP}^{2-}] = C_{\text{TBTPP}} - [\text{Hg}(\text{TBTPP})]$$

When C_{Hg} = total concentration of Hg^{2+}

C_{TBTPP} = total concentration of TBTPP

$[\text{Hg}(\text{TBTPP})]$:

$\text{Hg}(\text{TBTPP})$ was prepared by mixing of Hg^{2+} standard 0.1 mM with TBTPP 0.1 mM.

When $V_{\text{Hg}^{2+}}$ and $V_{\text{TBTPP}} = 0.500$ ml

So, initial concentration of C_{Hg} and C_{TBTPP} are

$$C_{\text{Hg}} = (0.500 \text{ ml})(1.0 \times 10^{-4} \text{ M}) = \frac{5.0 \times 10^{-6} \text{ M}}{10.0 \text{ ml}}$$

$$C_{\text{TBTPP}} = \frac{(0.500 \text{ ml})(1.0 \times 10^{-4} \text{ M})}{10.0 \text{ ml}} = 5.0 \times 10^{-6} \text{ M}$$

If the complex is stable, two straight lines are intercepted and thus the complex concentration is equal to the original concentration of metal ion.

When $[\text{ML}] = [\text{Hg}(\text{TBTPP})]$

$$\begin{aligned} [\text{Hg}(\text{TBTPP})]_{\text{ex}} &= [\text{ML}]_{\text{ex}} = C_{\text{Hg}} \\ A_{\text{ex}} &= \epsilon b [\text{ML}]_{\text{ex}} = \epsilon b C_{\text{Hg}} \end{aligned}$$

When A = The highest absorbance from the curvature of the experiment

A_{ex} = The highest absorbance from the theoretical straight line

but

$$A = \epsilon b [\text{ML}]$$

$$\frac{A}{A_{\text{ex}}} = \frac{\epsilon b [\text{ML}]}{\epsilon b C_{\text{Ru}}}$$

So,

$$[\text{ML}] = \frac{A}{A_{\text{ex}}} C_{\text{Hg}}$$

Thus,

$$\begin{aligned} K_{\text{stab}} &= \frac{[\text{Hg}(\text{TBTPP})]}{[\text{Hg}^{2+}][\text{TBTPP}^{2-}]} = \frac{[\text{ML}]}{[\text{Hg}^{2+}][\text{TBTPP}^{2-}]} \\ &= \frac{[\text{ML}]}{[C_{\text{Hg}} - \text{ML}][C_{\text{TBTPP}} - \text{ML}]} \end{aligned}$$

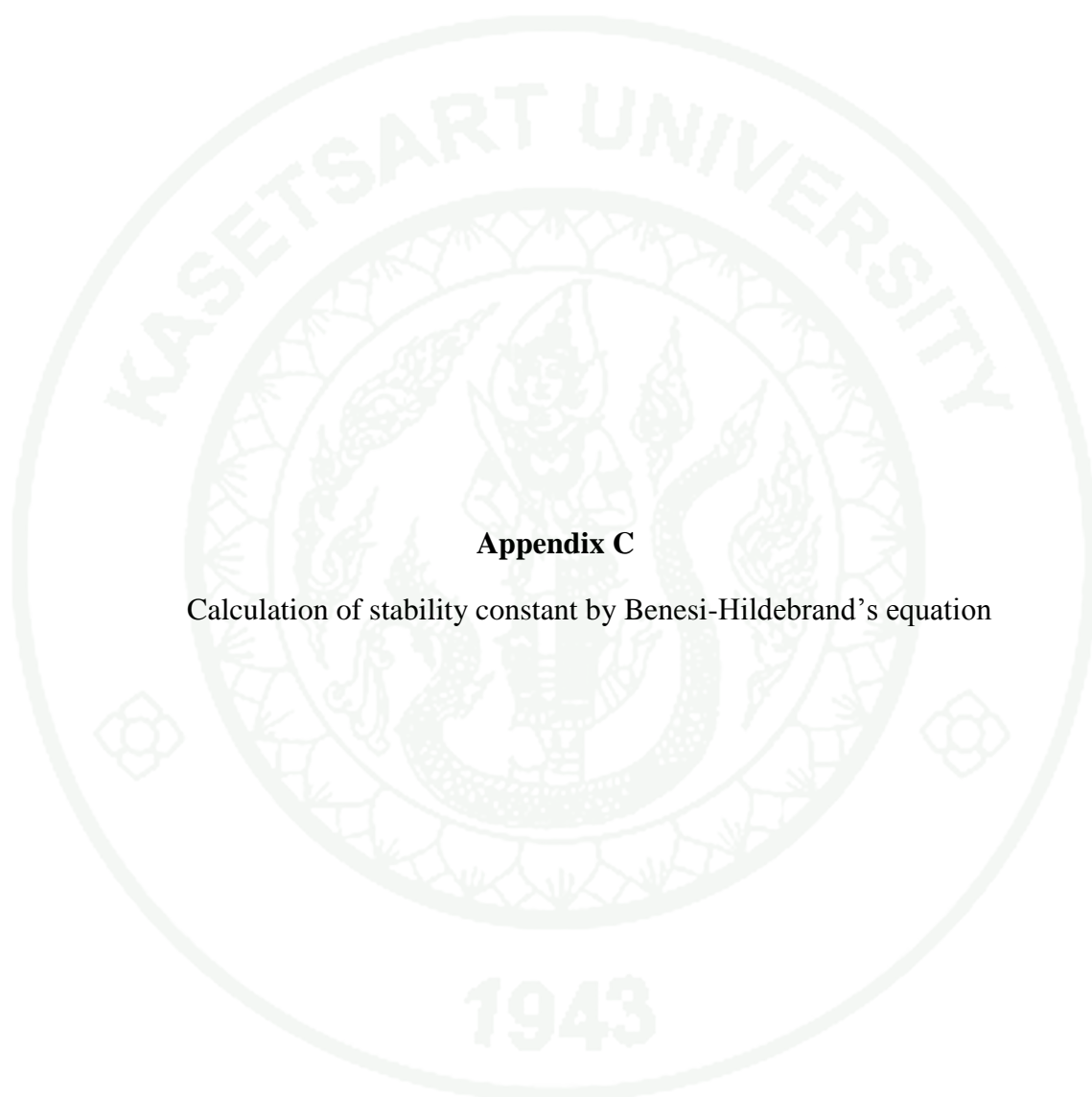
$$\begin{aligned} K_{\text{stab}} &= \frac{\frac{A}{A_{\text{ex}}} C_{\text{Hg}}}{(C_{\text{Hg}} - \frac{A}{A_{\text{ex}}} C_{\text{Hg}})(C_{\text{TBTPP}} - \frac{A}{A_{\text{ex}}} C_{\text{Hg}})} \end{aligned}$$

$$K_{\text{stab}} = \frac{\frac{A}{A_{\text{ex}}}}{\left(1 - \frac{A}{A_{\text{ex}}}\right) \left(C_{\text{TBTPP}} - \frac{A}{A_{\text{ex}}} C_{\text{Hg}}\right)}$$

When $A = 0.265$ and $A_{\text{ex}} = 0.296$

So,
$$K_{\text{stab}} = \frac{0.265 / 0.296}{[1 - (0.265 / 0.296)][5.0 \times 10^{-5} - (0.265 / 0.296)(5.0 \times 10^{-6})]}$$

$$K_{\text{stab}} = 1.87 \times 10^5$$



Appendix C

Calculation of stability constant by Benesi-Hildebrand's equation

The stoichiometric ratio between TBTPP and TNPP with mercury ion and is 1:1

The determination of equilibrium constant, K, the Benesi-Hildebrand equation was applied from equilibrium reaction of complex.



The equilibrium constant for the above reaction is defined by the equation

$$K = \frac{[ML]}{([M]-[ML])([L]-[ML])} \quad \text{----- (2)}$$

Where [ML] is molar concentration of the complex, [M]-[ML] is molar concentration of free metal ion and [L]-[ML] is molar concentration of free ligand.

From Beer's law, the true molar extinction coefficient, ϵ_0 , of the complex at the wavelength of maximum absorption will then be given by the equation

$$\epsilon_0 = \frac{A}{cb} = \frac{A}{[ML]b}$$

$$[ML] = \frac{A}{\epsilon_0 b} \quad \text{-----(3)}$$

In this reaction, ligand is added in excess. Therefore, [L] is much more than [ML]. The [ML] can be eliminated and the equation (2) can be rearranged and obtained as the relationship;

$$K = \frac{[ML]}{([M]-[ML])([L]-[ML])}$$

$$K = \frac{A/\epsilon_0 b}{([M]-A/\epsilon_0 b)[L]}$$

$$K = \frac{A}{\epsilon_0 b[M][L] - [L]A}$$

$$A = K\epsilon_0 b[M][L] - K[L]A$$

$$K\epsilon_0 b[M][L] = A + K[L]A$$

$$K\epsilon_0 b[M][L] = A(1 + K[L])$$

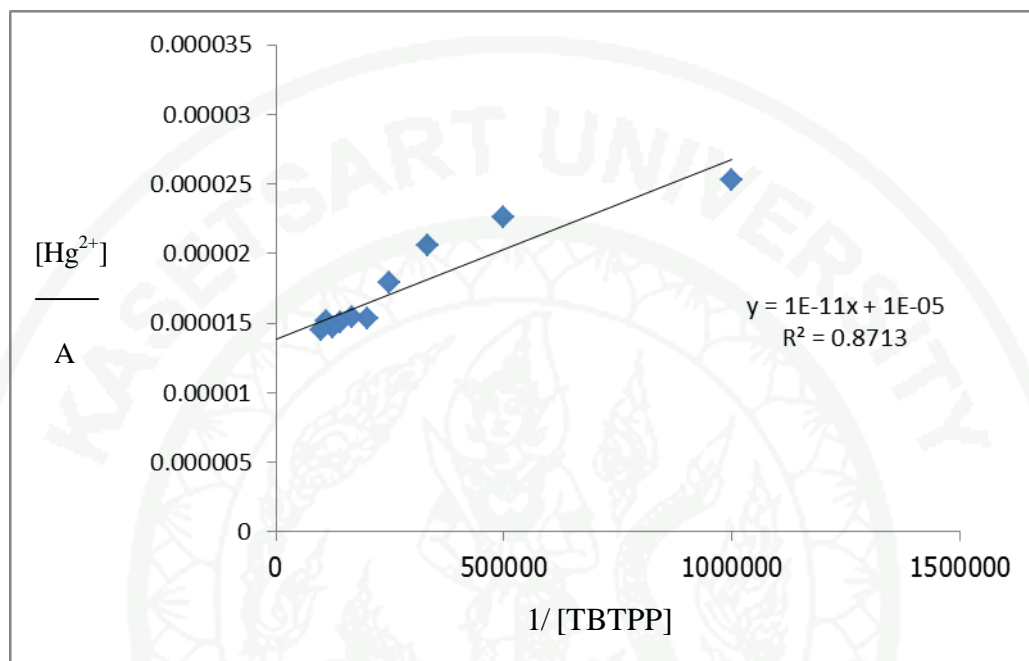
$$\frac{A}{[M]b} = \frac{K\epsilon[L]}{1} + \frac{\epsilon_0}{1} \quad \text{-----(4)}$$

The equation (4) is “Benesi-Hildebrand equation” which is in the form of the linear equation, $y = mx + c$.

For the experiment, the concentration of Hg^{2+} is fixed while the concentrations of ligand are varied. The relationship between $[M]/A$ and $1/[L]$ are plotted as shown in Appendix Figure C1 to Appendix Figure C2.

[Hg(TBTPP)];

The stoichiometric ratio between Hg^{2+} and TBTPP is 1:1.



Appendix Figure C1 The relationship between $[\text{Hg}^{2+}]/A$ and $1/[\text{TBTPP}]$.

The stability constant was obtained from the slope and y-intercept.

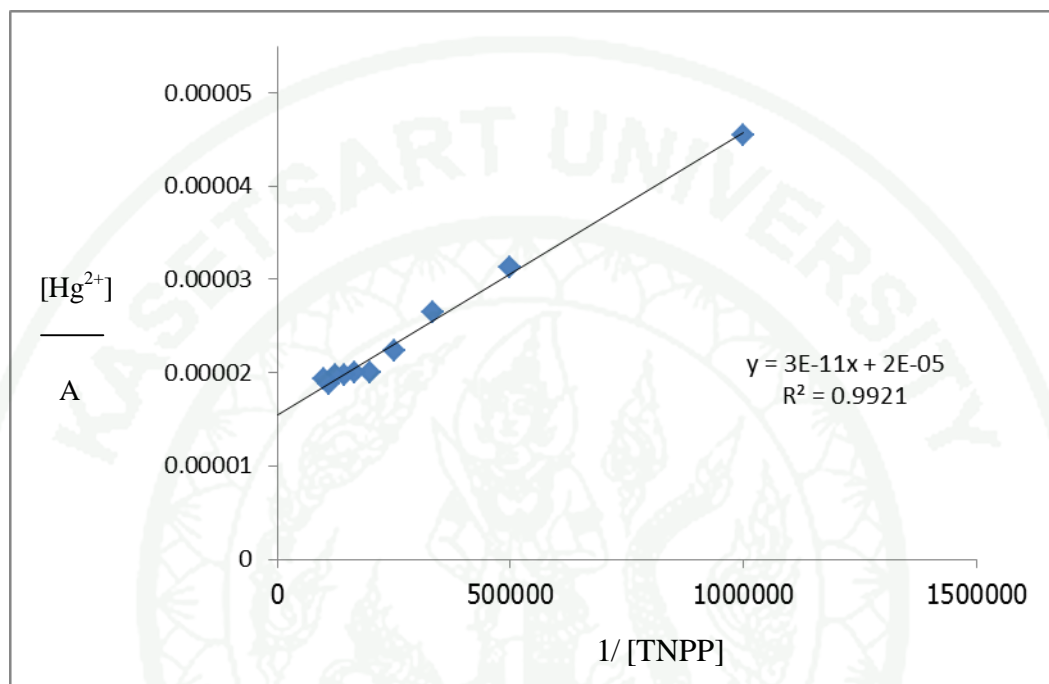
$$\text{Slope} = 1/K\varepsilon_0 = 1.00 \times 10^{-11}$$

$$\text{y-intercept} = 1/\varepsilon_0 = 1.00 \times 10^{-5}$$

$$\text{Stability constant (K}_{\text{stab}}) = \text{y-intercept/slope} = 1.00 \times 10^6$$

[Hg(TNPP)];

The stoichiometric ratio between Hg^{2+} and TNPP is 1:1.



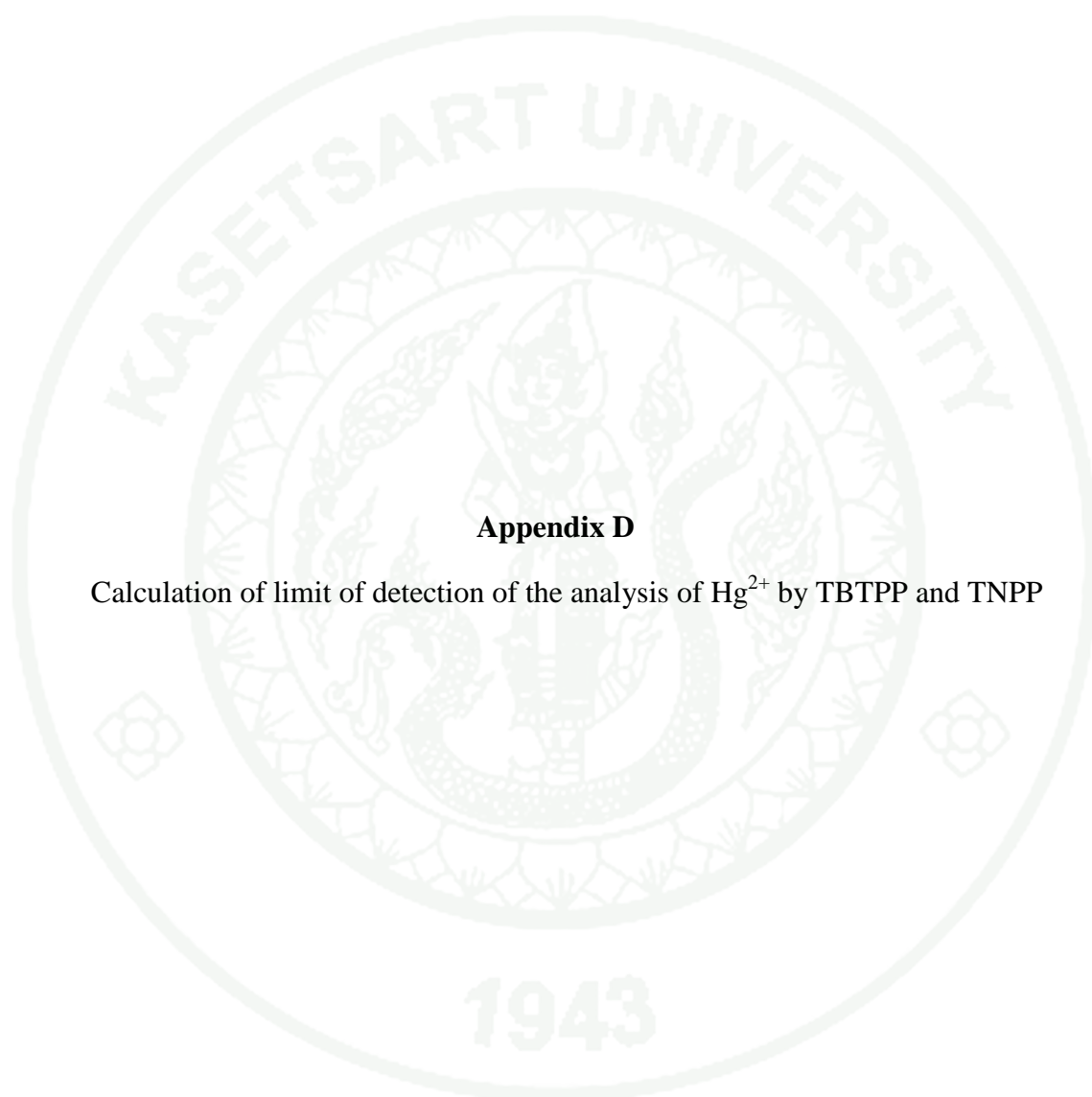
Appendix Figure C2 The relationship between $[\text{Hg}^{2+}]/A$ and $1/[\text{TNPP}]$.

The stability constant was obtained from the slope and y-intercept.

$$\text{Slope} = 1/K\varepsilon_0 = 3.00 \times 10^{-11}$$

$$\text{y-intercept} = 1/\varepsilon_0 = 2.00 \times 10^{-5}$$

$$\text{Stability constant } (K_{\text{stab}}) = \text{y-intercept/slope} = 6.67 \times 10^5$$



Appendix D

Calculation of limit of detection of the analysis of Hg^{2+} by TBTPP and TNPP

Appendix Table D1 Calibration curve of the analysis of Hg^{2+} by TBTPP.

Concentration (μM)	Fluorescence intensity (I)	$I_0/I (y_i)$	Signal from regression line $\hat{y} = 0.0922x + 0.3297$	$(y_i - \hat{y})^2$
0	661.8760000	1.000	0.3297	0.44930209
1	659.8963111	1.003	0.4219	0.33767721
2	620.8968105	1.066	0.5141	0.30459361
3	619.7340824	1.068	0.6063	0.21316689
4	619.1543499	1.069	0.6985	0.13727025
5	608.3419118	1.088	0.7907	0.08838729
6	627.9658444	1.054	0.8829	0.02927521
7	640.1121857	1.034	0.9751	0.00346921
8	578.0576419	1.145	1.0673	0.00603729
9	573.5493934	1.154	1.1595	3.025E-05
10	536.3662885	1.234	1.2517	0.00031329
11	510.7067901	1.296	1.3439	0.00229441
12	482.4169096	1.372	1.4361	0.00410881
13	453.9615912	1.458	1.5283	0.00494209
14	419.1741609	1.579	1.6205	0.00172225
15	370.7988796	1.785	1.7127	0.00522729
16	350.7556969	1.887	1.8049	0.00674041
17	340.8218332	1.942	1.8971	0.00201601
18	320.5210654	2.065	1.9893	0.00573049
19	329.6195219	2.008	2.0815	0.00540225
20	302.7795059	2.186	2.1737	0.00015129
21	301.5380410	2.195	2.2659	0.00502681
22	282.6114432	2.342	2.3581	0.00025921
23	261.4044234	2.532	2.4503	0.00667489
24	265.6003210	2.492	2.5425	0.00255025
25	272.2649116	2.431	2.6347	0.04149369
26	264.8563425	2.499	2.7269	0.05193841
27	274.5234343	2.411	2.8191	0.16654561
28	282.6114432	2.342	2.9113	0.32410249
29	272.1529605	2.432	3.0035	0.32661225
30	269.3838014	2.457	3.0957	0.40793769
$\Sigma(y_i - \hat{y})^2$				2.94099919

$$S_{y/x} = \frac{\sqrt{\sum [y_i - \hat{y}]^2}}{n-2}$$

$$= 0.059$$

When

$$S_{y/x} = S_B$$

$$y_{\text{intercept}} = y_B$$

$$\text{L.O.D} = y_B + 3S_B$$

$$= y_{\text{intercept}} + 3S_{y/x}$$

$$= 0.3297 + 3(0.059)$$

$$= 0.5067$$

L.O.D signal was transformed to L.O.D value by equation of regression line.

$$\hat{y} = 0.0922x + 0.3297$$

$$0.5067 = 0.0922x + 0.3297$$

$$x = 1.92 \mu\text{M}$$

Limit of detection for the analysis of Hg^{2+} by TBTPP is 1.92 μM .

Appendix Table D2 Calibration curve of the analysis of Hg^{2+} by TNPP.

Concentration (μM)	Fluorescence intensity (I)	I_0/I (y_i)	Signal from regression line $\hat{y} = 0.0913x + 0.292$	$(y_i - \hat{y})^2$
0	721.488	1.000	0.2920	0.50126400
1	689.994	1.046	0.3833	0.43917129
2	603.052	1.196	0.4746	0.52041796
3	603.046	1.196	0.5659	0.39702601
4	622.509	1.159	0.6572	0.25180324
5	605.275	1.192	0.7485	0.19669225
6	603.604	1.195	0.8398	0.12616704
7	601.254	1.200	0.9311	0.07230721
8	601.240	1.200	1.0224	0.03154176
9	641.893	1.124	1.1137	0.00010609
10	641.893	1.124	1.2050	0.00656100
11	635.672	1.135	1.2963	0.02601769
12	629.022	1.147	1.3876	0.05788836
13	494.848	1.458	1.4789	0.00043681
14	456.927	1.579	1.5702	7.744E-05
15	404.195	1.785	1.6615	0.01525225
16	418.012	1.726	1.7528	0.00071824
17	371.518	1.942	1.8441	0.00958441
18	361.648	1.995	1.9354	0.00355216
19	359.307	2.008	2.0267	0.00034969
20	367.544	1.963	2.1180	0.02402500
21	328.696	2.195	2.2093	0.00020449
22	344.221	2.096	2.3006	0.04186116
23	309.652	2.330	2.3919	0.00383161
24	289.522	2.492	2.4832	7.744E-05
25	280.407	2.573	2.5745	2.25E-06
26	258.783	2.788	2.6658	0.01493284
27	252.887	2.853	2.7571	0.00919681
28	262.933	2.744	2.8484	0.01089936
29	258.135	2.795	2.9397	0.02093809
30	272.260	2.650	3.0310	0.14516100
$\Sigma(y_i - \hat{y})^2$				2.92806495

$$S_{y/x} = \frac{\sqrt{\sum [y_i - \hat{y}]^2}}{n-2}$$

$$= 0.059$$

When

$$S_{y/x} = S_B$$

$$y_{\text{intercept}} = y_B$$

$$\text{L.O.D} = y_B + 3S_B$$

$$= y_{\text{intercept}} + 3S_{y/x}$$

$$= 0.292 + 3(0.059)$$

$$= 0.469$$

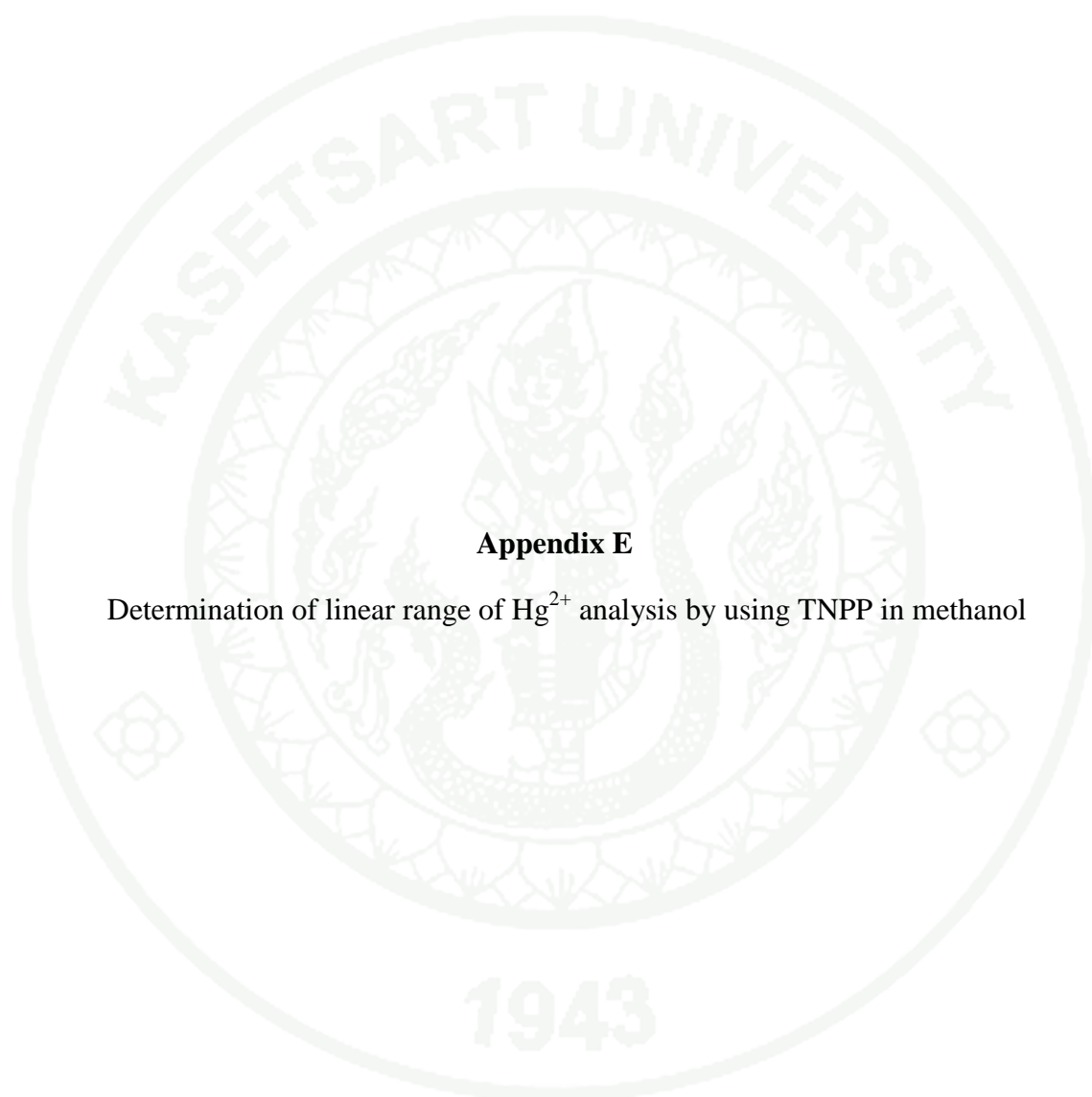
L.O.D signal was transformed to L.O.D value by equation of regression line.

$$\hat{y} = 0.0913x + 0.292$$

$$0.469 = 0.0913x + 0.292$$

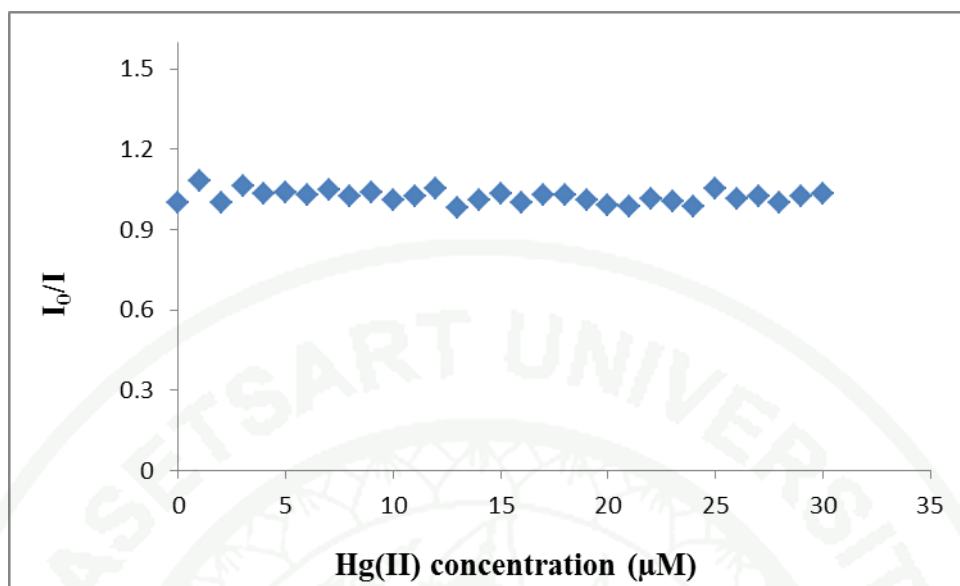
$$x = 1.94 \mu\text{M}$$

Limit of detection for the analysis of Hg^{2+} by TNPP is 1.94 μM .

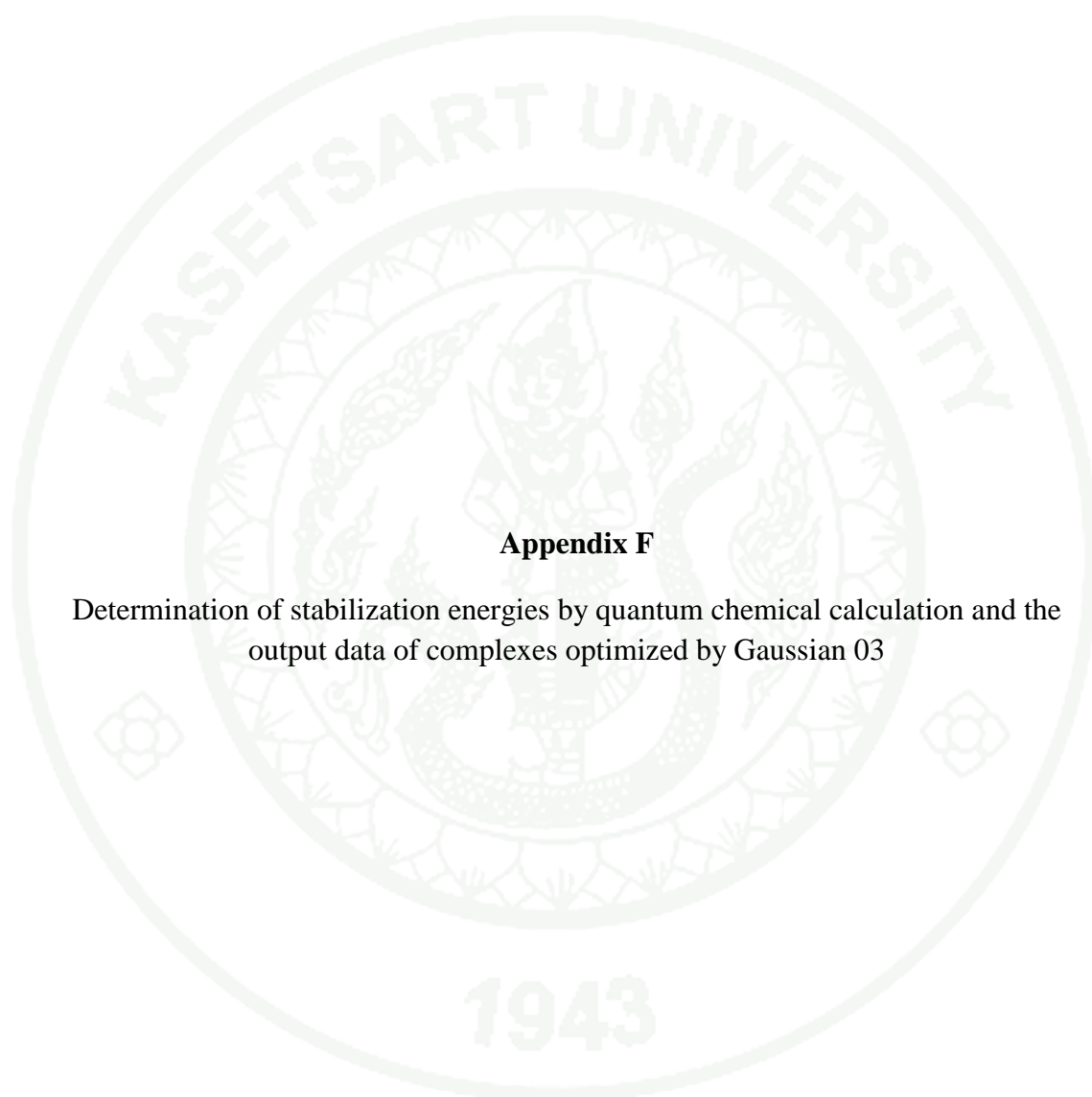


Appendix E

Determination of linear range of Hg^{2+} analysis by using TNPP in methanol



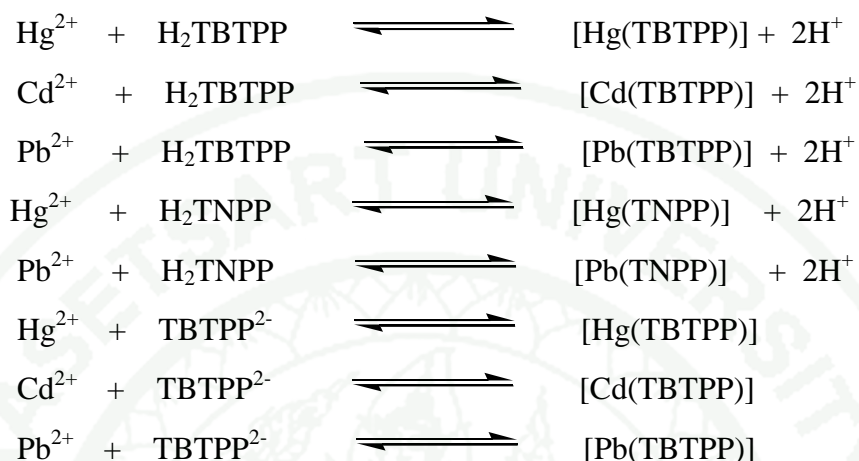
Appendix Figure E1 The plot of relative fluorescence intensity (I_0/I) as a function of Hg^{2+} concentration in methanol.



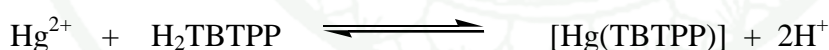
Appendix F

Determination of stabilization energies by quantum chemical calculation and the output data of complexes optimized by Gaussian 03

The formation of complexes between metal with TBTPP and TNPP should be as followed:

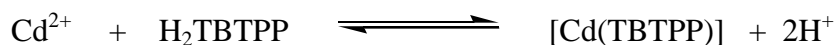


The molecular structures of reactants and products were created on GaussView version 3.0 and their cartesian coordinates were used as input structures on Gaussian03. The quantum chemical calculations were carried out at B3LYP (Lee, Yang and Parr correlation functional) level with 6-31G* basis set for all atoms and Lanl2DZ basis set for mercury atom.



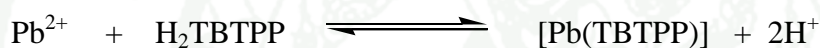
The stabilization energy, E, of [Hg(TBTPP)] complex was calculated as followed:

$$\begin{aligned}
 E &= (E_{\text{products}}) - (E_{\text{reactants}}) \\
 &= [(E_{\text{complex}}) + 2(E_{\text{proton}})] - [(E_{\text{Hg}}) + (E_{\text{H}_2\text{TBTPP}})] \\
 &= [(-12240.99139) - [(-41.7934727) + (-12198.169061)]] \\
 E &= -1.0288573 \text{ atomic unit} \\
 &= -1.0288573 \times 627.51 \\
 &= -645.618 \text{ kcal/mol}
 \end{aligned}$$



The stabilization energy, E, of [Cd(TBTPP)] complex was calculated as followed:

$$\begin{aligned} E &= (E_{\text{products}}) - (E_{\text{reactants}}) \\ &= [(E_{\text{complex}}) + 2(E_{\text{proton}})] - [(E_{\text{Cd}}) + (E_{\text{H}_2\text{TBTPP}})] \\ &= [(-12243.87062)] - [(-47.1558726) + (-12198.169061)] \\ E &= +1.4543126 \text{ atomic unit} \\ &= +1.4543126 \times 627.51 \\ &= +912.596 \text{ kcal/mol} \end{aligned}$$



The stabilization energy, E, of [Pb(TBTPP)] complex was calculated as followed:

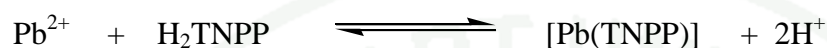
$$\begin{aligned} E &= (E_{\text{products}}) - (E_{\text{reactants}}) \\ &= [(E_{\text{complex}}) + 2(E_{\text{proton}})] - [(E_{\text{Pb}}) + (E_{\text{H}_2\text{TBTPP}})] \\ &= [(-12199.30282)] - [(-2.653458) + (-12198.169061)] \\ E &= +1.519698 \text{ atomic unit} \\ &= +1.519698 \times 627.51 \\ &= +953.626 \text{ kcal/mol} \end{aligned}$$



The stabilization energy, E, [Hg(TNPP)] complex was calculated as followed:

$$\begin{aligned} E &= (E_{\text{products}}) - (E_{\text{reactants}}) \\ &= [(E_{\text{complex}}) + 2(E_{\text{proton}})] - [(E_{\text{Hg}}) + (E_{\text{H}_2\text{TNPP}})] \\ &= [(-2773.97827)] - [(-41.7934727) + (-2731.753979)] \end{aligned}$$

$$\begin{aligned}
 E &= -0.40818 \text{ atomic unit} \\
 &= -0.40818 \times 627.51 \\
 &= -256.137 \text{ kcal/mol}
 \end{aligned}$$



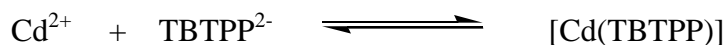
The stabilization energy, E, [Pb(TNPP)] complex was calculated as followed:

$$\begin{aligned}
 E &= (E_{\text{products}}) - (E_{\text{reactants}}) \\
 &= [(E_{\text{complex}}) + 2(E_{\text{proton}})] - [(E_{\text{Pb}}) + (E_{\text{H}_2\text{TNPP}})] \\
 &= [(-2733.99719) - [(-2.653458) + (-2731.753979)]] \\
 E &= +0.410247 \text{ atomic unit} \\
 &= +0.410247 \times 627.51 \\
 &= +257.434 \text{ kcal/mol}
 \end{aligned}$$



The stabilization energy, E, of [Hg(TBTPP)] complex was calculated as followed:

$$\begin{aligned}
 E &= (E_{\text{products}}) - (E_{\text{reactants}}) \\
 &= [(E_{\text{complex}}) + 2(E_{\text{proton}})] - [(E_{\text{Hg}}) + (E_{\text{TBTPP}^{2-}})] \\
 &= [(-12240.99139) - [(-41.7934727) + (-12196.9223424)]] \\
 E &= -2.27558 \text{ atomic unit} \\
 &= -2.27558 \times 627.51 \\
 &= -1427.930 \text{ kcal/mol}
 \end{aligned}$$



The stabilization energy, E, of [Cd(TBTPP)] complex was calculated as followed:

$$\begin{aligned} E &= (E_{\text{products}}) - (E_{\text{reactants}}) \\ &= [(E_{\text{complex}}) + 2(E_{\text{proton}})] - [(E_{\text{Cd}}) + (E_{\text{TBTPP}^{2-}})] \\ &= [(-12243.87062)] - [(-47.1558726) + (-12196.9223424)] \\ E &= +0.20759 \text{ atomic unit} \\ &= +0.20759 \times 627.51 \\ &= +130.265 \text{ kcal/mol} \end{aligned}$$



The stabilization energy, E, of [Pb(TBTPP)] complex was calculated as followed:

$$\begin{aligned} E &= (E_{\text{products}}) - (E_{\text{reactants}}) \\ &= [(E_{\text{complex}}) + 2(E_{\text{proton}})] - [(E_{\text{Cd}}) + (E_{\text{TBTPP}^{2-}})] \\ &= [(-12199.30282)] - [(-2.653458) + (-12196.9223424)] \\ E &= +0.27298 \text{ atomic unit} \\ &= +0.27298 \times 627.51 \\ &= +171.298 \text{ kcal/mol} \end{aligned}$$

1. The example of input data

1.1 The input data of H₂TBTPP;

%mem=1000MB

#p opt b3lyp/6-31g*

```

-----
0 1
C      -1.12934    2.93403   -0.10066
C      -0.69009    4.31029    0.06255
C       0.67553    4.31206    0.0287
C       1.10987    2.93398   -0.13515
N      -0.01256    2.1553    -0.22976
H      -1.33473    5.16424    0.21048
H       1.32317    5.17063    0.12654
H       5.11581   -1.3342    0.32503
C       4.27977   -0.68535    0.10892
C       4.2806     0.68037    0.10884
C       2.92042   -1.12062   -0.16834
C       2.92175    1.11724   -0.16837
H       5.11742    1.32825    0.32484
N       2.15614   -0.00123   -0.35238
N      -2.15266    0.00114   -0.09793
C      -2.9422    -1.11769   -0.0716
C      -2.94088    1.12094   -0.07173
C      -4.32887   -0.68056   -0.04451
C      -4.32807    0.68542   -0.04462
H      -5.19443   -1.32656   -0.03271
H      -5.19287    1.33242   -0.03301
H      -1.34067   -5.16292    0.20983
C      -0.69508   -4.30964    0.06221
C       0.67054   -4.31294    0.02831
C      -1.13276   -2.93283   -0.10051
C       1.10645   -2.93531   -0.13507
H       1.31722   -5.17229    0.12575
N      -0.01512   -2.1553    -0.22931
C       2.45595    2.46519   -0.12559
C      -2.47731    2.469     -0.05976
C      -2.4802    -2.46629   -0.05957
C       2.45305   -2.46803   -0.12554
C      -3.53133    3.52894    0.04343
C      -3.72755    4.45691   -0.99184
C      -4.34564    3.62689    1.18329
C      -4.70367    5.4492    -0.89981

```

H	-3.11294	4.39668	-1.88491
C	-5.32484	4.61391	1.29083
H	-4.20279	2.92713	2.00087
C	-5.49584	5.5189	0.24474
H	-4.84935	6.15571	-1.70922
H	-5.94235	4.68326	2.17911
C	3.52155	3.50958	0.02182
C	3.63021	4.2773	1.19237
C	4.45104	3.73337	-1.00606
C	4.6269	5.24236	1.33445
H	2.93195	4.10903	2.00637
C	5.45273	4.69605	-0.87973
H	4.38501	3.15051	-1.9198
C	5.531	5.44468	0.29313
H	4.70451	5.82441	2.24568
H	6.16051	4.8641	-1.68367
C	-3.53547	-3.52499	0.04367
C	-3.73292	-4.45268	-0.99159
C	-4.34979	-3.62191	1.18362
C	-4.71023	-5.44382	-0.89944
H	-3.11835	-4.39322	-1.88473
C	-5.33015	-4.60776	1.29126
H	-4.206	-2.92229	2.00115
C	-5.50235	-5.51256	0.2452
H	-4.85686	-6.15014	-1.70883
H	-5.94765	-4.67639	2.1796
C	3.51747	-3.51365	0.02167
C	4.44678	-3.73821	-1.00622
C	3.62527	-4.28174	1.19206
C	5.44744	-4.70198	-0.88005
H	4.38143	-3.15507	-1.91982
C	4.62093	-5.24787	1.33399
H	2.92717	-4.11285	2.00608
C	5.52485	-5.45094	0.29266
H	6.15508	-4.87062	-1.68398
H	4.69791	-5.83019	2.24511
Br	-6.8342	6.87552	0.38499
Br	-6.84229	-6.86759	0.38564
Br	6.89183	-6.77301	0.47934
Br	6.89931	6.76533	0.47998
H	1.18388	-0.00065	-0.58629
H	-1.15321	0.00054	-0.13121

1.2 The input data of H₂TNPP;

```
%mem=1000MB
```

```
#p opt b3lyp/6-31g*
```

```
-----
0 1
C      1.11811  -2.93557  -0.07257
C      0.68346  -4.32327  -0.09898
C     -0.68234  -4.32344  -0.09897
C     -1.11729  -2.93583  -0.07261
N      0.00031  -2.14684  -0.07386
H      1.32776  -5.18974  -0.12262
H     -1.32651  -5.19001  -0.12255
H     -5.10888   1.32844   0.53877
C     -4.27848   0.68218   0.29518
C     -4.2783   -0.68333   0.29513
C     -2.92915   1.11887  -0.02372
C     -2.92885  -1.11968  -0.0237
H     -5.10855  -1.32981   0.53867
N     -2.16779  -0.0003   -0.22175
N      2.16777   0.00033  -0.22173
C      2.92882   1.11969  -0.02363
C      2.92912  -1.11887  -0.02369
C      4.27827   0.68336   0.29519
C      4.27846  -0.68215   0.29518
H      5.1085    1.32985   0.53876
H      5.10886  -1.32841   0.53876
H      1.32644   5.18999  -0.12261
C      0.68229   4.32342  -0.09905
C     -0.68351   4.32326  -0.09904
C      1.11724   2.93581  -0.07261
C     -1.11814   2.93555  -0.07265
H     -1.32782   5.18972  -0.12266
N     -0.00035   2.14682  -0.0739
C     -2.46435  -2.46881  -0.02564
C      2.46501  -2.46817  -0.02559
C      2.46431   2.46882  -0.02556
C     -2.46504   2.46817  -0.02567
C      3.52616  -3.5176    0.08338
C      4.51647  -3.63848  -0.90839
C      3.56302  -4.39671   1.18131
C      5.50993  -4.60873  -0.81743
H      4.49678  -2.96976  -1.76269
C      4.5514   -5.37027   1.2886
H      2.81609  -4.30296   1.96257
```

C	5.51173	-5.46289	0.28324
H	6.27236	-4.71776	-1.5786
H	4.59668	-6.04757	2.13225
C	-3.52517	-3.51859	0.08338
C	-3.56186	-4.39751	1.18146
C	-4.51532	-3.64	-0.90848
C	-4.54992	-5.37137	1.28884
H	-2.81503	-4.30337	1.96278
C	-5.50849	-4.61054	-0.81742
H	-4.49578	-2.97145	-1.76292
C	-5.51014	-5.4645	0.28341
H	-4.59501	-6.04856	2.13259
H	-6.27081	-4.71992	-1.57864
C	3.52512	3.51861	0.08342
C	4.51521	3.64003	-0.9085
C	3.56191	4.39746	1.18154
C	5.50841	4.61055	-0.81746
H	4.4956	2.97152	-1.76296
C	4.54999	5.3713	1.28889
H	2.81513	4.3033	1.96291
C	5.51014	5.46447	0.2834
H	6.27068	4.71995	-1.57874
H	4.59516	6.04845	2.13267
C	-3.52616	3.51762	0.08334
C	-4.51652	3.63851	-0.90839
C	-3.56295	4.39674	1.18125
C	-5.50996	4.60878	-0.81738
H	-4.49689	2.96978	-1.76268
C	-4.55129	5.37033	1.28858
H	-2.81596	4.30301	1.96246
C	-5.51168	5.46296	0.28327
H	-6.27242	4.71779	-1.57852
H	-4.59648	6.04766	2.13221
N	6.55728	6.49286	0.38891
O	7.39356	6.54884	-0.51196
O	6.53155	7.23318	1.37138
N	6.55919	-6.49099	0.38868
O	6.53392	-7.23111	1.37132
O	7.39533	-6.54682	-0.51232
N	-6.55725	-6.49292	0.38895
O	-6.53144	-7.23328	1.37139
O	-7.3936	-6.54887	-0.51186
N	-6.55911	6.49109	0.38875
O	-7.39533	6.5469	-0.51218
O	-6.53368	7.23134	1.37128
H	0.00019	-1.14684	-0.07548
H	-0.00023	1.14682	-0.07551

1.3 The input data of Hg-TBTPP complex;

%mem=5000MB

#P B3LYP/gen pseudo=read Opt

```

-----
0 1
C      1.08767  -2.95025  -0.05592
C      0.62658  -4.31142   0.16866
C     -0.7396   -4.29348   0.13415
C     -1.15344  -2.9182    -0.09118
N     -0.01817  -2.16203  -0.22023
H      1.25824  -5.16647   0.35956
H     -1.40257  -5.13419   0.27555
H     -5.13027   1.40649   0.18049
C     -4.29183   0.74083   0.03361
C     -4.31261  -0.62568   0.03988
C     -2.9093    1.15284  -0.15308
C     -2.94352  -1.0824   -0.14908
H     -5.1709   -1.2632    0.19502
N     -2.15164   0.02231  -0.28033
N      2.15157  -0.03197  -0.04034
C      2.95539   1.07619  -0.0656
C      2.92502  -1.1618   -0.06021
C      4.33583   0.62261  -0.10744
C      4.31779  -0.74479  -0.108
H      5.20835   1.25858  -0.14165
H      5.17428  -1.40199  -0.14595
H      1.39803   5.11415   0.39136
C      0.74211   4.28119   0.18439
C     -0.62443   4.29749   0.15507
C      1.16844   2.91265  -0.06328
C     -1.07043   2.93806  -0.10335
H     -1.26948   5.1474    0.32455
N      0.04465   2.1567   -0.24956
C     -2.49395  -2.43362  -0.09873
C      2.4436    -2.50497  -0.03429
C      2.51025   2.43109  -0.03961
C     -2.42124   2.4888   -0.10791
C      3.48138  -3.57817   0.05562
C      3.60738  -4.54729  -0.95338
C      4.35398  -3.65283   1.15424
C      4.5717    -5.55179  -0.87857
H      2.94842  -4.50644  -1.81538
C      5.32224  -4.65191   1.24439
H      4.26451  -2.92473   1.95452

```

C	5.42381	-5.59546	0.22348
H	4.66303	-6.28782	-1.66916
H	5.98443	-4.70134	2.10117
C	-3.57346	-3.46936	0.03079
C	-3.76153	-4.17614	1.2282
C	-4.43242	-3.74116	-1.0444
C	-4.77273	-5.12939	1.35289
H	-3.1145	-3.97064	2.07562
C	-5.44798	-4.69193	-0.93558
H	-4.30453	-3.20244	-1.97857
C	-5.60782	-5.37994	0.26565
H	-4.91407	-5.66474	2.28471
H	-6.10527	-4.89582	-1.77304
C	3.57757	3.4775	0.05815
C	3.72457	4.44866	-0.94505
C	4.45067	3.5211	1.15673
C	4.71379	5.42866	-0.86418
H	3.06101	4.4313	-1.80434
C	5.44277	4.49671	1.25351
H	4.3459	2.78628	1.94903
C	5.56618	5.44396	0.23845
H	4.82358	6.16779	-1.6494
H	6.1076	4.52383	2.10929
C	-3.46784	3.56008	0.02792
C	-4.07536	4.11183	-1.10862
C	-3.86292	4.02682	1.28975
C	-5.05282	5.10161	-0.99563
H	-3.78213	3.76208	-2.09415
C	-4.83842	5.01641	1.41955
H	-3.40349	3.60896	2.18062
C	-5.42531	5.54554	0.2715
H	-5.51714	5.52272	-1.87989
H	-5.13901	5.36982	2.39922
Br	6.74569	-6.97011	0.33955
Br	6.92282	6.78415	0.36092
Br	-6.7626	6.90173	0.43696
Br	-6.99796	-6.68228	0.42652
Hg	0.03293	-0.00773	-0.88969

Hg 0

LanL2DZ

N C H Br 0

6-31G (d,p)

Un saludo desde Leioa

Pablo

1.4 The input data of Hg-TNPP complex;

%mem=5000MB

#P B3LYP/gen pseudo=read Opt

```

-----
0 1
C          2.7963      1.49745  -0.0016
C          4.23106     1.23882  -0.00018
C          4.40685    -0.11964  -0.00007
C          3.08569    -0.73617  -0.00231
N          2.18037     0.28257  -0.00322
H          5.00744     1.99084   0.00122
H          5.35233    -0.64385   0.00123
H          -0.6436    -5.34935   0.0012
C          -0.11926   -4.40401  -0.00084
C          1.23857    -4.22984  -0.00086
C          -0.73653   -3.08164  -0.00284
C          1.50035    -2.79402  -0.00314
H          1.98931    -5.00754   0.00108
N          0.28493    -2.17849  -0.00477
N          -0.28271    2.17828  -0.00369
C          -1.4988     2.79284  -0.00177
C          0.73772     3.08246  -0.00151
C          -1.23808    4.22896   0.00106
C          0.11955     4.40432   0.00108
H          -1.98932    5.00619   0.00339
H          0.64329     5.35      0.00346
H          -5.35285    0.64379   0.00146
C          -4.40743    0.11954   0.00012
C          -4.23151    -1.23904  -0.00051
C          -3.08615     0.73633  -0.0017
C          -2.7964     -1.49774  -0.00202
H          -5.00784    -1.99112   0.00045
N          -2.18117    -0.28253  -0.00315
C          2.77311     -2.13455  -0.00246
C          2.13454     2.77104  -0.00115
C          -2.77205     2.13437  -0.00129
C          -2.13365    -2.77063  -0.00222
C          3.05596     3.96027   0.00099
C          3.49141     4.52718  -1.20705
C          3.49424     4.51987   1.2115
C          4.34392     5.6298   -1.21526
H          3.15686     4.09887  -2.14666
C          4.34664     5.62246   1.22427
H          3.1619     4.08605   2.14935
C          4.7598     6.1623   0.00562

```

H	4.68862	6.07876	-2.1378
H	4.69345	6.06598	2.14868
C	3.96209	-3.05422	-0.00014
C	4.53048	-3.48291	1.20953
C	4.52114	-3.49909	-1.20866
C	5.633	-4.33564	1.22182
H	4.10206	-3.14334	2.14726
C	5.62392	-4.35099	-1.21717
H	4.08693	-3.17266	-2.14834
C	6.16461	-4.75825	0.00307
H	6.08239	-4.67546	2.14591
H	6.06675	-4.70304	-2.13999
C	-3.9612	3.05443	0.00132
C	-4.51894	3.50112	-1.20713
C	-4.53078	3.48135	1.21109
C	-5.62171	4.35306	-1.21563
H	-4.08376	3.17588	-2.14679
C	-5.63334	4.334	1.22339
H	-4.1035	3.14042	2.14886
C	-6.16361	4.75829	0.00471
H	-6.06366	4.70637	-2.13839
H	-6.08375	4.67246	2.14751
C	-3.05446	-3.96033	-0.00062
C	-3.48817	-4.52815	-1.20885
C	-3.49396	-4.51946	1.20968
C	-4.34021	-5.63115	-1.21749
H	-3.15271	-4.10011	-2.14826
C	-4.34578	-5.62247	1.222
H	-3.163	-4.08501	2.14773
C	-4.75708	-6.1633	0.00316
H	-4.6836	-6.08079	-2.14019
H	-4.69346	-6.06568	2.14624
N	-7.32984	5.66141	0.00642
O	-7.78138	6.00819	-1.07933
O	-7.79328	5.98956	1.09317
N	5.66278	7.32904	0.00811
O	6.00154	7.78356	1.09612
O	5.99896	7.79023	-1.07791
N	7.33075	-5.66157	0.00459
O	7.79259	-5.99193	1.091
O	7.78239	-6.00769	-1.08089
N	-5.65917	-7.33067	0.00519
O	-6.0039	-7.78494	-1.08124
O	-6.00914	-7.77693	1.09318
Hg	-0.00106	-0.00058	-0.00909

Hg 0

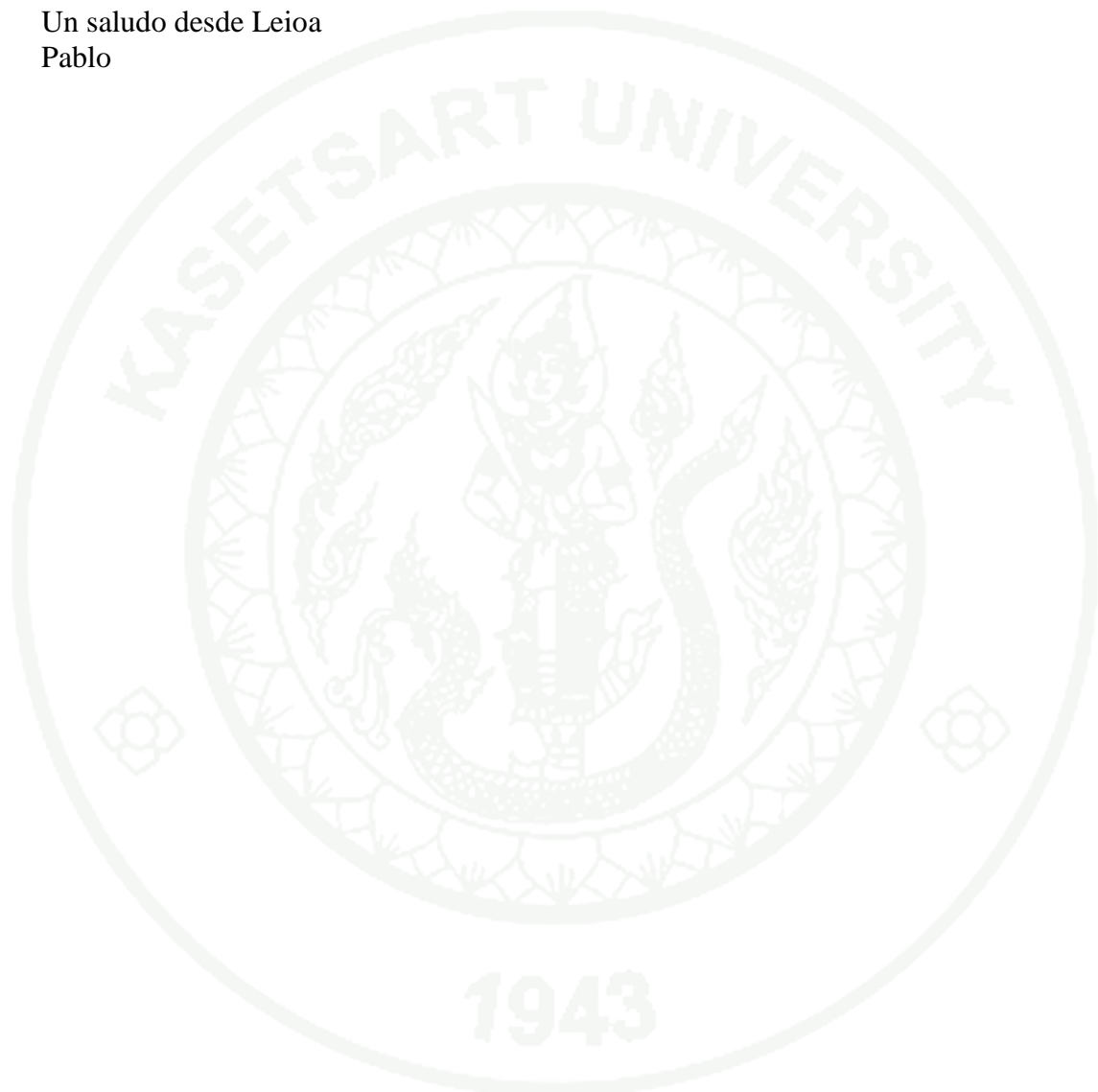
LanL2DZ

N C H O 0

6-31G (d,p)

Un saludo desde Leioa

Pablo



CIRRICULUM VITAE

NAME : Miss. Suwaluck Chaitong

BIRTH DATE : January 2, 1988

BIRTH PLACE : Nakhon Si Thammarat, Thailand

EDUCATION	: <u>YEAR</u>	<u>INSTITUTE</u>	<u>DEGREE/DIPLOMA</u>
	2010	Kasetsart Univ.	B.Sc. (Chemistry)

POSITION/TITLE : Postgraduated student

WORKPLACE : Faculty of Science, Kasetsart University

SCHOLARSHIP/AWARDS : -Center for Innovation in Chemistry:
Postgraduate Education and Research Program in Chemistry (PERCH-CIC)